NAVAL POSTGRADUATE SCHOOL
Monterey, California

THESIS

PERFORMANCE MEASUREMENTS, FLOW VISUALIZATION, AND NUMERICAL SIMULATION OF A CROSSFLOW FAN

by

M. Scot Seaton

March 2003

Thesis Advisor: Garth V. Hobson
Second Reader: Raymond P. Shreeve

Approved for public release; distribution is unlimited

THIS PAGE INTENTIONALLY LEFT BLANK

REPORT DOCUMENTATION PAGE			Form Approved OMB No. 0704-0188
Public reporting burden for this collection of information is estimated to average 1 hour per response, including the time for reviewing instruction, searching existing data sources, gathering and maintaining the data needed, and completing and reviewing the collection of information. Send comments regarding this burden estimate or any other aspect of this collection of information, including suggestions for reducing this burden, to Washington headquarters Services, Directorate for Information Operations and Reports, 1215 Jefferson Davis Highway, Suite 1204, Arlington, VA 22202-4302, and to the Office of Management and Budget, Paperwork Reduction Project (0704-0188) Washington DC 20503.			
1. AGENCY USE ONLY *(Leave blank)*	**2. REPORT DATE** March 2003	**3. REPORT TYPE AND DATES COVERED** Master's Thesis	
4. TITLE AND SUBTITLE: Performance Measurements, Flow Visualization, and Numerical Simulation of a Crossflow Fan			**5. FUNDING NUMBERS**
6. AUTHOR(S) Seaton, M. Scot			
7. PERFORMING ORGANIZATION NAME(S) AND ADDRESS(ES) Naval Postgraduate School Monterey, CA 93943-5000			**8. PERFORMING ORGANIZATION REPORT NUMBER**
9. SPONSORING / MONITORING AGENCY NAME(S) AND ADDRESS(ES) N/A			**10. SPONSORING / MONITORING AGENCY REPORT NUMBER**
11. SUPPLEMENTARY NOTES The views expressed in this thesis are those of the author and do not reflect the official policy or position of the Department of Defense or the U.S. Government.			
12a. DISTRIBUTION / AVAILABILITY STATEMENT Approved for public use; distribution is unlimited			**12b. DISTRIBUTION CODE**

13. ABSTRACT ***(maximum 200 words)***

A 12-inch diameter, 1.5-inch span crossflow fan test apparatus was constructed and tested using the existing Turbine Test Rig (TTR) as a power source. Instrumentation was installed and a data acquisition program was developed to measure the performance of the crossflow fan. Performance measurements were taken over a speed range of 1,000 to 7,000 RPM. Results comparable to those measured by Vought Systems Division of LTV Aerospace in 1975 were obtained. At 6,000 RPM, a thrust-to-power ratio of one was determined; however, at 3,000 RPM twice the thrust-to-power ratio was measured. Flow visualization was conducted using dye-injection methods. Performance and flow visualization results were compared to predictions obtained from 2-D numerical simulation conducted using Flo++, a commercial PC-based computational fluid dynamics software package by Softflo. A possible design for a light civil V/STOL aircraft was suggested using a similar crossflow fan apparatus for both lift and propulsion.

14. SUBJECT TERMS Crossflow fan, cross flow fan, VTOL			**15. NUMBER OF PAGES** 127
			16. PRICE CODE
17. SECURITY CLASSIFICATION OF REPORT Unclassified	**18. SECURITY CLASSIFICATION OF THIS PAGE** Unclassified	**19. SECURITY CLASSIFICATION OF ABSTRACT** Unclassified	**20. LIMITATION OF ABSTRACT** UL

NSN 7540-01-280-5500 Standard Form 298 (Rev. 2-89)
Prescribed by ANSI Std. 239-18

THIS PAGE INTENTIONALLY LEFT BLANK

Approved for public release; distribution is unlimited

PERFORMANCE MEASUREMENTS, FLOW VISUALIZATION, AND NUMERICAL SIMULATION OF A CROSSFLOW FAN

M. Scot Seaton
Lieutenant, United States Navy
B.S., Purdue University, 1993

Submitted in partial fulfillment of the
requirements for the degree of

MASTER OF SCIENCE IN AERONAUTICAL ENGINEERING

from the

NAVAL POSTGRADUATE SCHOOL
March 2003

Author: M. Scot Seaton

Approved by: Garth V. Hobson
Thesis Advisor

Raymond P. Shreeve
Second Reader

Max F. Platzer
Chairman, Department of Aeronautics and Astronautics

THIS PAGE INTENTIONALLY LEFT BLANK

ABSTRACT

A 12-inch diameter, 1.5-inch span crossflow fan test apparatus was constructed and tested using the existing Turbine Test Rig (TTR) as a power source. Instrumentation was installed and a data acquisition program was developed to measure the performance of the crossflow fan. Performance measurements were taken over a speed range of 1,000 to 7,000 RPM. Results comparable to those measured by Vought Systems Division of LTV Aerospace in 1975 were obtained. At 6,000 RPM, a thrust-to-power ratio of one was determined; however, at 3,000 RPM twice the thrust-to-power ratio was measured. Flow visualization was conducted using dye-injection methods. Performance and flow visualization results were compared to predictions obtained from 2-D numerical simulation conducted using Flo++, a commercial PC-based computational fluid dynamics software package by Softflo. A possible design for a light civil V/STOL aircraft was suggested using a similar crossflow fan apparatus for both lift and propulsion.

THIS PAGE INTENTIONALLY LEFT BLANK

TABLE OF CONTENTS

LIST OF FIGURES

LIST OF TABLES

THIS PAGE INTENTIONALLY LEFT BLANK

ACKNOWLEDGEMENTS

I would like to express my sincere thanks to the following people:

Professor Garth Hobson, for sparking my interest in this project. Without his expert guidance I would not have finished; without his attitude it would not have been half as much fun.

Professor Ray Shreeve, for his dedication to his students and for being a true educator, not just a teacher.

Professor Max Platzer, for his interest in this project, but specifically for his forthright and uncompromising leadership of the Aero Department during a particularly difficult time.

Doug Seivwright, Rick Still, and John Gibson, for all their assistance and for making the Turbo Lab such a great place to work.

Anthony Gannon and Louis LeGrange, vir die assistensie in FLO++ en computational fluid dynamics. Dankie here, sonder julle sou ek dit nie kon gedoen het nie.

My family, for their boundless support in my military and academic career.

Juan, Wendy, and Gabby Gutierrez, for keeping me fed and relatively sane throughout my time at NPS.

Finally, I would like to thank Rebecca Lindell for her love, support, and patience. Although I've tested the latter of these in the last two years, it's been worth it. Thanks for inspiring my return to academics and for being my best friend.

THIS PAGE INTENTIONALLY LEFT BLANK

I. INTRODUCTION

A. OVERVIEW

Recently, NASA has placed emphasis on the need for a more robust civil transport system intended to alleviate congestion in ground and air traffic near major cities. This has resulted in the creation of several programs to provide funding for research into various aspects of this broad goal. One such program encourages the development of civil alternatives to private ground transport; the intent being to reduce ground traffic by replacing the private automobile with a similarly-sized and purposed vertical takeoff and landing (VTOL) vehicle. This would serve the triple purpose of reducing ground traffic without requiring traditional airfields while simplifying the takeoff and landing process. At first glance, helicopter-type designs may seem the obvious choice, but these aircraft are more complex than fixed-wing types and require capabilities far beyond those required to operate a private automobile - capabilities which the average civilian is not likely to possess. Additionally, the potential for serious bodily harm and property damage involved in the operation of numerous rotary-winged aircraft in relatively close proximity makes these types of aircraft extremely risky for the general population. Similarly, jet engines could create a serious fire, noise, and foreign object debris (FOD) hazard when used outside the controlled atmosphere of the traditional airfield. They also have the additional drawback of being prohibitively expensive to purchase and maintain in relation to the automobile's internal combustion engine. Therefore, VTOL designs that do not incorporate exposed or otherwise hazardous lifting and propulsive devices are preferable. The research conducted in preparation for this thesis was intended to evaluate one such device, the crossflow fan, to determine its suitability for such a purpose.

The Crossflow Fan Test Assembly (CFTA) was established at the Naval Postgraduate School Turbopropulsion Laboratory using the previously existing Turbine Test Rig. This assembly was initiated by Studevan [Ref. 1] in order to test the turbine of the Space Shuttle Main Engine High Pressure Fuel Turbopump (SSME HPFTP). This work was continued by Rutkowski [Ref. 2] and Greco [Ref. 3] and refined for laser-

Doppler-velocimetry measurements by Southward [Ref. 4]. The primary goal of research on the crossflow fan was to determine performance characteristics by measuring parameters along an operating line. Provision was made in the CFTA for optical access to the rotor, which allowed for flow visualization studies to be performed as part of the experimental testing.

Viscous flow through the crossflow fan was numerically modeled using the commercially-available FLO++ software package from Softflo. A significant effort was undertaken to represent the numerical model as accurately as possible by generating a two-dimensional grid from computer-aided design (CAD) drawings of the CFTA. The results of this simulation were compared to pressure and velocity measurements determined experimentally in the test cell. FLO++ was also used to model a theoretical "fan-in-wing" concept in order to determine its usefulness as a high-lift device in a VTOL aircraft.

B. HISTORY

Crossflow devices have been theorized and utilized for many years. One early concept that used a type of crossflow device was the Banki turbine, which was most often used as a hydraulic turbine generator. In this configuration, as shown in Figure 1, water passed radially through the turbine and thus encountered the rotor twice, which allowed a more efficient passage of kinetic energy from the moving water to the turbine. Use of the Banki turbine was predominantly limited to the field of hydraulic power generation, where low-pressure head was available at high flow rates.

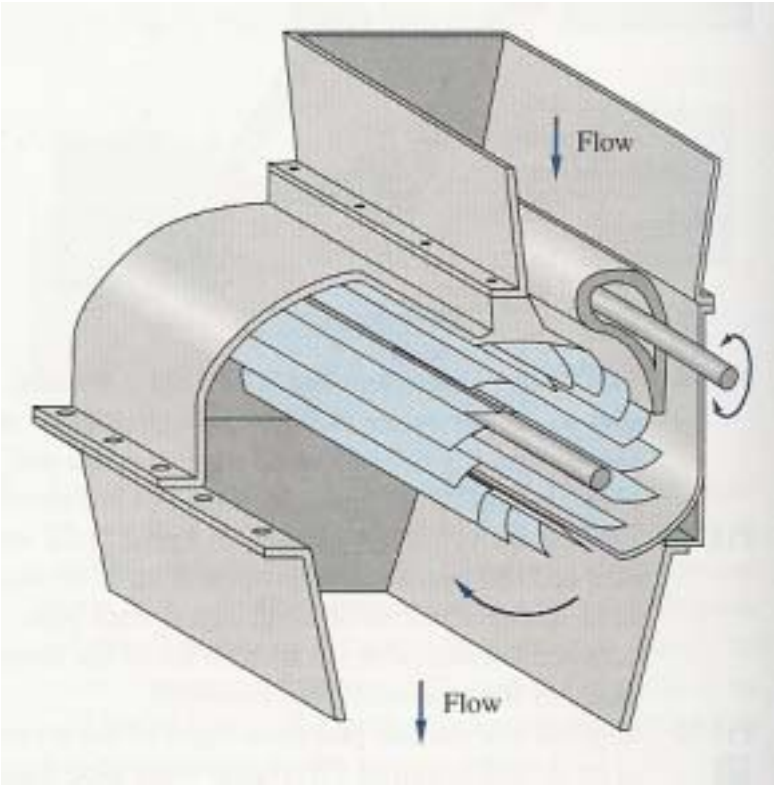

Figure 1. Banki Turbine (From Ref. 5)

Crossflow fans intended to move air have also seen much use in commercial and industrial applications. Primarily, these fans are designed to move air in a linear fashion for heating and ventilation purposes such as “air curtains” which maintain heating and cooling boundaries by providing a steep velocity gradient between two temperature zones. Such fans are often seen in open-bay freezers and refrigerators at supermarkets and above the entrances and exits of air-conditioned offices and restaurants.

In 1975, Vought Systems Division (VSD) of LTV Aerospace Corporation studied the application of crossflow fan technology to aircraft propulsion in their Multi-Bypass Ratio Propulsion System Development program [Ref. 6]. This program sought to take advantage of the crossflow fan's relatively compact size and form factor in developing a propulsion device that could easily be incorporated into conventional aircraft configurations with a minimum of added drag. Another advantage cited by VSD was the ability to accomplish thrust vectoring with ease since the fan was insensitive to the angular position of inlets, outlets, and cavities. VSD initially tested a 12-inch diameter, 1.5-inch span crossflow fan in various configurations between 6,000 and 13,000 RPM in order to establish baseline performance. Additionally, different housing or cavity configurations and exhaust duct shapes were tested, affording the opportunity to measure the performance of various crossflow fan configurations. This allowed some measure of optimization to be performed. A total of 46 different fan and housing configurations were tested, primarily including modifications to fan blade angles, resizing and reshaping of recirculation-inducing cavities, and variations in the total number of blades.

More recently, Moller International pioneered the design of a type of aircraft called the volantor, which relied primarily on thrust-producing devices for lift vice lifting surfaces. Moller's M400 Skycar was but one example of several models that were flight-tested and are in continuing development. This aircraft is shown in the figure below undergoing tethered hover tests.

Figure 2. Moller M400 Skycar (From Ref. 7)

The Skycar concept used four vectored-thrust ducted fans to provide both lift and thrust in all phases of flight. Eight Wankel engines were used to power the fans due to their characteristically high power-to-weight ratio.

Recognizing the inefficiency of using thrust-producing devices to create lift, Dean H. Gossett [Ref. 8] incorporated a crossflow fan as a lifting device in his proposal for a light civil VTOL aircraft. His concept utilized a Wankel-driven crossflow fan solely for lift in order to augment two Wankel-driven ducted fan assemblies that acted in a "lift and cruise" capacity. Gossett's model, shown in Figure 3, was a wing-and-canard type air vehicle that relied more heavily on lifting surfaces in forward flight than the Moller Skycar. The crossflow fan could be shut down in forward flight in order to improve fuel consumption, and reengaged upon preparation for landing. It was felt that low reliance on lifting surfaces during the takeoff and landing phases of flight would eliminate some of the more dangerous aspects of controlling conventional fixed- and rotary-wing aircraft, and therefore help reduce complexity of operation to something nearly on par with the average automobile. The concept eliminated the extra weight of two ducted fan assemblies and associated engines.

The crossflow fan configuration evaluated by Gossett was one of the types tested in the Multi-Bypass Ratio System development project. Performance data for this application were taken from the project report [Ref. 6] and were used to develop the design shown below.

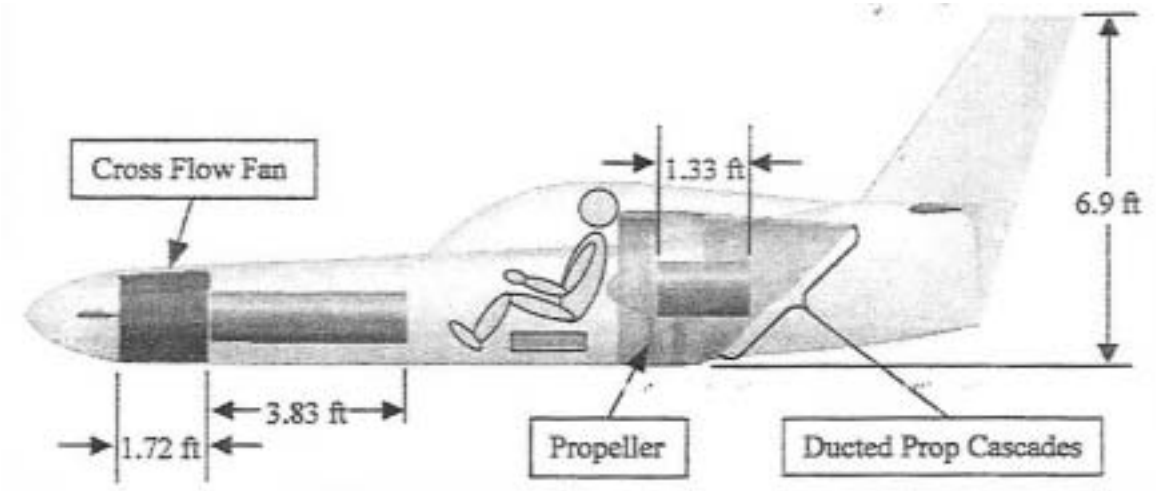

Figure 3. Gossett's Conceptual Civil Light VTOL Aircraft (From Ref. 8)

A most recent development of the crossflow fan in a lift and propulsion application was the prototypical Fanwing short takeoff and landing (STOL) aircraft. This design used an exposed, large-diameter, low revolutions-per-minute (~1,300 RPM), full-span crossflow fan to direct high-speed airflow across the upper surface of a thick wing section, thereby generating lift even at zero forward airspeed. There were no casewalls and no pressure cavities, since the primary purpose of the fan was to energize and redirect airflow over the wing providing both thrust and lift. The concept is illustrated below in Figure 4.

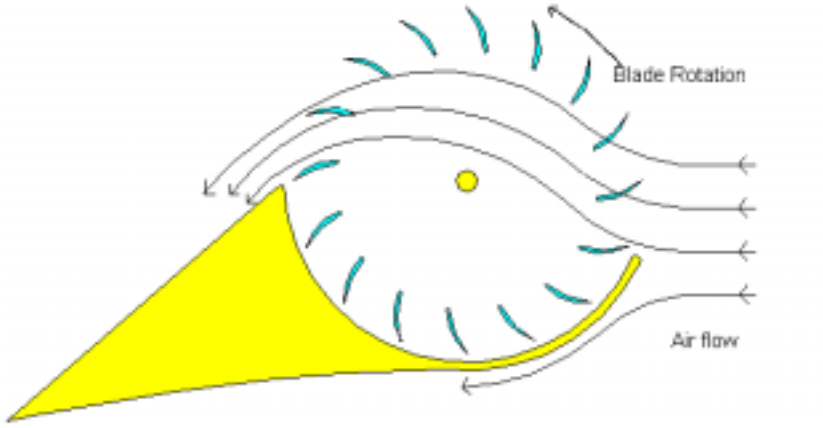

Figure 4. Fanwing Conceptual Diagram (From Ref. 9)

Advantages of this arrangement included: significantly increased lift as compared to a static wing section of similar dimension and shape; very short-takeoff capability; high maneuverability and stability due to relative insensitivity of the fan to the direction of incoming airflow; and lack of a true stall point due to continuous fan-driven airflow over the wing. Wing sections were tested in wind tunnels and small-scale models were successfully flight-tested, which demonstrated the strong potential of the Fanwing. The advantages of the Fanwing lend themselves to application to the light civil VTOL aircraft market. However, vertical takeoff has not yet been demonstrated, and the presence of a partially exposed crossflow fan rotor may render this aircraft hazardous. Further information on the Fanwing can be obtained from Ref. 9.

The research presented in this thesis therefore seeks to investigate the potential of enclosed crossflow fans as propulsion and lift devices in the personal air vehicle market.

Since relatively little research has been performed on the crossflow fan in aircraft propulsion applications, the VSD study stands as the most thorough reference on the topic. Therefore, a VSD-tested design was selected to form the basis for the CFTA used in this ongoing research, which was complemented by a significant computational fluid dynamics (CFD) analysis of the unsteady flow through the device. As reported in Ref. 6, VSD Fan #6 demonstrated the best power efficiency. This fan design was therefore selected as the base crossflow fan model. The general configuration of VSD Fan #6 is shown in Figure 5. Performance data for this configuration is shown in Figure 6.

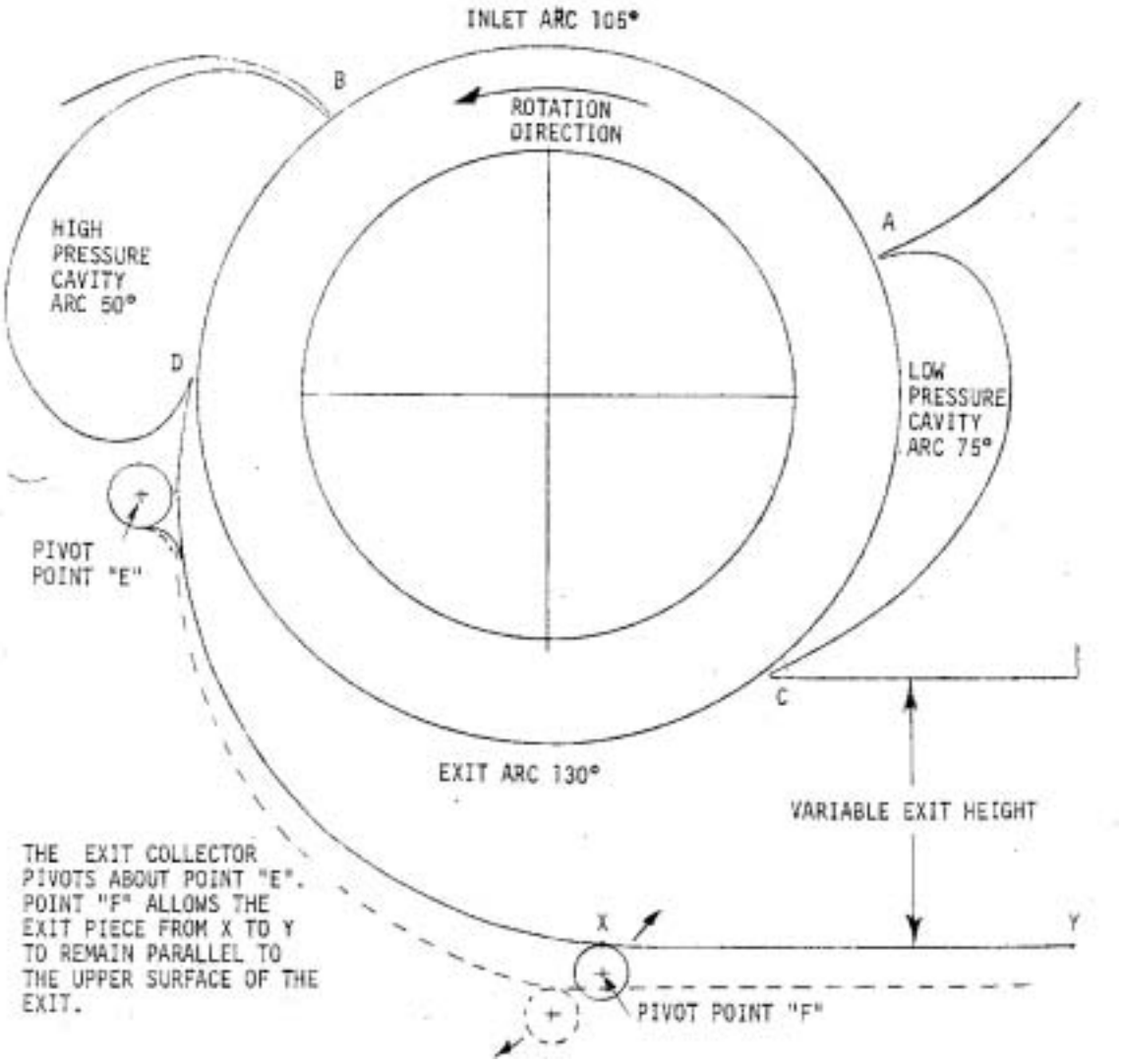

Figure 5. Vought Systems Division Fan #6 General Layout (From Ref. 6)

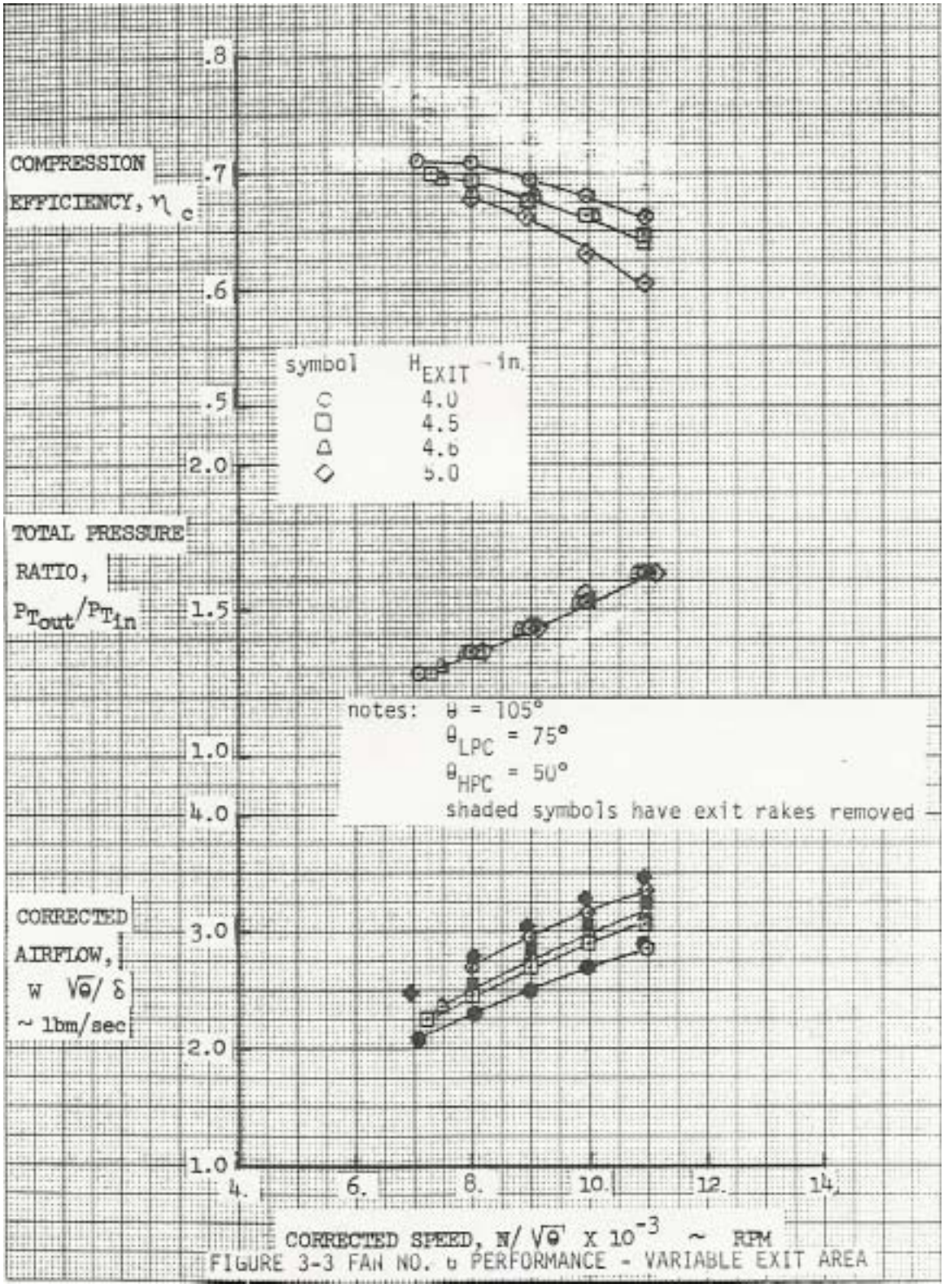

FIGURE 3-3 FAN NO. 6 PERFORMANCE - VARIABLE EXIT AREA

Figure 6. Vought Systems Division Fan #6 Performance Data (From Ref. 6)

II. EXPERIMENTAL APPARATUS

A. HARDWARE DESCRIPTION

1. Turbine Test Rig (TTR)

The previously-existing Turbine Test Rig (TTR) at the Naval Postgraduate School Turbopropulsion Lab was used as a power source for the Crossflow Fan Test Assembly (CFTA). The TTR was comprised of an air supply system and associated piping, test cell, data acquisition system, and the turbine from the Space Shuttle Main Engine High-Pressure Fuel Turbopump (SSME HPFTP).

A schematic of the air supply system is shown in Figure 7. The air supply system consisted of a 1,250-horsepower (HP) electric motor which drove an Allis-Chalmers 12-stage axial compressor at 12,000 RPM through a gearbox. The compressor was capable of providing 10,000 cubic feet per minute of air at a maximum pressure of 30 psig. The compressed air was cooled to approximately 560ºR in a water/air heat exchanger, relieved of moisture in a moisture trap, and measured for flow rate via an orifice plate prior to being supplied through piping to the test cell plenum chamber. A separate reciprocal compressor and reservoir provided shop air for various uses such as supplying the oil mister lubrication systems and calibration of pressure instrumentation.

Air from the test cell plenum chamber was fed into the turbine of the SSME HPFTP via flow straighteners and piping. The HPFTP assembly remained as reported in Ref. 4 with the exception of a longer aluminum splined drive shaft, which transferred power from the TTR to the CFTA. The existing bearing housing, associated bearing temperature and vibration monitoring systems, and the installed once-per-revolution measurement system remained unmodified. A schematic of the drive turbine is shown in Figure 8(a).

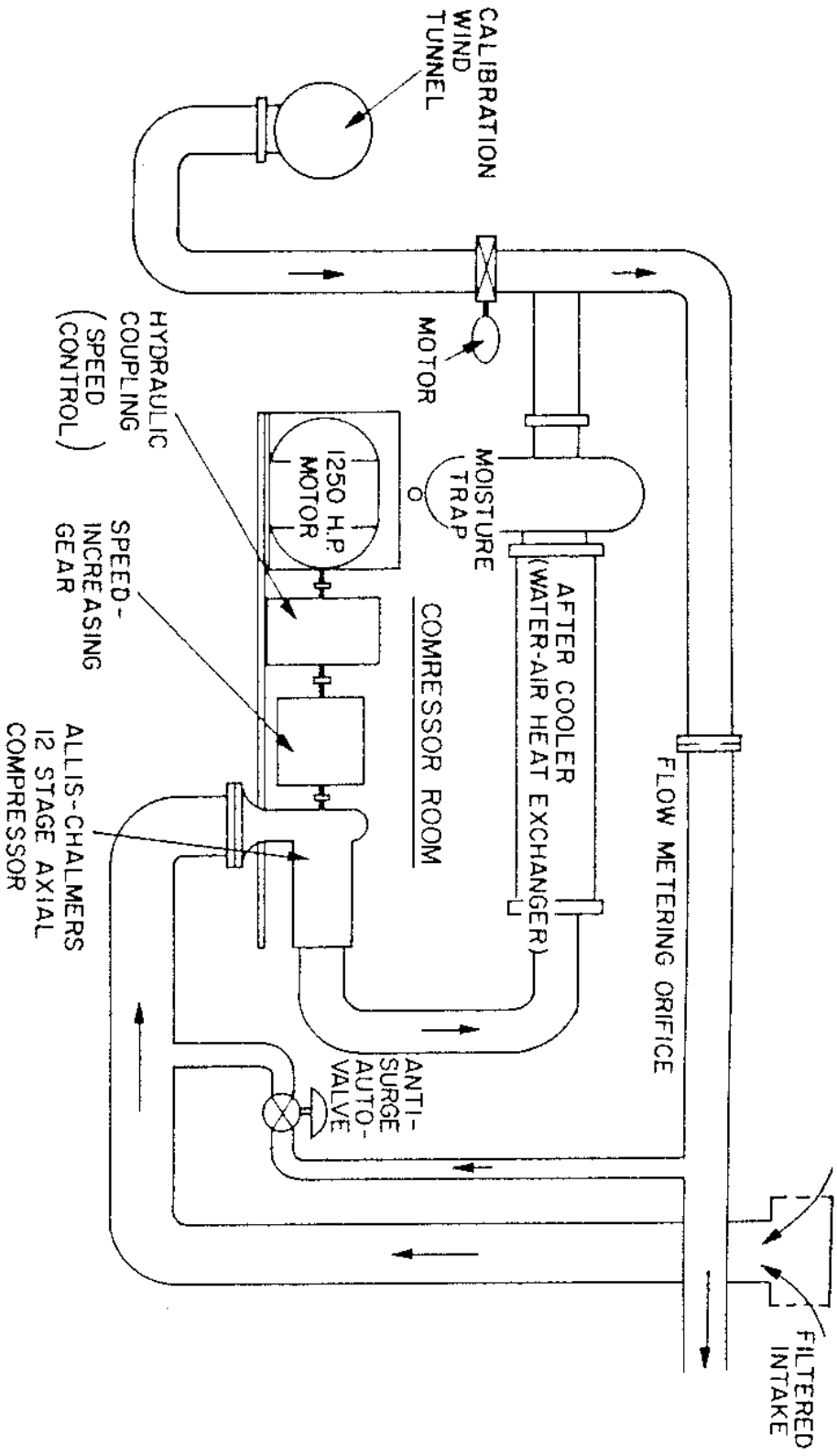

Figure 7. Schematic of Air Supply System

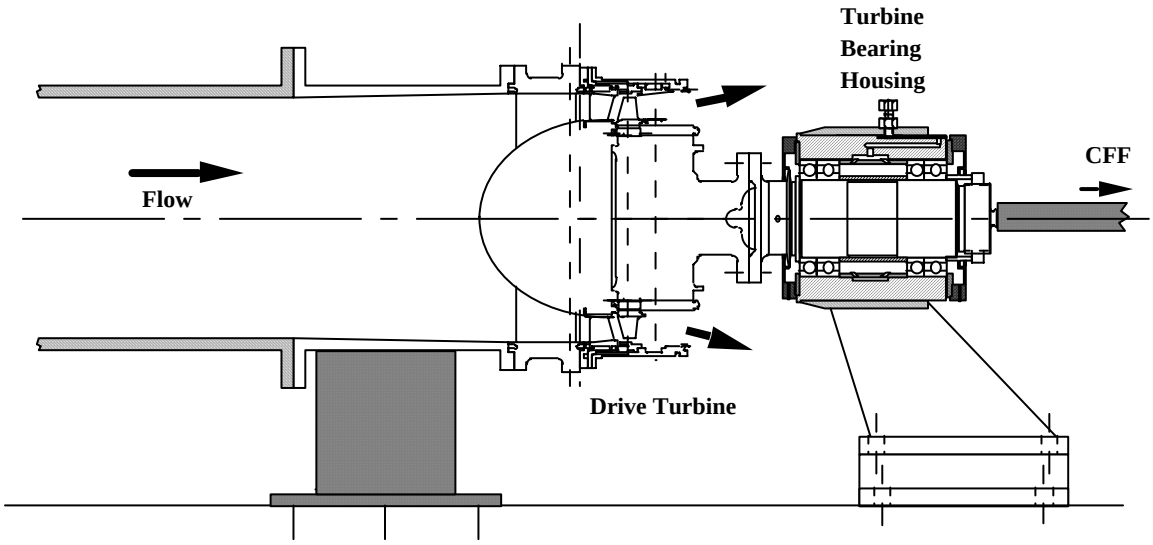

(a)

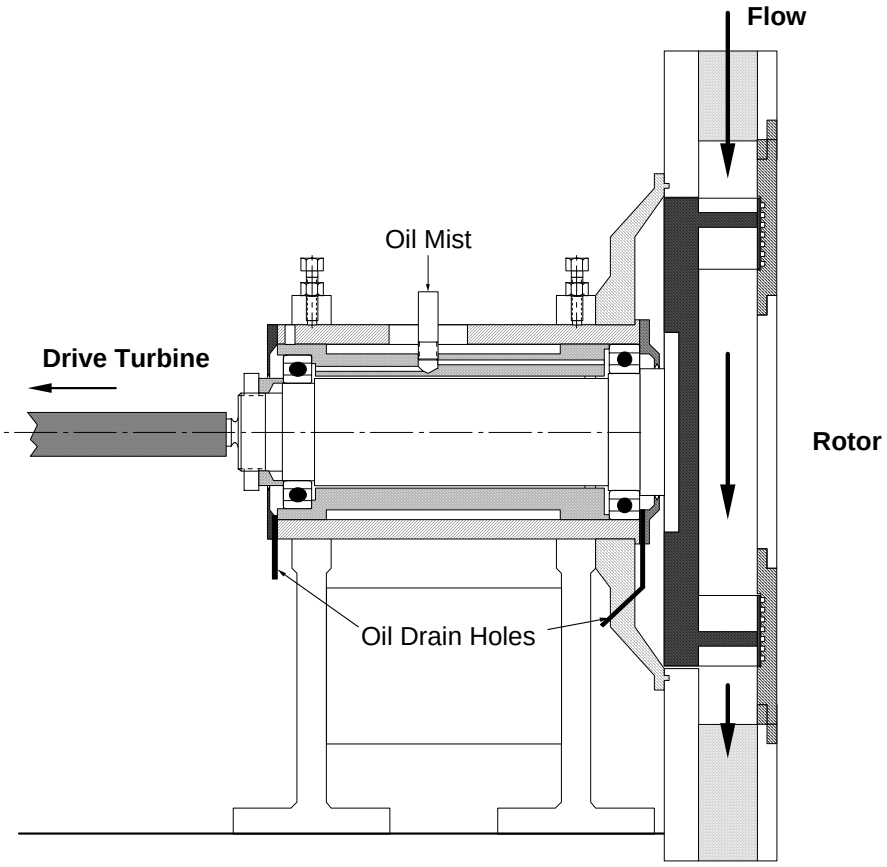

(b)

Figure 8. Schematic of Turbine Test Rig (a) and Crossflow Fan Test Assembly (b)

2. Crossflow Fan Test Assembly (CFTA)

A schematic of the Crossflow Fan Test Assembly is shown in Figure 8(b). The CFTA was based on VSD Multi-Bypass Ratio System test assembly #6. The assembly consisted of a 12-inch diameter, 1.5-inch span, 30-bladed crossflow fan rotor; two intake/cavity components; an exhaust duct wall; a drive shaft, arbor, and associated bearing housing. The front face plate had identically-dimensioned aluminum and Plexiglas inserts, the latter to be used as a viewing window for flow visualization. The primary construction material was 7065-T6 aluminum, although the bearing housing was constructed of SAE 4130 cold-rolled steel with a hot-rolled bearing spacer, and the drive shaft was of SAE 4340-300M cold-rolled annealed steel.

The fan rotor was assembled from machined disc, 30 identical rotor blade sections, and a front retaining ring. Each blade was pinned in place using dowels and secured with Hysol epoxy E-120HP. Prior to assembly, the blades were weighed and arranged in ascending order according to weight in order to to minimize subsequent rotor balance efforts. The rotor disc was designed to be recessed into the back plate, seating flush with the back wall of the assembly. A labyrinth seal on the tip of the rotor disc was used to minimize mass flow between the rotor and test assembly back plate cavity. Figure 9 depicts the fan in a partially assembled state.

The rotor disc was secured to the drive shaft with machined screws. Fafnir bearings were fitted between the drive shaft and the bearing housing, separated by a bearing spacer. Oil misters pressurized by 40 psia shop air lubricated the bearings at a rate of approximately one drop of oil per minute. Provision was made for vibration monitoring on the CFTA bearing set; however, no bearing temperatures were recorded.

The test assembly front plate provided for the replacement of the aluminum blanking plate with a Plexiglas viewing window. Both the blanking plate and the viewing window contained inner blanks that could be rotated to provide for alternate positioning of pressure/temperature probes and/or dye injectors. A labyrinth seal was utilized between the rotor retaining ring and the blanking plate/viewing window to

minimize leakage in the radial direction. The intake/cavity components and exhaust duct wall were secured in place between the CFTA front and back plates using machine bolts. This arrangement will allow for relatively ease of replacement of the intake, exhaust, and cavities without the need for a complete redesign and remanufacture of the CFTA.

The test cell itself was equipped with a test stand to which all components of the SSME HPFTP and CFTA were secured. The steel surface of the stand allowed precise location and alignment of the bearing housings and CFTA. All components were bolted to the test stand using machine bolts. The CFTA could be monitored from the control station through a ballistic-tolerant glass window. Additional monitoring capability was provided by a TV monitor connected to a remote video camera, which recorded the view through the Plexiglas viewing window of the CFTA. Figure 10 is a view of the partially assembled CFTA.

Figure 9. Partially Assembled Fan

Figure 10. Partially Assembled Crossflow Fan Test Assembly

B. OPERATING CONTROLS AND INSTRUMENTATION

1. Control Station

The TTR and CFTA were manually operated from the control station. The remotely-operated butterfly valves referred to in the air supply system description were controlled electrically from the operator's console, shown in Figure 11.

Two thermocouples measured the TTR bearing temperatures. Both temperatures were displayed on the operator's console for continuous monitoring of bearing performance. One accelerometer monitored the TTR vibrations and another monitored vibration levels in the CFTA. This information was recorded in a logbook during test runs.

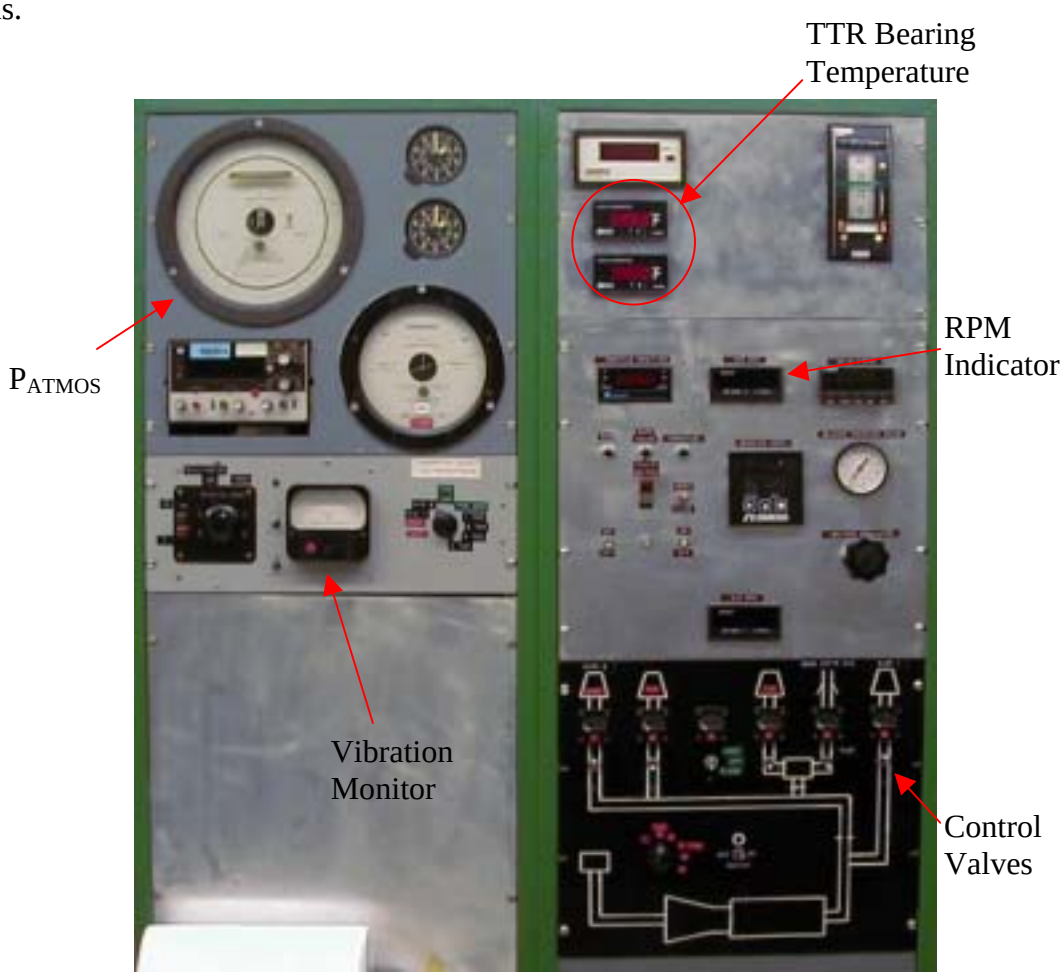

Figure 11. Control Station Operator's Console

2. Instrumentation

Instrumentation for data collection consisted of five United Sensor Devices model USD-C-161 1/8-inch combination thermocouple/pressure probes (hereafter referred to as "combo probes"), 12 static pressure taps, and the TTR total pressure, total temperature, and once-per-revolution (OPR) measurement systems as described by Southward [Ref. 4]. Additional equipment included the previously mentioned video camera and various digital still cameras for recording flow visualization results.

Two combo probes were installed at roughly the 10 o'clock and 2 o'clock (viewed from front) positions in the test assembly intake section, aligned with the anticipated flow direction, as shown in Figure 12 as T1 and T2. Three combo probes (T3, T4, and T5 in Figure 12) were installed in the exhaust duct section in a configuration intended to detect pressure or temperature profiles along the centerline of the exhaust duct. The combo probes were mounted through the front plate to such a depth that the pitot opening of each probe was at the midpoint axially between the front and back plate.

The 12 1/32-inch diameter static pressure taps (P_A through P_L in Figure 12) were drilled as closely as possible to the normal of the intake, cavity, or exhaust duct walls. Associated tubing was routed so as to remain free of the airflow, with the exception of the upper High Pressure Cavity tap (P_G) which was routed along the intake sidewall to minimize interference with fan inflow.

All pressure taps were drilled at the midpoint of their respective assembly component as measured in the axial direction. Instrument nomenclature is provided in Table 1.

Probe/Tap	Type	Nomenclature
T1	Combo	P_{in} CFF / T_{in} CFF (10 o'clock)
T2	Combo	P_{in} CFF / T_{in} CFF (2 o'clock)
T3	Combo	P_{out} CFF / T_{out} CFF (Top)
T4	Combo	P_{out} CFF / T_{out} CFF (Mid)
T5	Combo	P_{out} CFF / T_{out} CFF (Bot)
A	Static	P_A
B	Static	P_B
C	Static	P_C
D	Static	P_D
E	Static	P_E
F	Static	P_F
G	Static	P_G
H	Static	P_H
I	Static	P_I
J	Static	P_J
K	Static	P_K
L	Static	P_L

Table 1. Combo Probe / Pressure Tap Nomenclature

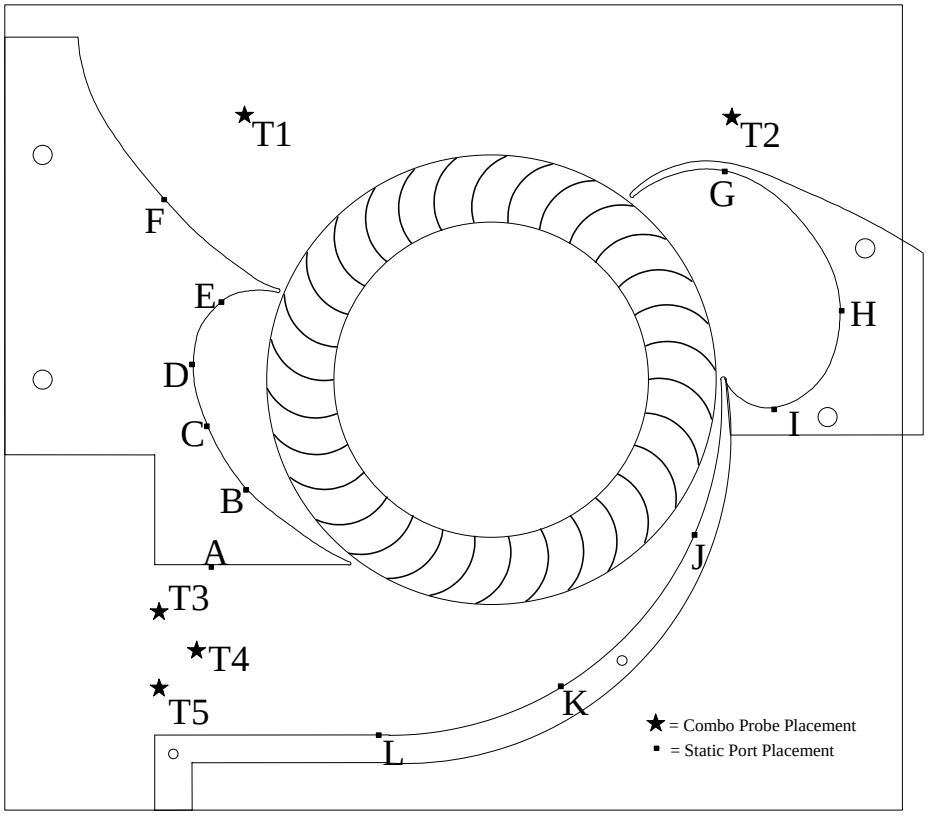

Figure 12. Combo Probe and Pressure Tap Placement

C. FLOW VISUALIZATION

Flow patterns in the areas viewable through the Plexiglas viewing window were visualized using dye injection methods. The viewing window contained a movable inner blank with an instrumentation port meant for future use. Figure 13 shows the arrangement of the dye injection ports. One dye injection port was drilled through the center of the plug which sealed the instrumentation port at exactly two inches radius from the center of the fan. For the final data run, two more holes were drilled through the inner blank on either side of the instrumentation port for expanded flow visualization capability

Dye injectors consisted of large-bore syringes and/or squeeze bottles connected to the injection ports via surgical tubing. These injectors were manually operated from the test cell. A mixture of distilled water and commercially available food coloring served as the dye. The same video recorder used to monitor the fan from the control station was used to record the flow visualization results. Several digital cameras were also available to record still pictures of the results.

Figure 13. Dye Injection Ports on Inner Blank

D. DATA ACQUISITION SYSTEM

1. Hardware

The data acquisition system remained essentially unchanged from that described in Ref. 10. A schematic of the system is shown in Figure 14.

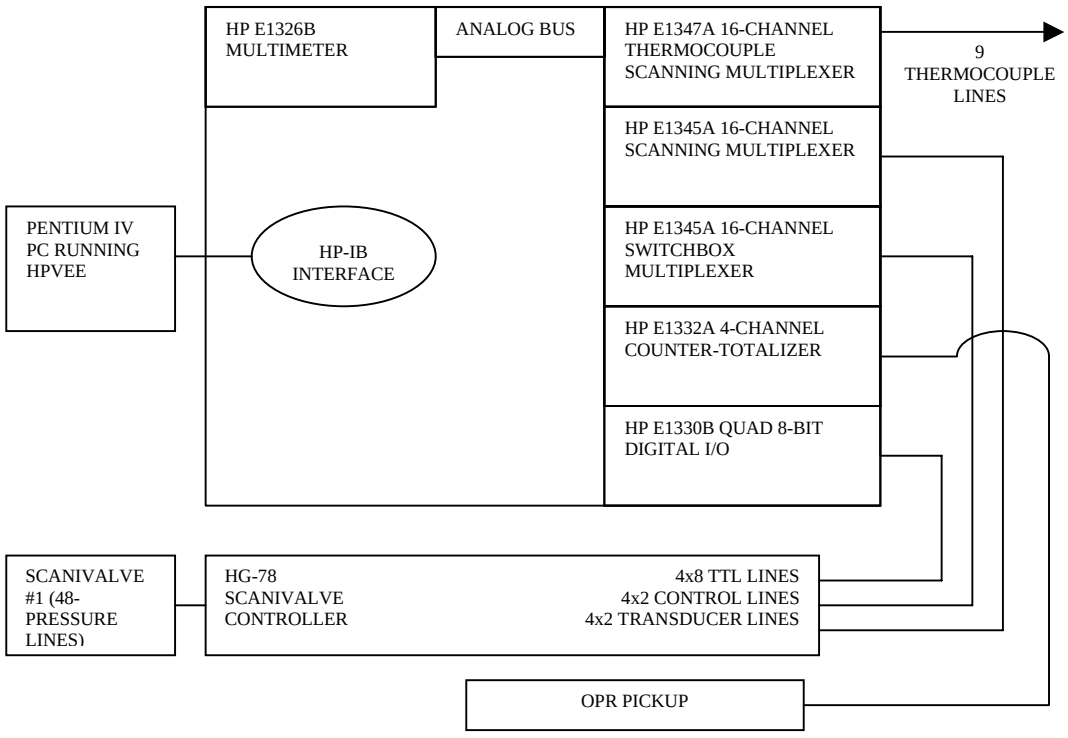

Figure 14. Data Acquisition System Hardware (After Ref. 10)

Major changes included the addition of four thermocouple lines and the deletion of the dynamometer load cell strain gauge signal lines used in Ref. 3. Thermocouple and pressure lines were reassigned as necessary. Control of the thermocouple multiplexer, Scanivalve 48-port transducer, and counter / totalizer was accomplished as outlined in Ref. 10.

Table 2 lists the Scanivalve port assignments for the pressure lines. Table 3 lists thermocouple multiplexer channel assignments for thermocouple lines

Port #	Type	Nomenclature
1	Static	P_{ATMOS}
2	Static	P_{CAL}
3	Total	P_{in}TTR (5 o'clock)
4	Total	P_{out}TTR
5	Total	P_{in}TTR (8 o'clock)
6	Total	P_{in}CFF (2 o'clock)
7	Total	P_{in}CFF (10 o'clock)
8	Total	P_{out}CFF (Top)
9	Total	P_{out}CFF (Mid)
10	Total	P_{out}CFF (Bot)
11	Static	P_A
12	Static	P_B
13	Static	P_C
14	Static	P_D
15	Static	P_E
16	Static	P_F
17	Static	P_G
18	Static	P_H
19	Static	P_I
20	Static	P_J
21	Static	P_K
22	Static	P_L
32	Static	P_{in}
33	Static	P_{in}(Flange)
34	Static	P_{out}(Flange)
35	Static	P_{out}(Vena)

Table 2. Scanivalve Port Assignments

Multiplexer Channel	Nomenclature
6	T_{in}CFF (2 o'clock)
8	T_{in}CFF (10 o'clock)
9	T_{in}TTR (8 o'clock)
10	T_{in}TTR (5 o'clock)
11	T_{out}TTR
12	T_{in}Orifice
13	T_{out}CFF (Bot)
14	T_{out}CFF (Mid)
15	T_{out}CFF (Top)

Table 3. Thermocouple Scanning Multiplexer Channel Assignments

2. Software

Elements of the data acquisition and instrumentation control program [Ref. 10] were incorporated into the HPVEE-based program used in this research. Appropriate changes were made to Scanivalve ports and thermocouple multiplexer channels. A routine was created to write raw and reduced data to a single tab-delimited file as opposed to the previous scheme's multiple output files. The new export file was designed to be imported into Microsoft Excel for further data manipulation, with a minimum of effort. Finally, the user control panel was redesigned to provide immediate display of both raw and reduced data upon cycling through all the instruments. Figure 15 shows the user control panel. Further HPVEE schematics for this data acquisition program can be found in Appendix A.

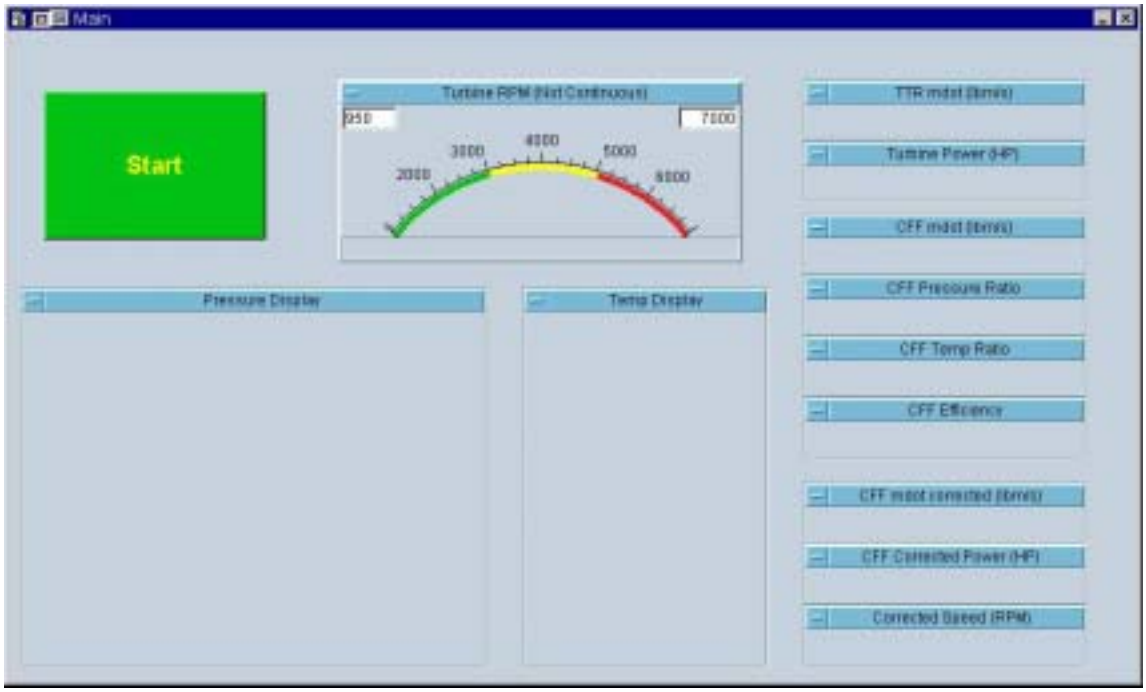

Figure 15. Data Acquisition System User Control Panel

E. OPERATIONAL PROCEDURES AND TEST PROGRAM

1. Procedures

The Allis-Chalmers compressor was started by a technician and brought up to speed slowly, normally over a period of one to two hours. Flow control was achieved using two remotely-operated butterfly-type valves. One valve was located upstream of the orifice plate and was used to control mass flow to the SSME HPFTP, thereby controlling power output to the CFTA and thus RPM. The other valve was located downstream of the orifice plate and was used as an atmospheric dump. It was necessary to close this valve completely in order to obtain reliable mass flow measurements for power calculations. After the compressor startup period, the crossflow fan was started by opening the test cell butterfly valve slowly while simultaneously closing the dump valve downstream of the TTR. With the TTR valve open approximately 20% and the first dump valve fully closed, the CFTA attained about 2,000 RPM. At this condition mass flow rate measurements through the TTR were accurate. Orifice plate mass flow rate measurements were performed in accordance with Vavra's technical note describing the method [Ref. 11].

A typical test began once speed reached 2,000 RPM. After allowing approximately one minute for the system to stabilize, the HPVEE program was activated. This initiated the Scanivalve pressure port scanning cycle, the thermocouple multiplexer, and a routine which calculated the average fan speed over the pressure scanning cycle. Once the cycle was complete, raw data were automatically reduced and recorded as a new line on a text file. A combination of raw and reduced data was then displayed on the user control panel.

Once data had been recorded at a particular RPM, speed was increased in 500- or 1,000-RPM increments by manipulating the dump valve and the turbine inlet valve. Typically, 500-RPM increments were used when increasing speed above 3,000 RPM, and 1,000-RPM increments were used when decreasing speed. The CFTA was tested up to a

maximum of 7,022 RPM during the course of this research. Flow visualization was performed at 5,000 RPM after data had been recorded.

Once all desired measurements and flow visualizations were made, shutdown was accomplished by opening both the valves and closing the TTR valve. The CFTA typically came to a full stop within 30 seconds.

2. Test Program

Table 4 summarizes the program of data-collection runs. The CFTA was run on seven separate dates. The first two were uninstrumented runs for the purpose of verifying bearing temperature and vibration levels as well as crossflow fan integrity. The third run was an instrumented run for the purpose of debugging and refining the data acquisition system. The fourth through seventh runs produced the data reported here. The final two dates involved multiple startup/shutdown procedures in order to make configuration changes.

Date	Start Time	Stop Time	Maximum RPM Reached	Number of Measurement Sets	Flow Visualization Performed
29 Jan 03	1000	1138	5503	9	
7 Feb 03	1005	1130	6517	18	
19 Feb 03	1040	1127	5015	9	✓
	1136	1200	5036	7	✓
	1211	1228	5006	6	✓
12 Mar 03	1023	1058	5020	4	✓
	1130	1209	7022	12	

Table 4 Summary of Test Program

F. DATA REDUCTION

Primary data reduction was performed in the HPVEE data acquisition program. Additional data reduction was performed using Microsoft Excel spreadsheets.

As previously stated, mass flow through the TTR was calculated in accordance with Ref. 11. Work produced by the TTR was then given by

$$W_{TTR} = \dot{m}_{TTR} C_p (T_{out,TTR} - T_{in,TTR(avg)}) \tag{1}$$

where W_{TTR} was in Btu/s, $\dot{m}_{TTR}$ was in lbm/s, C_p = 0.24 Btu/lbm-°R, and $T_{in,TTR(avg)}$ was the average of the two TTR inlet total temperatures. Mechanical efficiency of the bearing and shaft systems was not estimated and it was therefore assumed that W_{TTR} = -W_{CFF}, where W_{CFF} was the work input to the crossflow fan. Mass flow through the crossflow fan was calculated as follows:

$$\dot{m}_{CFF} = \frac{W_{CFF}}{C_p (T_{out,CFF(avg)} - T_{in,CFF(avg)})} \tag{2}$$

where $T_{out,CFF,(avg)}$ was the average of the three crossflow fan exhaust duct total temperatures and $T_{in\ CFF(avg)}$ was the average of the two crossflow fan inlet total temperatures. Total-to-total pressure and temperature ratios were similarly calculated using pressure averages, such that:

$$\pi_{CFF} = \frac{P_{out,CFF(avg)}}{P_{in,CFF(avg)}} \qquad \text{and} \qquad \tau_{CFF} = \frac{T_{out,CFF(avg)}}{T_{in,CFF(avg)}} \tag{3}$$

Compression efficiency through the crossflow fan was calculated from the values found in (3) above, in the following manner:

$$\eta_{CFF} = \frac{\pi_{CFF}^{\left(\frac{\gamma-1}{\gamma}\right)} - 1}{\tau_{CFF} - 1} \tag{4}$$

with γ=1.4. Crossflow fan performance values were corrected to standard atmospheric conditions, such that

$$\dot{m}_{corr} = \dot{m}\frac{\sqrt{\theta}}{\delta}\ , \qquad N_{corr} = \frac{N}{\sqrt{\theta}}, \qquad HP_{corr} = \frac{HP}{\delta\sqrt{\theta}} \tag{5}$$

where N is fan speed in RPM, $\theta = \frac{T_{in,CFF(avg)}}{T_{ref}}$, and $\delta = \frac{P_{in,CFF(avg)}}{P_{ref}}$. T_{ref} and P_{ref} were standard atmospheric temperature (518.7 °R) and pressure (29.92 inHg), respectively.

Microsoft Excel was used to produce plots of the results and to perform further data reduction, which became necessary as a result of error in the TTR mass flow and temperature measurements. Mass flow through the crossflow fan was calculated independently of the work produced by the TTR, by separating the exhaust duct area into three zones, in each of which the flow was assumed to be uniform. Each zone was roughly centered around one of the three exhaust duct combo probes, with zone 1 surrounding the top probe, zone 2 around the middle probe, and zone 3 around the bottom probe. Mass flow in each zone was calculated as a function of total pressure and temperature measurements from that zone's probe in accordance with Ref. 12:

$$\dot{m}_i = X_i(1 - X_i^2)^{\frac{1}{\gamma-1}} \frac{P_{t_i}(70.929)}{RT_{t_i}} \sqrt{2C_p g_c T_{t_i}} A_i \tag{6}$$

where $\dot{m}_i$ is the mass flow through zone i, P_{t_i} and T_{t_i} are the total pressure and temperature measured at the top probe, and A_i is the area of zone i. A conversion factor of 70.929 lbf/ft^2-inHg was applied to maintain unit consistency. X_i is called the dimensionless velocity in zone i and is defined as follows:

$$X_i = \frac{V_i}{V_{t_i}}$$

where V_t is the "total velocity" obtained from the definition of total enthalpy ,

$$h_t = h + \frac{V^2}{2g_c} \qquad \text{or} \qquad C_p T_t = C_p T + \frac{V^2}{2g_c},$$

as T→0 giving $V_{t_i} = \sqrt{2C_p g_c T_{t_i}}$. In this case V_i is unknown, but it can be shown that

$$\frac{P_i}{P_{t_i}} = (1 - X_i^2)^{\frac{\gamma}{\gamma-1}} \tag{7}$$

with $P_i = P_A$, the static pressure in the exhaust duct. Solving this expression for X_i gives the remaining term needed to find the mass flow in zone i.

Mass flow through the three zones was calculated using the following values:

$A_1 = A_3 = 0.018229155$ ft^2

$A_2 = 0.01041666$ ft^2

$R = 53.3$ lbf-ft/lbm-°R

$C_p = 186.72$ lbf-ft/lbm-°R

It was then a simple task to calculate the total mass flow through the exhaust duct by summing the three zonal mass flows as shown in Eq. 7:

$$\dot{m}_{tot} = \dot{m}_1 + \dot{m}_2 + \dot{m}_3 = \sum_{i=1}^{3} \dot{m}_i \tag{8}$$

Mass flow-averaged total pressures and temperatures in the exhaust duct were then calculated using

$$\overline{T_t} = \frac{\dot{m}_1 T_{t_1} + \dot{m}_2 T_{t_2} + \dot{m}_3 T_{t_3}}{\sum_3 \dot{m}} \text{ and } \overline{P_t} = \frac{\dot{m}_1 P_{t_1} + \dot{m}_2 P_{t_2} + \dot{m}_3 P_{t_3}}{\sum_3 \dot{m}} \quad (9)$$

Work used by the crossflow fan was calculated using:

$$W_{CFF} = \dot{m}_{tot} C_p (\overline{T_t} - T_{in,CFF(avg)}) \quad (10)$$

Parameters subsequently derived from these TTR-independent quantities are hereafter referred to as “computed” parameters.

Exit Mach number was calculated using

$$M_{exit} = \sqrt{\frac{2}{\gamma - 1}\left(\left(\frac{\overline{P_t}}{P_A}\right)^{\frac{\gamma-1}{\gamma}} - 1\right)} \quad (11)$$

Exit static temperature was calculated using

$$T_{exit} = \frac{\overline{T_t}}{1 + \frac{\gamma - 1}{2} M_{exit}^2} \quad (12)$$

Exit velocity was calculated using

$$u_{exit} = M_{exit}\left(\sqrt{\gamma g_c R T_{exit}}\right) \quad (13)$$

Finally, corrected thrust was calculated using

$$F_{corr} = \frac{\dot{m}_{tot}}{g_c \delta}\left(u_{exit} - u_0\right) \quad (14)$$

with $u_0 = 0$.

G. RESULTS AND DISCUSSION

1. Introduction

The reduced data available from the HPVEE data acquisition program were exported to a Microsoft Excel spreadsheet for post-processing. Performance data plotted included total-to-total pressure ratio versus corrected mass flow (Figure 16, showing an "open throttle" operating line), total-to-total pressure ratio versus corrected speed (Figure 17), corrected mass flow versus corrected speed (Figure 18), corrected power versus corrected speed (Figure 19), and efficiency versus corrected speed (Figure 20). For comparison to the VSD study performance information, exit velocities (Figure 21) were calculated in English engineering units but were also presented in SI units for later comparison with CFD results. The exit velocities were used to calculate thrust. These values were calculated for the present fan and scaled linearly to predict a 12-inch span fan for comparison with published results (Figures 22 and 23).

Initially the mass flow rate through the crossflow fan was deduced from equation (2); however, the data obtained were not consistent. In some cases, different mass flow rates were calculated at the same fan speed. An example of this is the 7 Feb Run #1 (Not Computed) series shown in Figure 18. Analysis of reduced and raw data led to the belief that either the TTR total temperature measurements or the orifice plate mass flow contained some error. The temperature measurements were the most suspect due to the fact that there was only a single combo probe on the outlet side of the TTR. This arrangement did not allow an average temperature at the outlet to be recorded. Therefore, the mass flow rate was calculated as in equations (6) through (8).

The result of the additional data reduction was that a “computed” crossflow fan mass flow rate and power were obtained without reliance on measurements from the TTR. The total temperature and total pressure at the exit to the crossflow fan were also mass flow-averaged, as described in equation (9) The resulting performance plots showed a marked improvement in consistency.

2. Performance Plots

All performance plots were made using computed values described above, corrected for standard conditions as described in the Data Reduction section. Data from all runs were plotted as separate series on the same plot for each type of plot. Trendlines were used to demonstrate the consistent nature of the data

Figure 16 is a fan operating line, or crossflow fan pressure ratio versus corrected mass flow rate. Despite the wide range of test dates, the data showed excellent consistency and smoothness. Since an operating line plot from the VSD fan #6 was not available, no direct comparison could be made. A second-order trendline was used.

Figure 17 is a plot of total-to-total pressure ratio versus corrected speed. Again, the data showed excellent consistency and smoothness. The data compared favorably to the VSD fan #6 performance information available in Figure 6. This fan demonstrated a pressure ratio of 1.33 at approximately 7,000 RPM, as compared to the VSD fan's 1.28 measured at approximately 7,300 RPM. A second-order trendline was used.

Figure 18 is a plot of corrected mass flow rate versus corrected speed. The data showed the same degree of consistency and smoothness found in the plots described above. Mass flow compared favorably with the VSD study, with this fan achieving a mass flow rate of 2.5 lbm/s at approximately 7,000 RPM vice the VSD fan's 2.25 lbm/s at 7,300 RPM. A linear trendline was used.

Figure 19 is a plot of corrected mass-averaged computed power versus corrected speed. Data consistency and smoothness was of the same degree as the previous plots. Power consumption peaked at approximately 59 HP at approximately 7,000 RPM. No comparison to the VSD fan #6 was made since this information was not presented for a 1.5-inch span fan in the VSD study. A third-order trendline was used.

Figure 20 is a plot of crossflow fan efficiency versus corrected speed. The data in this plot were not as consistent for a given speed. Since efficiency was calculated as a function of the fan total-to-total pressure and temperature ratios, there was no dependence on TTR mass flow or temperature measurements and these can be discounted as factors. It is likely that the variance shown was the result of the sensitivity of the efficiency

calculation to slight changes in the crossflow fan total-to-total pressure or temperature ratios. A third-order trendline was used.

Efficiency did not compare as favorably with the VSD fan #6 information. Figure 6 shows a peak efficiency for the VSD fan of 0.7 at 7,300 RPM, while Figure 20 shows a peak efficiency of approximately 0.65 at ~4,000 RPM. A trendline plotted for the 12 March Run #2, which reached the highest RPM tested, indicated a distinct downward trend above 5,000 RPM and showed an efficiency of approximately .625 at ~7,000 RPM. The reason for the discrepancy between VSD fan #6 and the test assembly efficiency is unknown. It may be traceable to a difference in the methods used to take pressure and temperature measurements. The manner in which these measurements were taken in the VSD study is not specified in Ref. 6. Use of mass-averaged total-to-total pressure and temperature ratios in the expression for efficiency was investigated, but resulted only in negligible change to the plot.

Figure 21 is a plot of exit velocity versus corrected speed. Peak exit velocity was recorded at 718.2 ft/s (218.9 m/s) at 6,990 corrected RPM This information was not available for the VSD fan. Exit velocity was also reported in meters per second for later comparison to figures derived from the numerical simulation. A linear trendline was used.

Figure 22 is a plot of corrected thrust per foot of span versus corrected speed. For this plot, corrected thrust was scaled by a factor of eight. This was done to facilitate comparison to the VSD fan, for which this information was available only for the 12-inch span fan. A maximum thrust per foot of span of 447 lbf was achieved at 6,990 corrected RPM. A second-order trendline was used.

Figure 23 is a plot of corrected thrust per foot of span versus corrected power per foot of span. Both axes of this plot were scaled by a factor of eight for comparison to the VSD fan. Per foot of span, maximum corrected thrust was recorded at 447 lbf, while drawing 473 HP. A second-order trendline was used.

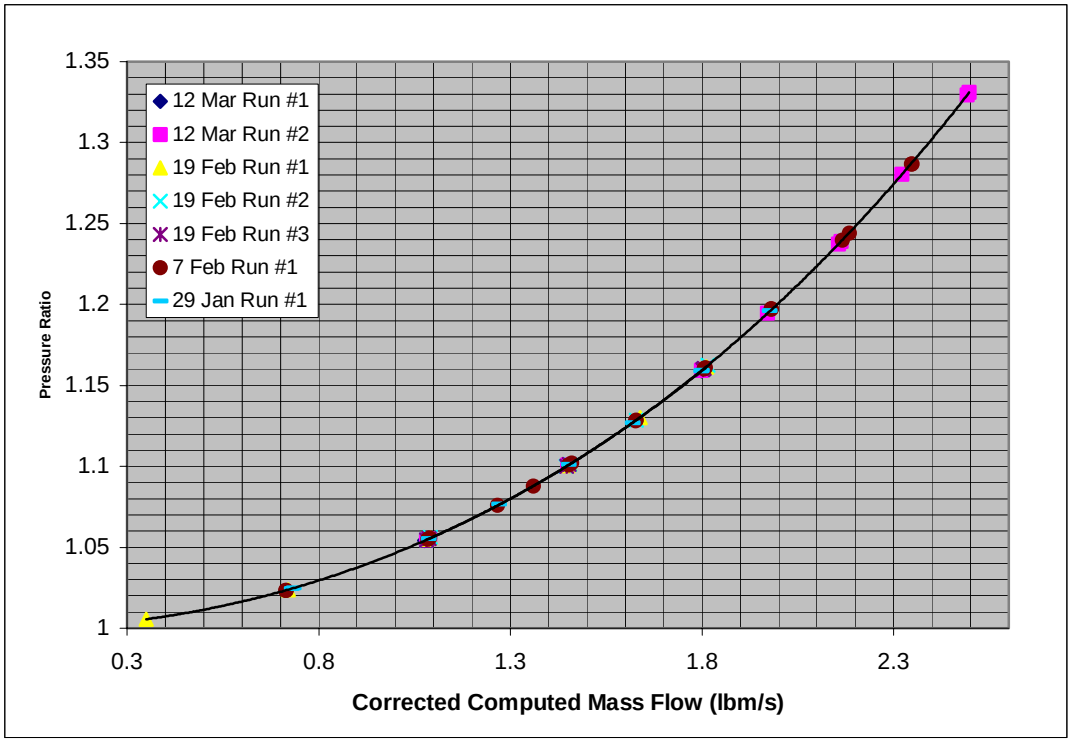

Figure 16. Operating Line

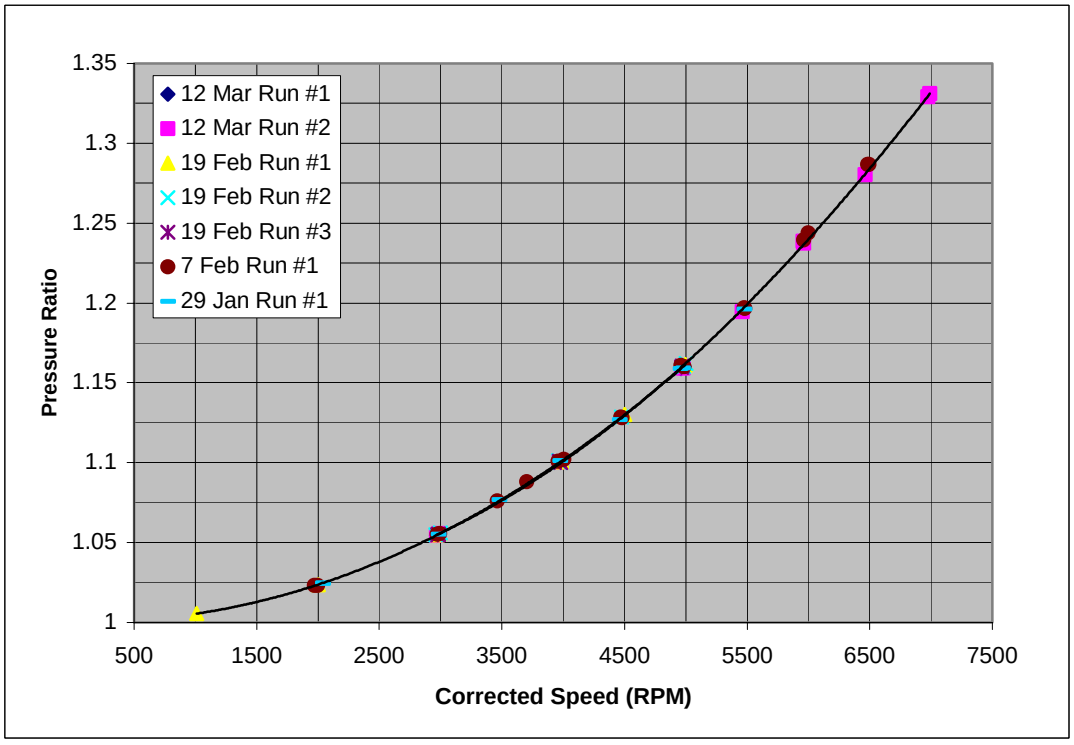

Figure 17. Pressure Ratio vs. Corrected Speed

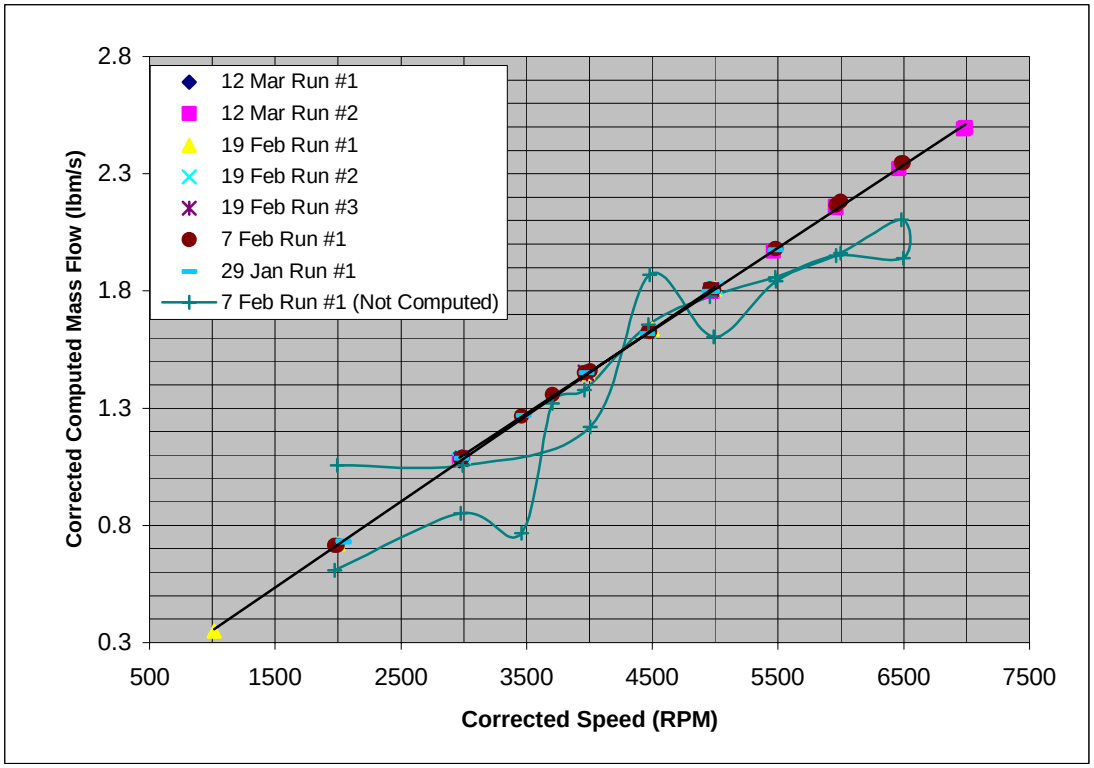

Figure 18. Corrected Computed Mass Flow vs. Corrected Speed

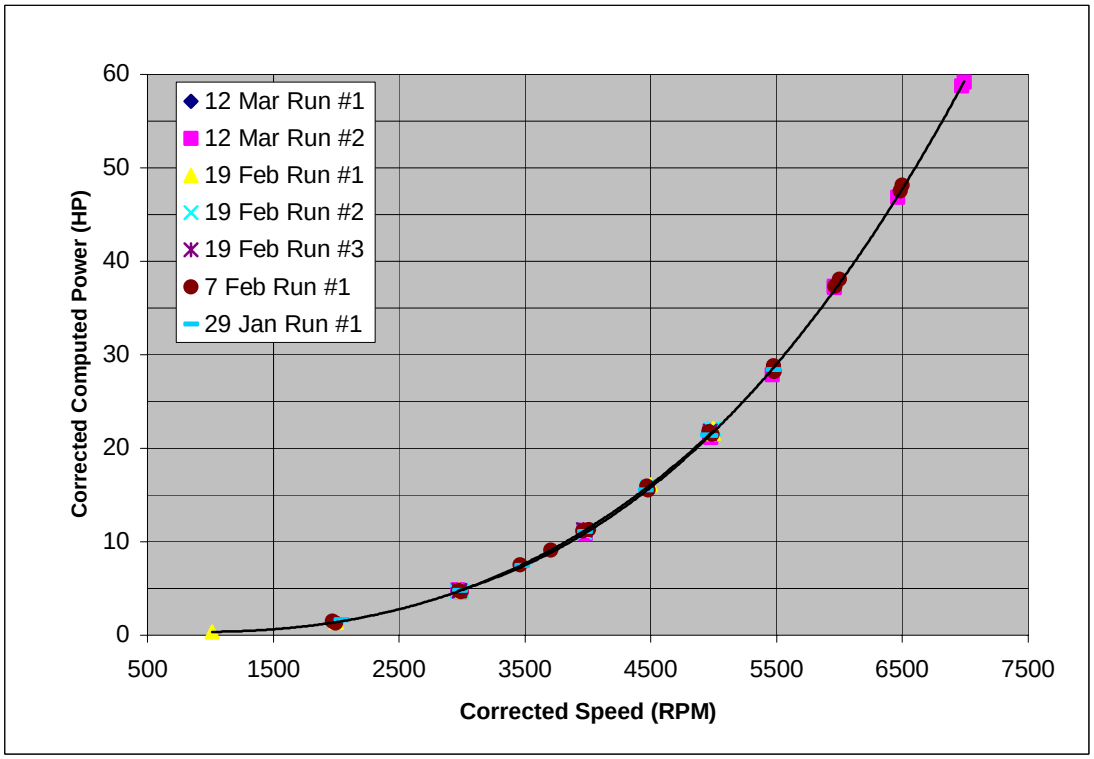

Figure 19. Corrected Computed Power vs. Corrected Speed

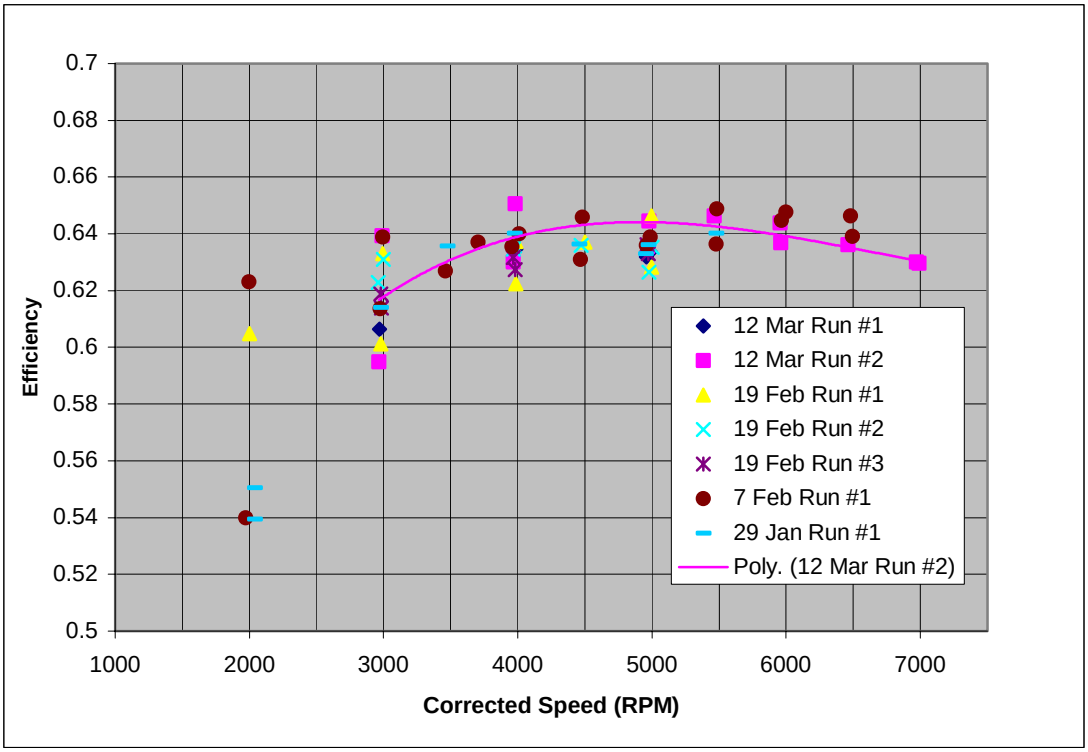

Figure 20. Compression Efficiency vs. Corrected Speed

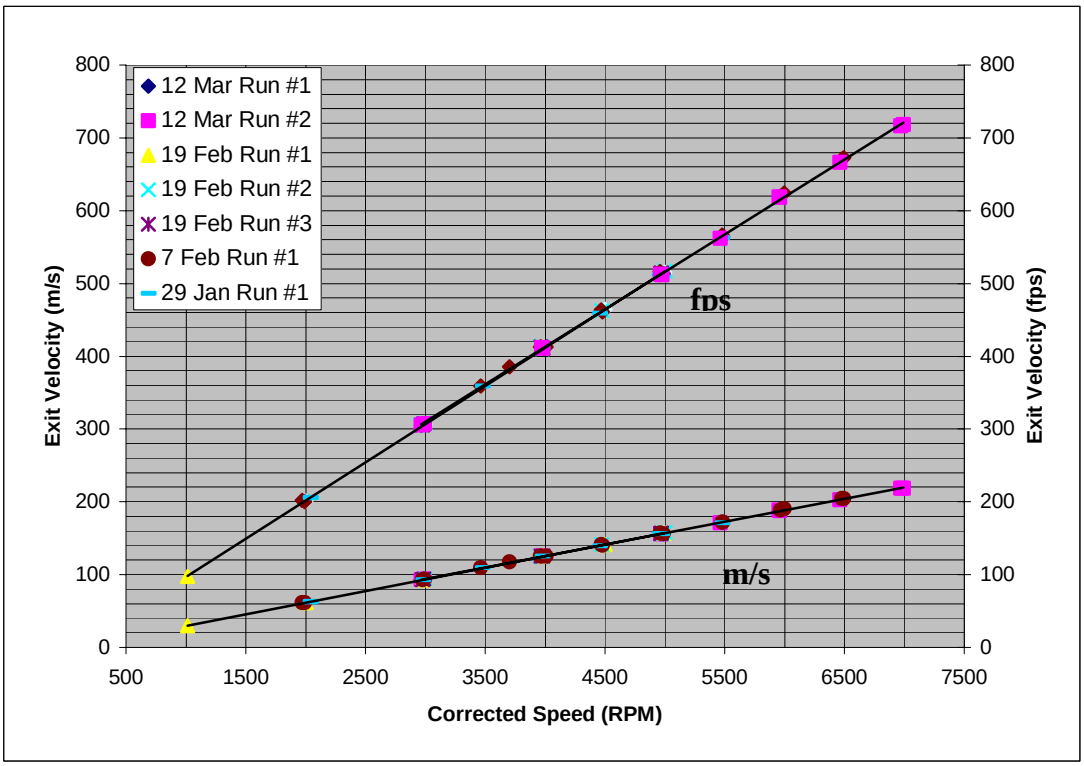

Figure 21. Exit Velocity vs. Corrected Speed

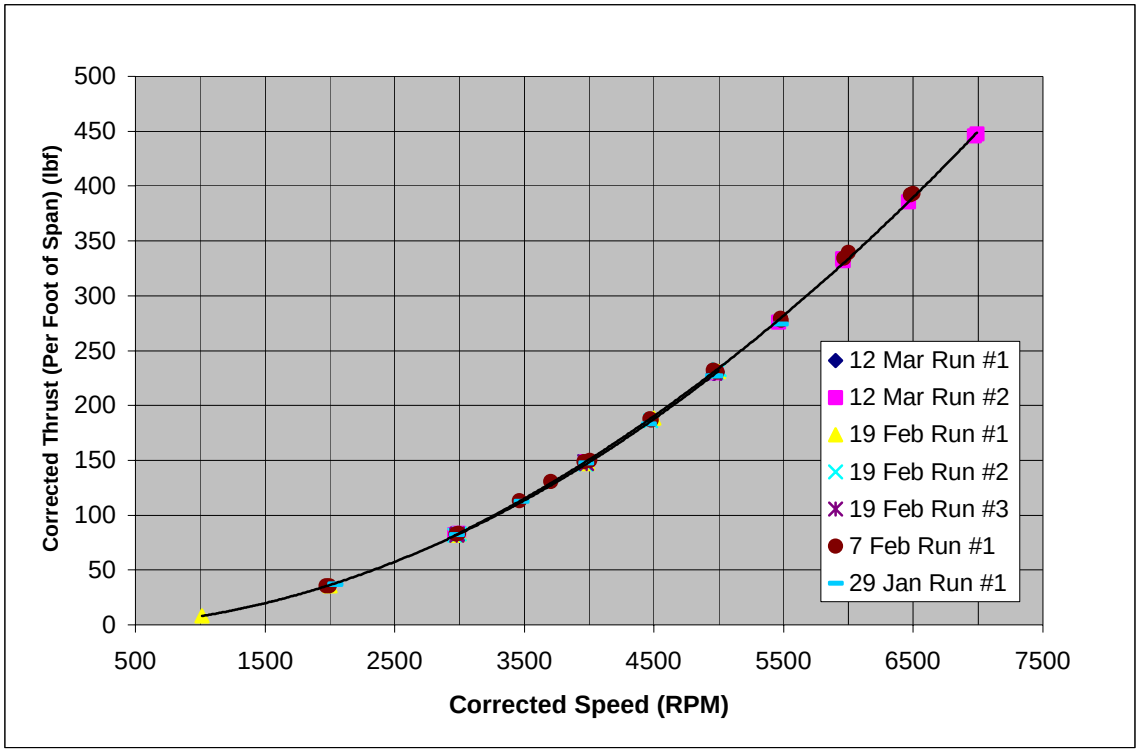

Figure 22. Corrected Thrust Per Foot of Span vs. Corrected Speed

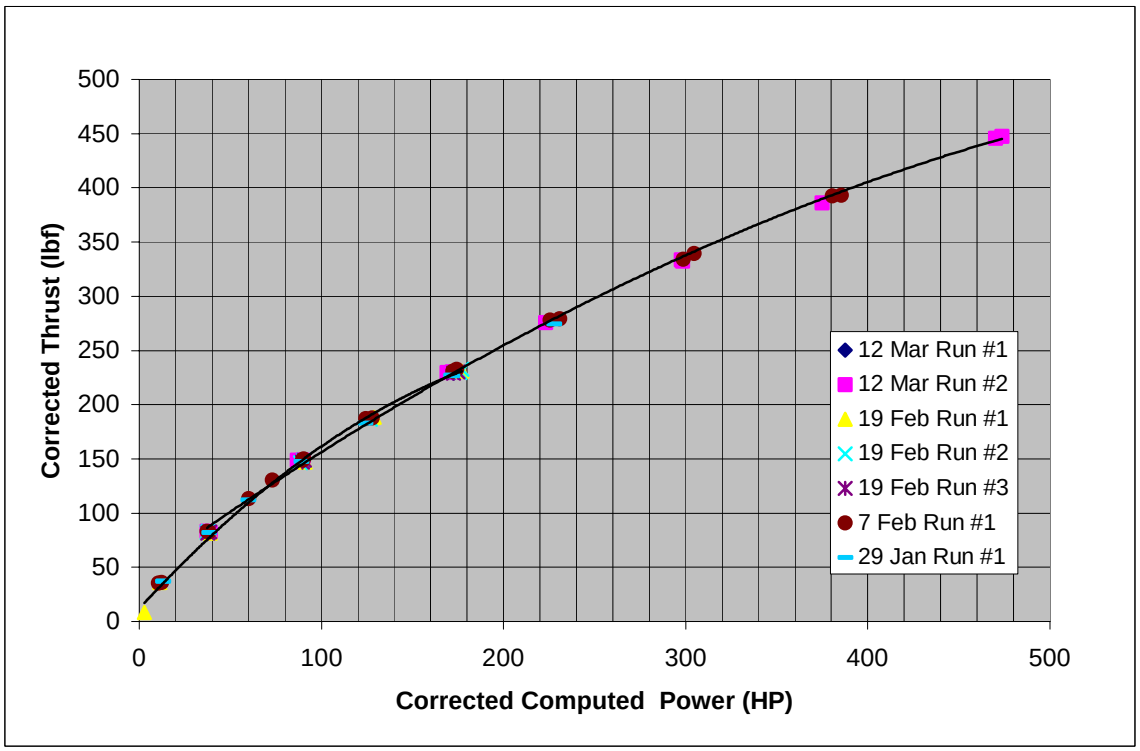

Figure 23. Corrected Thrust vs. Corrected Computed Power (Per Foot of Span)

3. Flow Visualization

Flow visualization results were recorded on digital still and video media. This allowed a qualitative comparison to be made with the flow patterns reported in the VSD study as well as current computational fluid dynamics efforts. All flow visualization measurements were performed at a rotational speed of 5,000 RPM.

Figure 24 presents the overall flow pattern using three dyes injected in the left, center, and right ports of the Plexiglas inner blank. The image shows the distinct central streamlines in the rotor and the circulation in the high-pressure cavity. To a lesser degree, the circulation in and through the low-pressure cavity is also evident. Figure 25 depicts close-ups of the high-pressure cavity recirculation pattern (a) and the recirculation pattern near the low pressure cavity (b).

Figure 26 is an overlay of a typical flow pattern obtained from the VSD study onto the image from Figure 24. The streamline patterns are noticeably similar. Also, the centers of the high-pressure and low-pressure cavity-induced recirculations are in the same locations as those in the VSD study.

Although not directly related to the flow visualization efforts, the effectiveness of the labyrinth seals between the crossflow fan and the Plexiglas viewing window should be noted. No leakage of dye through this seal was evident. This was not the case in the mating surfaces between the Plexiglas inner blank and the viewing window, nor between the inner blank and the instrumentation port. A substantial amount of dye leaked between these seals and led to some obscuration of the flow visualization.

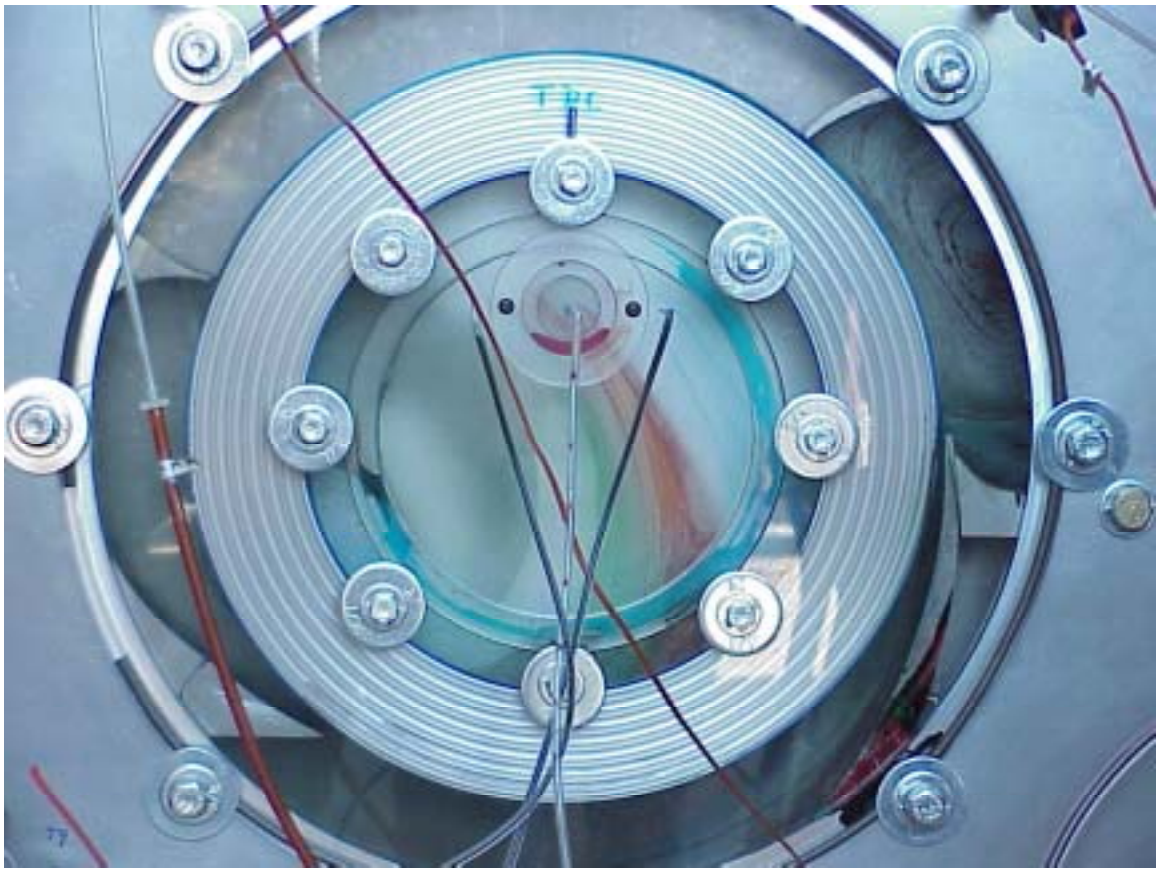

Figure 24. Flow Visualization Trial (12 March Run #1)

(a)

(b)

Figure 25. Closeups of (a)HP Cavity and (b)LP Cavity Circulation Patterns

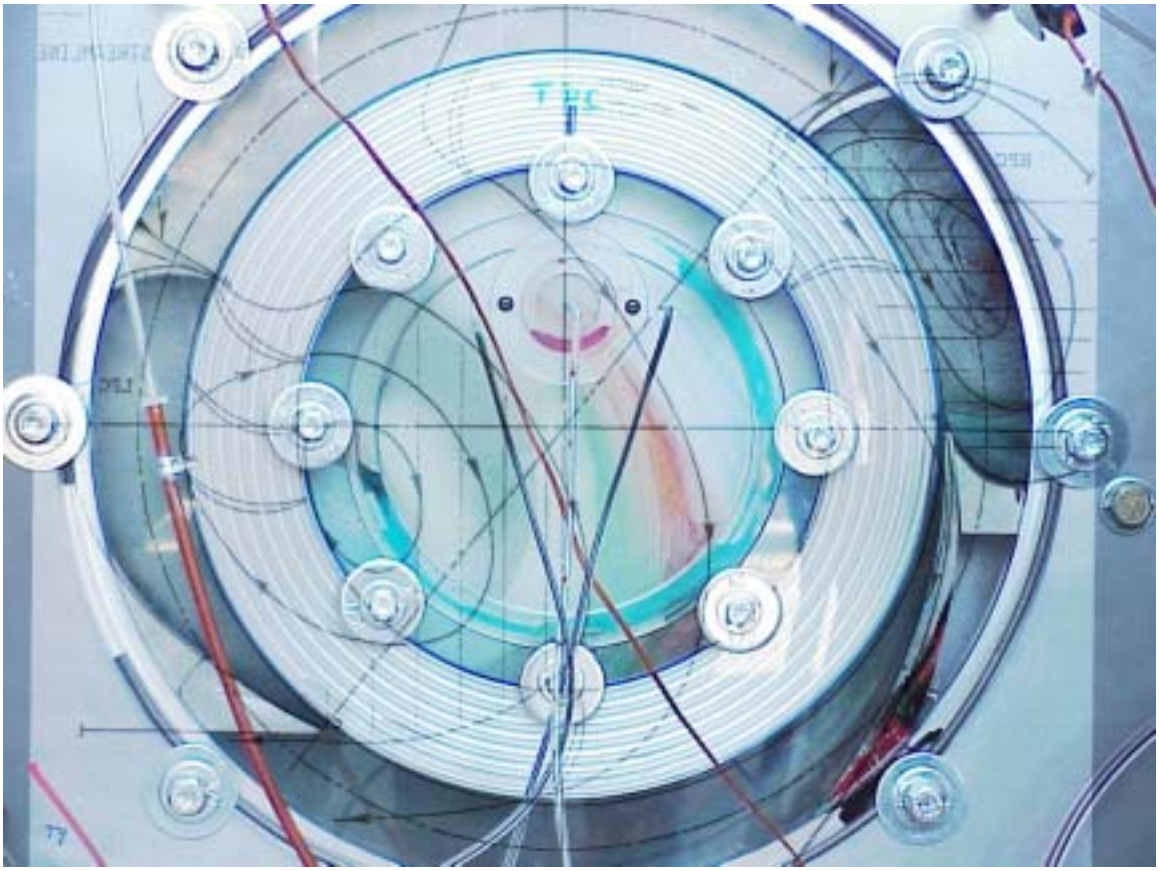

Figure 26. Overlay of Streamline Patterns (After Ref. 6)

III. NUMERICAL SIMULATION

A. FLO++ OVERVIEW

The software used for numerical simulation of the CFTA was FLO++, by Softflo of South Africa. FLO++ is a Windows-based computational fluid dynamics (CFD) software package capable of handling a wide range of fluid-flow and heat transfer problems. It combines an easy-to-use graphic user interface (GUI) with a powerful grid generator, preprocessor and postprocessor (PFLO), and solver (FLO) in one package. Both the solver, pre- and postprocessor executables can be recompiled based on the size and complexity of the problem in order to provide minimum memory usage. The postprocessor was used to visualize the solution in steady and unsteady mode in either contour (scalar) or velocity vector form.

FLO++ is capable of handling incompressible or compressible, laminar or turbulent flows. A high-Reynolds number k-ε model is used to model turbulent flows. FLO++ is also capable of handling steady or unsteady solutions. It uses a modified SIMPLE algorithm for solving steady cases, or a time-marching upwind-differencing modified PISO algorithm to solve unsteady cases. Sliding meshes are used to model moving or rotating machinery.

B. GRID GENERATION

Grid generation was performed using MATLAB and FLO++. A 15-bladed fan was initially modeled in order to limit the total number of cells in the grid. A MATLAB script file was used to generate a text file of vertex coordinates corresponding to the upper and lower surfaces of a blade section and the inner and outer radii of the fan. The MATLAB script file and vertex coordinate text file are included in Appendix B. Figure 27 shows the vertices plotted with MATLAB.

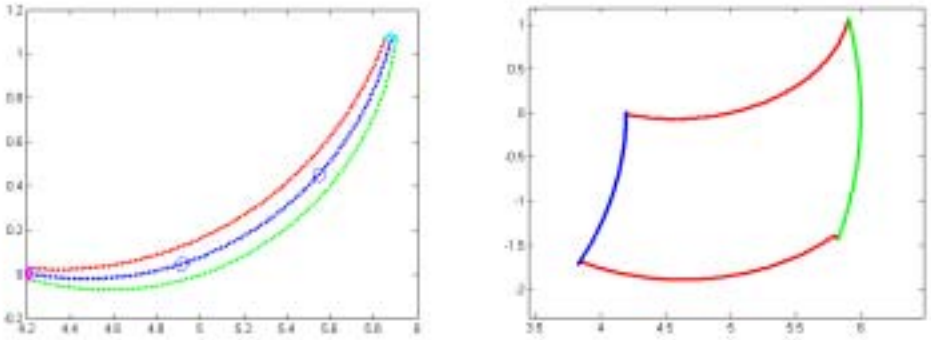

Figure 27. MATLAB-Generated Blade and Blade Passage Vertices

After the creation of the vertex coordinate file, the FLO++ preprocessor PFLO was opened and a new script file was created, starting with commands that read the vertex coordinates directly from the previously created text file. Once these vertices had been created in PFLO, they were splined together appropriately and copied in the spanwise direction to provide a basis for the definition of a block. Once the block was defined, cell dimensions and distributions were assigned on all three directions, and the block command was executed, which physically created the cells. Two thin layers of cells on the outside and inside radii of the fan were added to smooth the interface between the fan cells and interior and exterior cells. In this manner the grid describing the passage between two blades was modeled. This cell group is depicted in Figure 28.

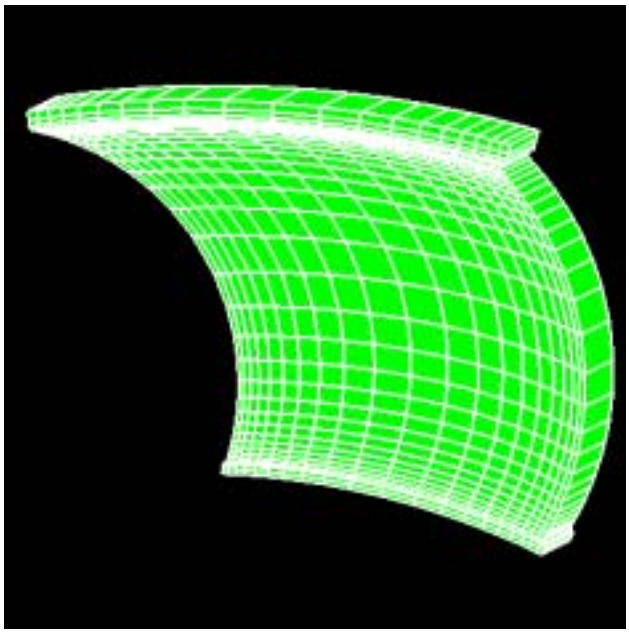

Figure 28. Blade Passage Grid

The blade passage cell group was then copied with 24-degree increments added successively in a cylindrical coordinate system. The resulting structure represented a complete rotor grid. All cells of the rotor grid were assigned to a single cell group for later definition as a sliding set. Figure 29 shows close-ups of the rotor grid detail.

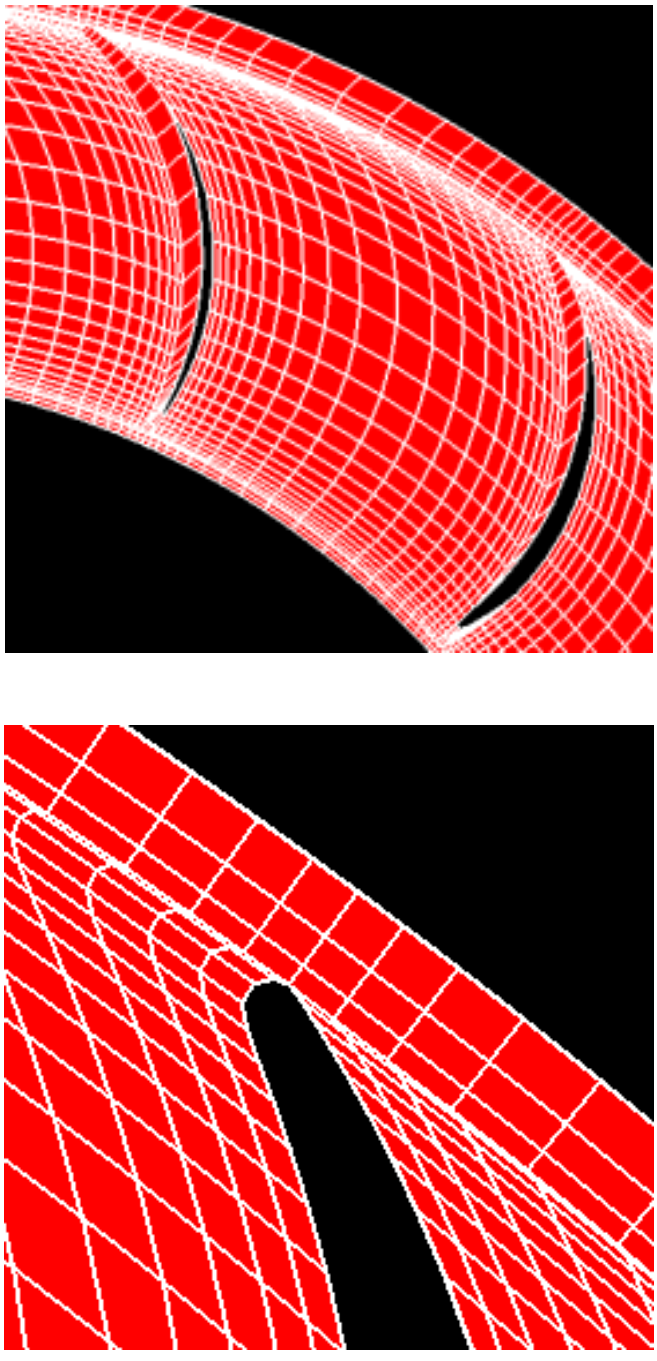

Figure 29. Crossflow Fan Rotor Grid Detail

Remaining components of the CFTA numerical model were constructed in a similar manner, with vertex coordinates chosen directly from the CAD drawings used to machine the physical components. These consisted of the intake, low pressure (LP) cavity, exhaust duct and extension, high pressure (HP) cavity, and inner fan mesh. The cells in each cell group were dimensioned and distributed appropriately to provide acceptable detail with a minimum of skewness of the individual cells.

Some components in the CFTA had regions of relatively small radius of curvature, which required refined modelling. However, increasing the number of cells in these areas was not necessarily an option since it often had an impact on the shape and skewness of the cells in the group. Fine detail was therefore achieved using "detail layers" – thin subgroups of cells in a component cell group covering the areas of small radius of curvature. Figure 30 shows the level of detail achieved through the use of these cell layers

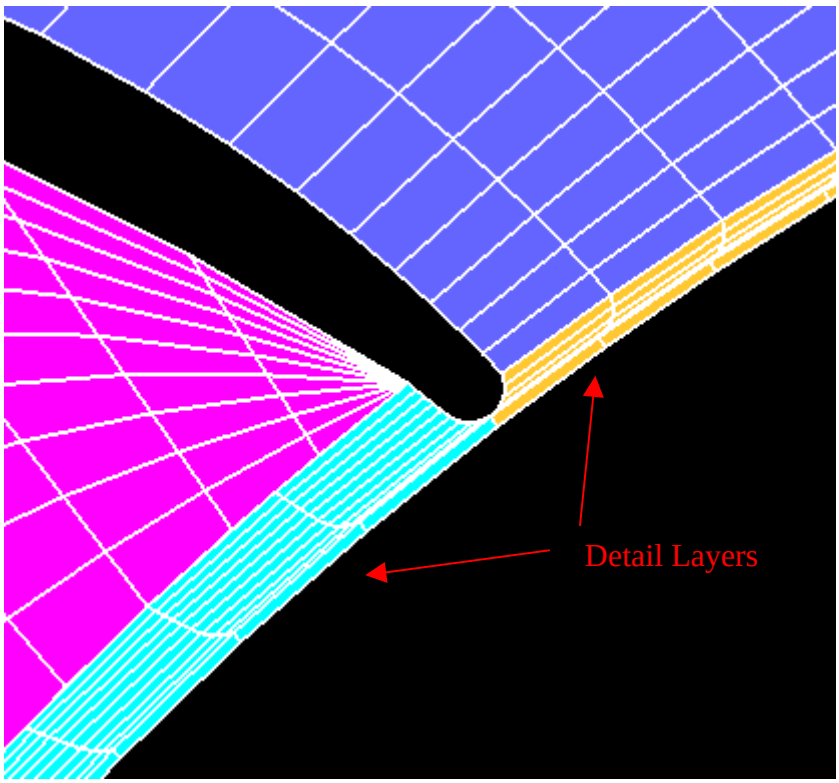

Figure 30. Close-up of HP Cavity and Intake Detail Layers

After many trials and refinements, the grid shown in Figure 31 was adopted. This grid demonstrated a high level of detail and proved error-free in the preprocessing stage. The grid contained a thin clearance layer cell group, which allowed the assignment of a single boundary between the outer radius of the moving inner fan and the rest of the external components. This helped to simplify the setup for the solution stage. Figure 32 shows a close-up of the grid to highlight the interface between the moving and non-moving surfaces. A total of 36,130 vertices and 16,630 cells were used.

Some adjoining cell groups were not of the same cell dimension or distribution. In these cases, the ESFIND command was used to define the manner in which the two dissimilar meshes were coupled. This command invoked the FLO++ arbitrary mesh coupling to produce a seamless interface between meshes of differing cell dimension or distribution.

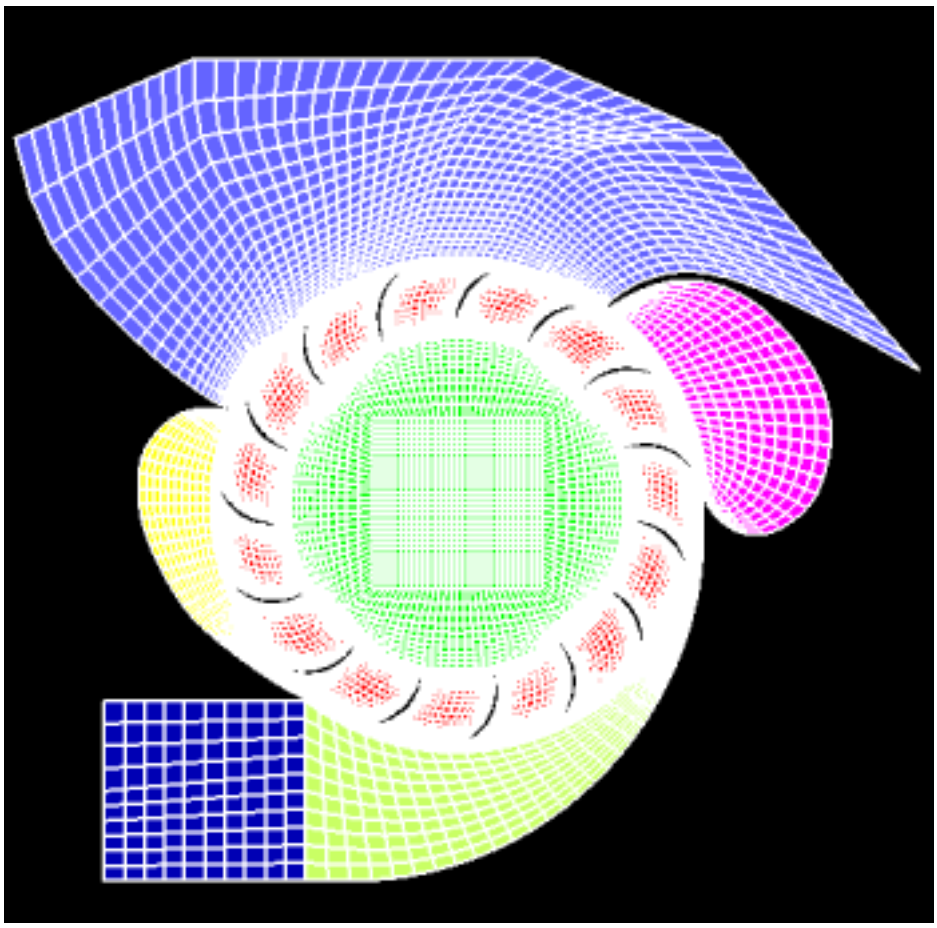

Figure 31. Complete Test Assembly Computational Grid

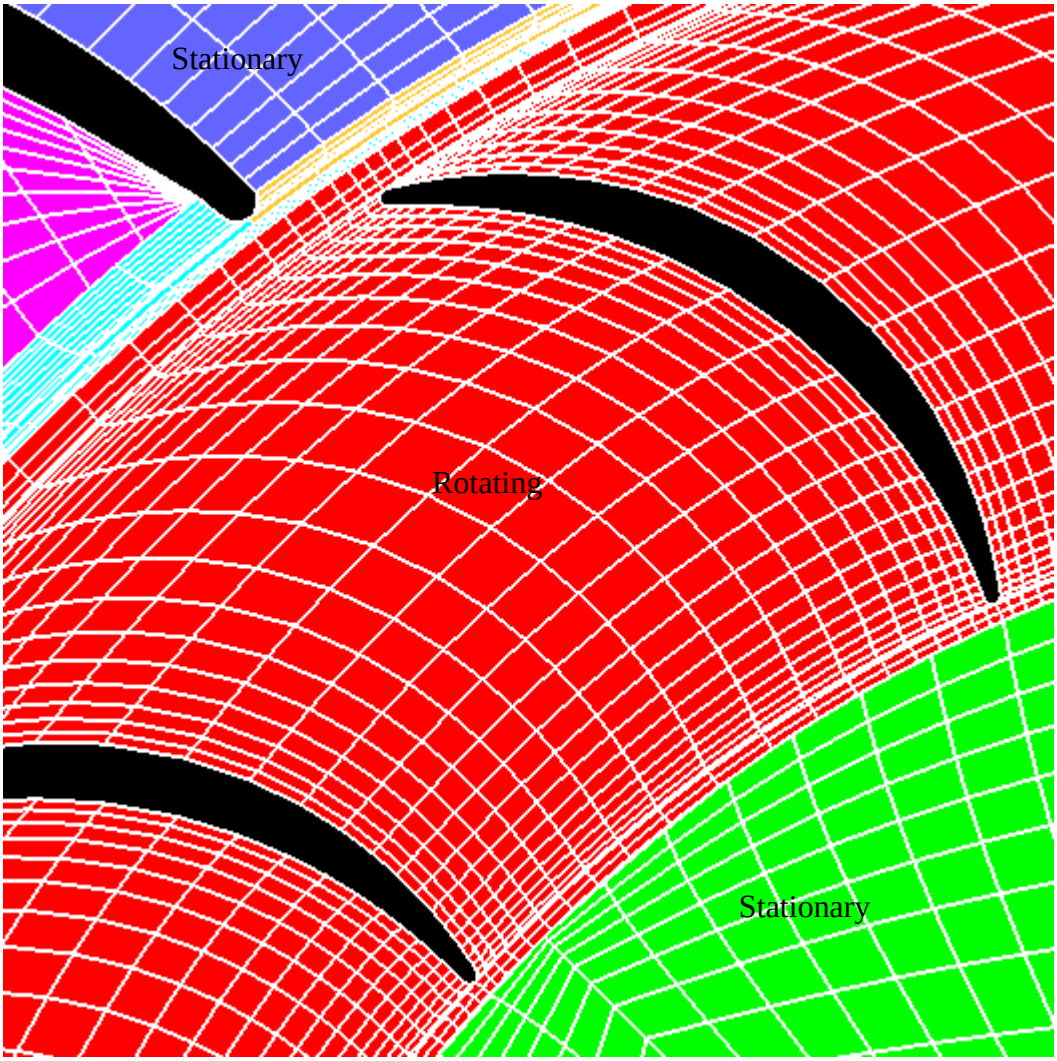

Figure 32. Grid Moving Surfaces Detail

Once the grid was fully constructed and the mesh coupling completed, boundary cells were chosen and defined. Initially the assembly inlet and outlet were defined as PRESSURE type boundaries, with atmospheric pressure specified. The outer and inner surfaces of the fan rotor, inner surface of the fan clearance layer, and the outer surface of the inner fan mesh were defined as ATTACHED type boundaries, which facilitated their later use as sliding sets. The front and back faces of the entire assembly model (corresponding to the areas covered by the front and back plates of the physical assembly) were defined as SYMMETRY type boundary conditions. This was done to minimize demand on the solver by reducing the test assembly to a pseudo-2D problem instead of a full 3D problem. All other boundaries were assigned as WALL type by

default. Figure 33 shows the assigned boundaries, with the exception of the SYMMETRY boundaries.

Once boundaries were assigned, the sliding sets were defined using the SSDEF command with which the boundaries of type ATTACHED were instructed to slide against each other. The fan rotor cell group rotated in the negative θ-direction based on a cylindrical coordinate system defined with the z-axis aligned with the axis of rotation of the CFTA. Additionally, material properties such as density, viscosity, and reference pressure and temperature were specified. Density was defined as either constant at 1.205 kg/m^3 for incompressible solutions or as dictated by the ideal gas law for compressible solutions. Viscosity was defined as constant at 1.8×10^{-5} $N\text{-}s/m^2$. Reference pressure and temperature were fixed at 1×10^5 Pa and 300 K respectively.

The presence of moving meshes necessitated an unsteady solution. This was selected using the UNSTEADY command. Also specified in this command line was information regarding the time step, maximum Courant number, and modifiers to the PISO (Pressure Implicit Split Operator) algorithm. The time step could be specified as FIXED or ADJUSTABLE. If ADUSTABLE was chosen the time step would adjust during each iteration to maintain the specified maximum Courant number. Also, a minimum number of corrector loops used in the PISO algorithm could be specified.

The remainder of the commands in the script file were dedicated to solver commands and instructions regarding how to save the results. The PFLO command script file is included as Appendix B.

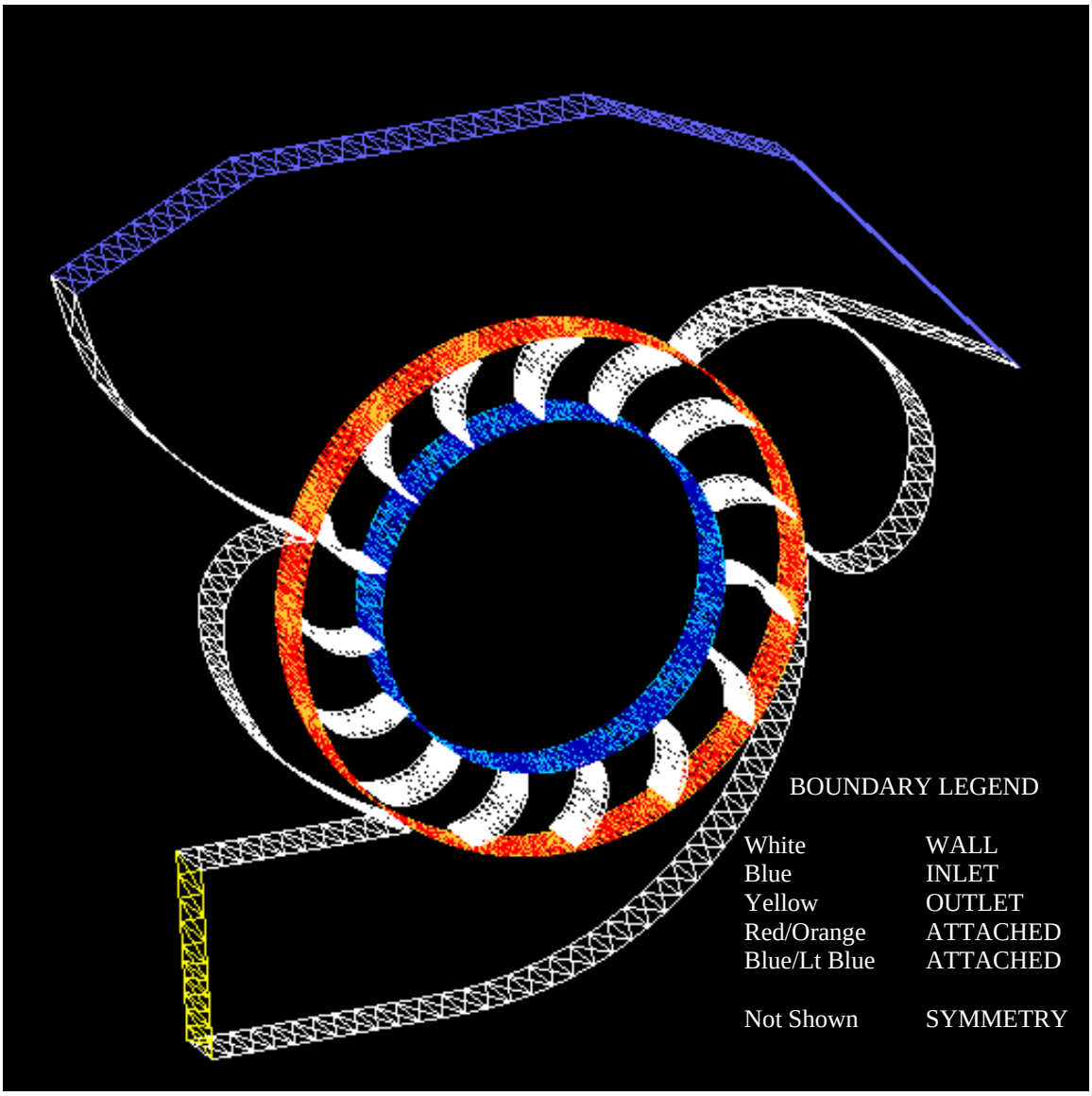

Figure 33. Boundary Groups

C. FLOW SOLUTION

Once the PFLO command input file was complete, the solver FLO was initiated. Initially, a compressible solution at 5,000 RPM was attempted. The maximum Courant number was set at 1 in order to preserve time-accuracy of the solution. This was considered important in visualizing how the flow developed inside the crossflow fan. However, this had a significant effect on the time step, which was adjusted by FLO each iteration in order to remain below the specified maximum time step. Time steps on the order of 10^{-7} seconds or smaller were frequently encountered, making the solution time unreasonably long. A fan speed of 5,000 RPM corresponded to one rotation in .012 seconds. It was considered desirable to obtain a solution of at least one fan revolution to ensure proper function of the grid. With a time step of 10^{-7} seconds, this would have required 120,000 iterations of solver. Given that each iteration took approximately 20 seconds to process, the solution time would have been approximately 667 hours, or 27 days.

Additionally problematic was the fact that the solver had a tendency to become unstable, even well into the solution time. This instability manifested itself as unrealistic velocities in the intake and / or inflow at the exhaust duct, both of which eventually became unbounded. Therefore, several modifications to the original grid were made in the hope of alleviating these problems.

The unbounded intake velocity consistently occurred at the corner nearest the high-pressure cavity. It was thought that highly skew cell geometry in close proximity to the intake pressure boundary was at fault. Consequently, the grid was reshaped to improve the geometry of the intake grid. The intake was extended and the boundary was reshaped into an arc of 24 inches radius as measured from the center of the fan. This had a favorable effect on the shape and dimension of the cells in the intake. The wall boundaries of the initial grid were extended to intersect the 24-inch arc. It was felt that the wall extensions would have little effect at such a large radius relative to the radius of the fan. The modified grid contained 36,124 vertices, while the number of cells remained unchanged. The modified grid is shown in Figure 34.

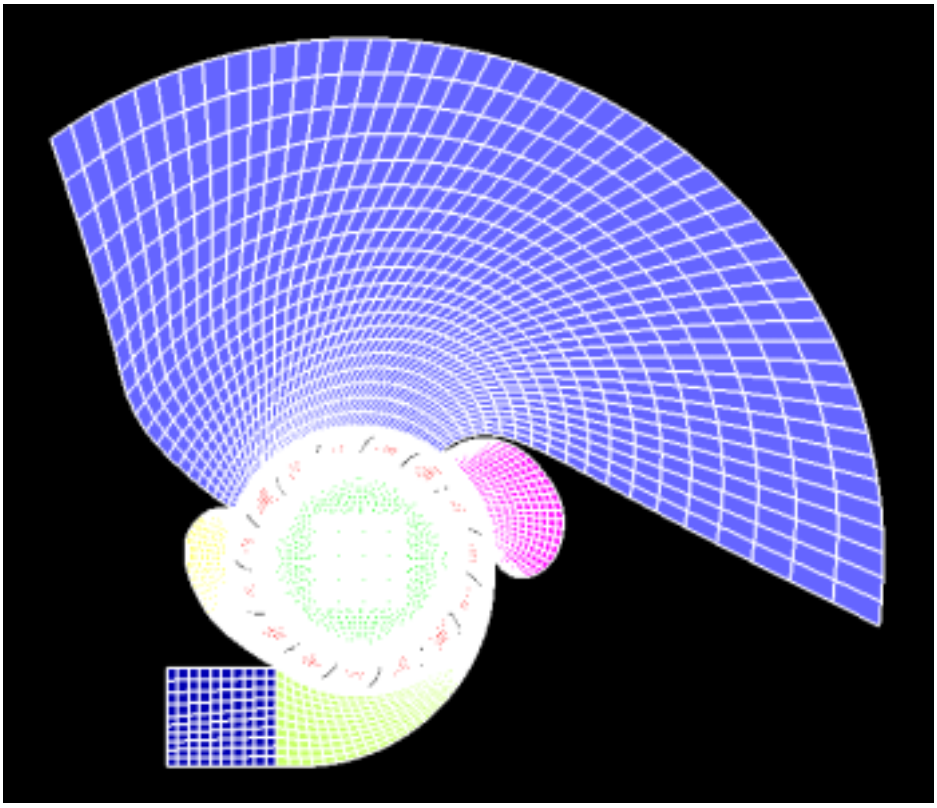

Figure 34. Modified Grid

In an attempt to correct the inflow that occurred at the exhaust duct boundary, a slight pressure gradient was applied between the intake and exhaust duct pressure boundaries. The intake boundary remained at 1×10^{5} Pa, while the exit velocity was reduced by 5,000 Pa. It was felt that the slight pressure gradient would create flow in the proper direction from the outset of the solution, thus assisting the solver in the early stages of the solution.

Finally, the solution definition was changed to an incompressible one. This made a reduction in fan speed necessary, since the rotor tip speed of approximately 80 m/s made speeds approaching compressibility a possibility elsewhere in the fan. The fan speed was therefore reduced to 3,000 RPM and density was set to "constant".

D. RESULTS AND DISCUSSION

The solver processed for a total of 24,200 iterations at a fan speed of 3,000 RPM. This corresponded to a solution time of 2.13×10^{-2} seconds, or 1.065 revolutions of the

fan. After approximately 18,000 iterations, the solver was stopped and the input file was modified to eliminate the pressure differential between the intake and exhaust boundaries. It was felt that the pressure differential was not necessary after flow had been established through the fan. The solution was restarted from the 16,400th iteration, and exhibited some oscillation caused by the instantaneous change in boundary conditions which appeared to damp out prior to reaching 20,000 iterations. The flow resumed its previous pattern prior to reaching 24,200 iterations.

The results of the 24,200th iteration were examined. Contour plots of velocity magnitude, Mach number, static pressure, and total pressure were created using the post-processing functions in PFLO. Vector plots of velocity magnitude were also created. These images are shown in Figures 35 through 42.

Figure 35 is a contour plot of velocity magnitude. Examination of the high- and low-velocity areas of the plot reveals similar flow patterns to those found in the experimental phase of this research, as well as those found by VSD in their pressure gradient analysis. It must be acknowledged that although this problem was solved as an incompressible solution, the maximum velocity depicted on this plot is at a level sufficient for compressible effects to exist. However, these areas of high velocity or possible compressible flow are extremely small and may be limited to computationally insignificant pockets near the surfaces of the fan blades.

Figure 36 is a contour plot of Mach number. This plot demonstrates similar results to the previous plot. From inspection of the Mach number plot, it can be seen that the exit Mach number is in the range of .29 to .32. This is supported by experimental data, which suggests an exit Mach number of approximately .27 at 3,000 RPM. Frictional effects of the front and back plates of the test assembly may explain the lower Mach number in the experimental data.

Figure 37 is a contour plot of static pressure. Inspection of this plot further verifies the locations of the high- and low-pressure circulation regions within the crossflow fan. The reason for the choice of names of the two cavities is also clear. Although the lowest recorded pressure does not actually occur inside the low-pressure cavity, this cavity creates the circulation area in which the lowest pressure is seen. The

high-pressure cavity shows a pressure lower than reference pressure in this image; however, the pressure in this cavity is definitely higher than anywhere within the circulation region caused by the low-pressure cavity.

Figure 38. is a contour plot of total pressure. It must be acknowledged that the total-to-total pressure ratio in this image is less than the experimentally obtained values. Figure 17 shows a pressure ratio of approximately 1.055 at a fan speed of 3,000 corrected RPM. Figure 38 shows an approximate pressure ratio of up to 1.017. The reason for this discrepancy may lie with use of specified inlet and exit pressure boundaries. Additionally, the numerically derived total pressures may still show effects from the restart at the 16,400th iteration. Although this information was not available due to some of the results files being overwritten after the restart, a plot of total pressure derived from roughly the 18,000th iteration, prior to the restart of the solver, showed a pressure ratio approaching 1.05.

Several different velocity magnitude vector plots were examined. Figure 39 is a plot of the entire test assembly. The large difference in velocity magnitudes and the large number of vectors in the plot makes flow patterns somewhat difficult to discern. Therefore, separate plots were created showing only certain cell groups of interest. These are given as Figures 40 through 42. Comparison with experimentally derived flow velocities and flow patterns further testifies to the validity of the numerical solution.

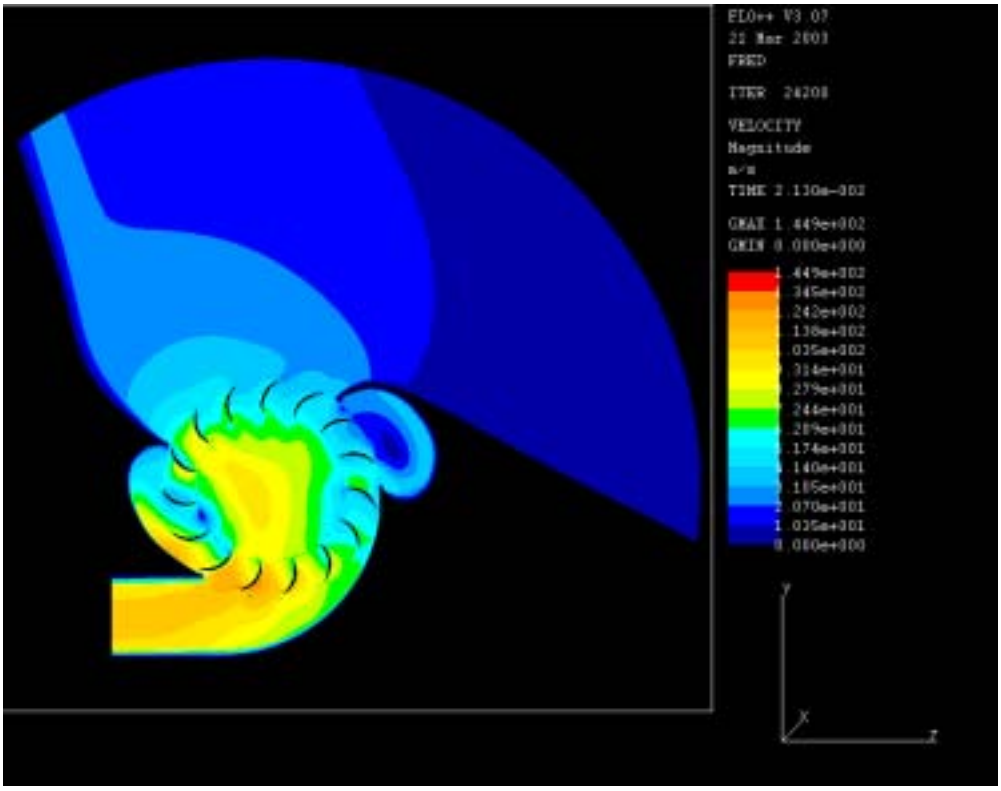

Figure 35. Contour Plot of Velocity Magnitude

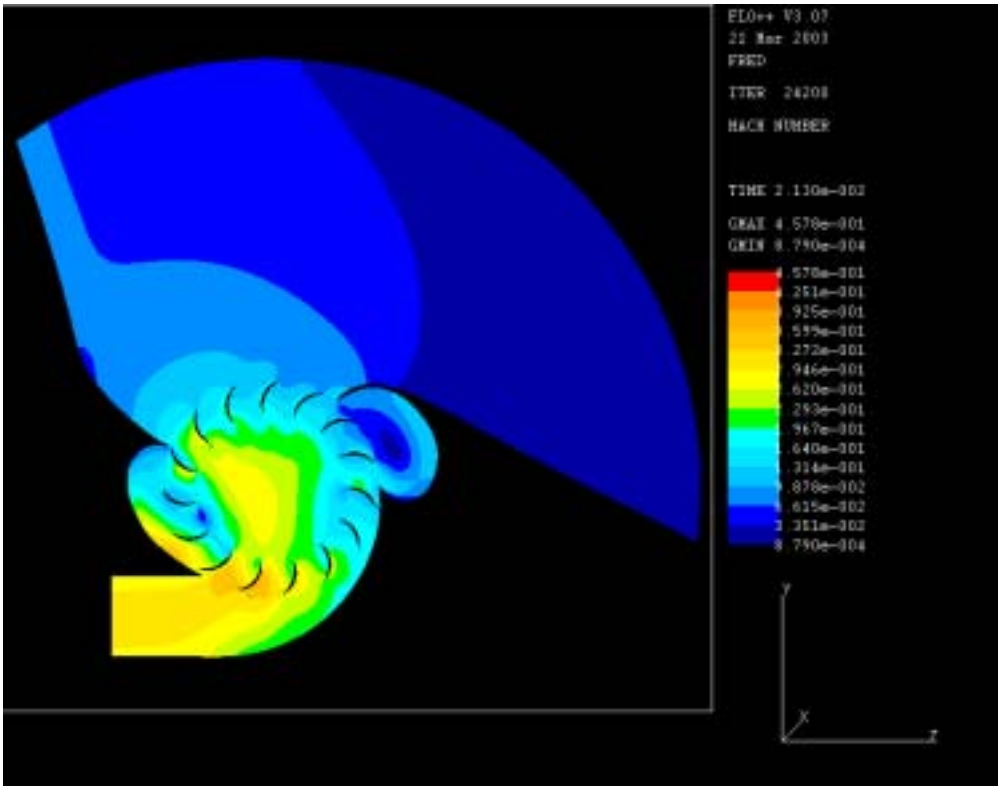

Figure 36. Contour Plot of Mach Number

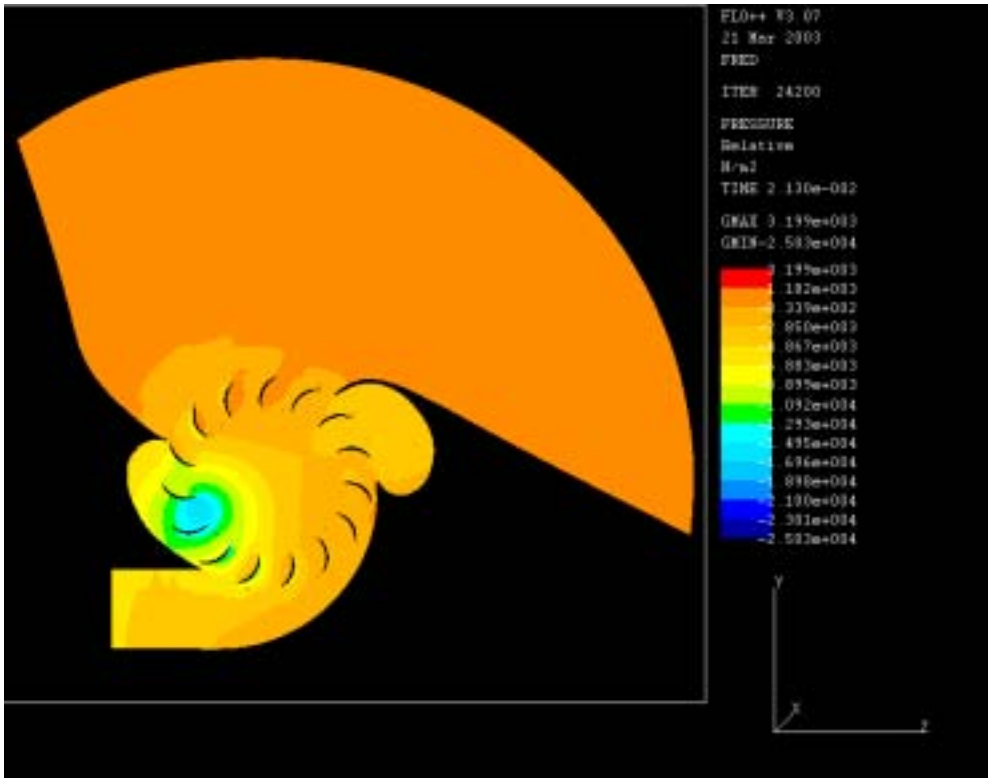

Figure 37. Contour Plot of Static Pressure

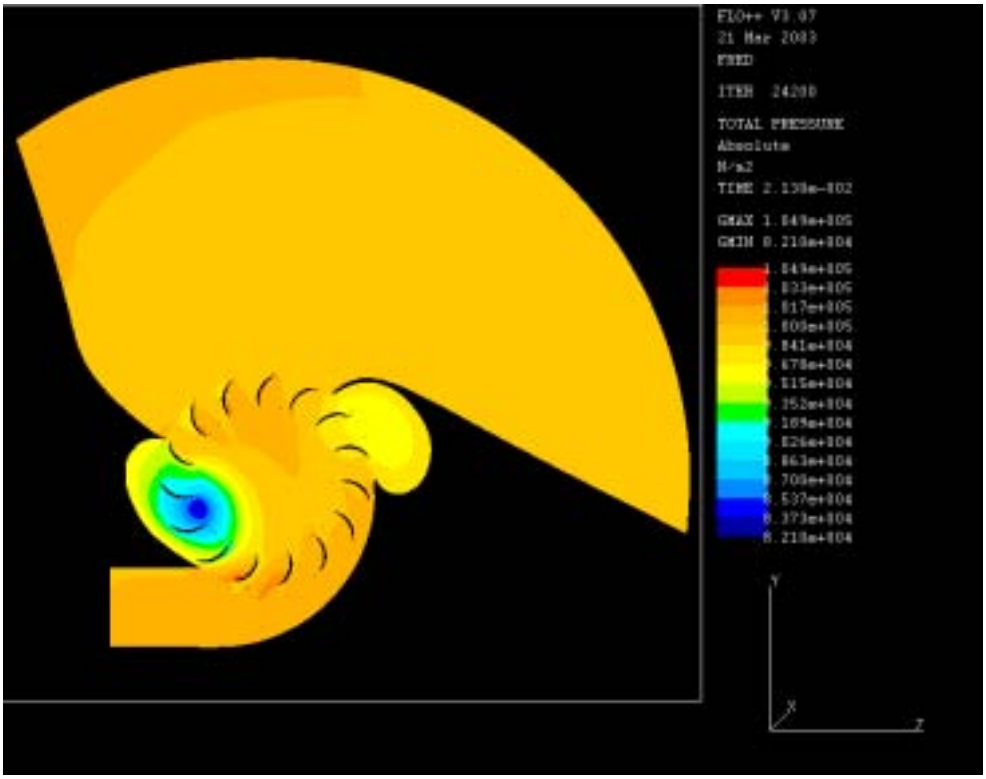

Figure 38. Contour Plot of Total Pressure

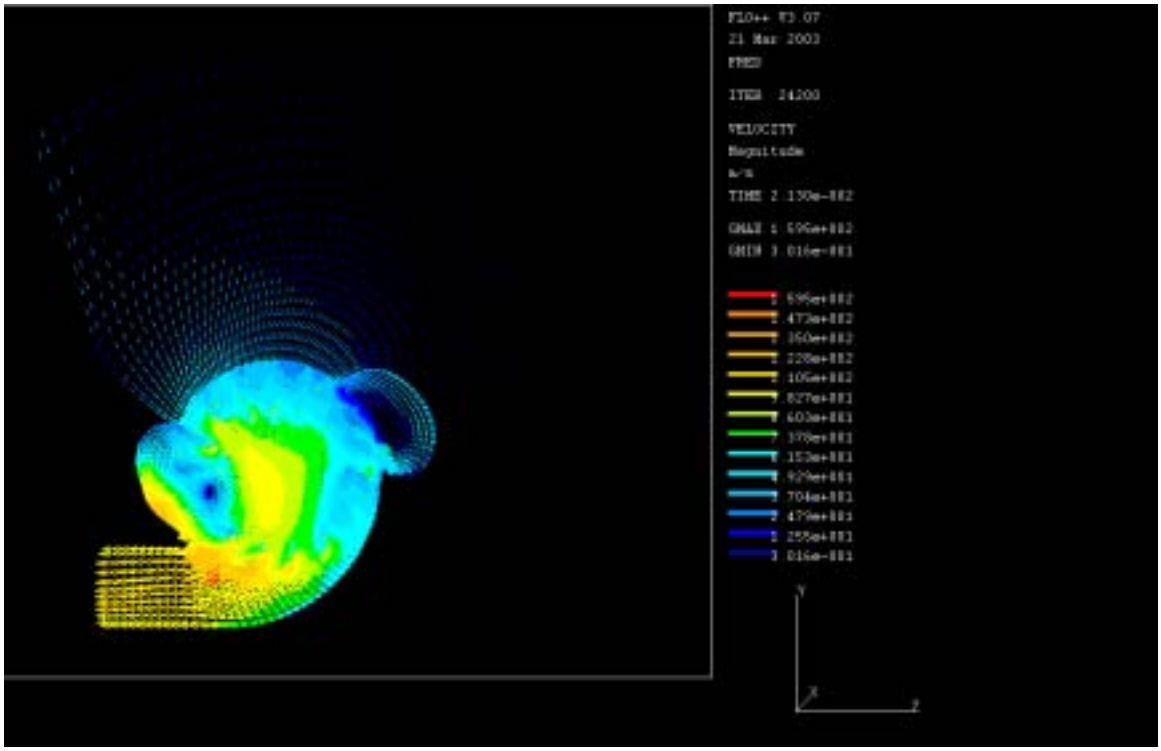

Figure 39. Vector Plot of Velocity

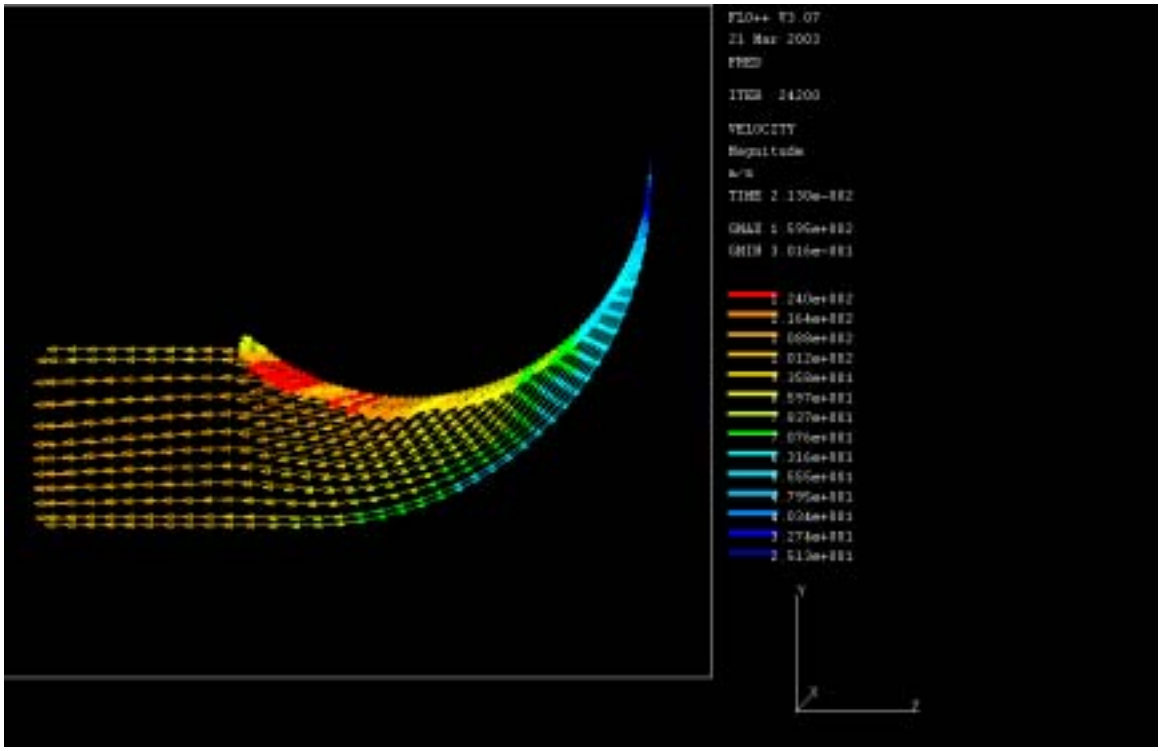

Figure 40. Vector Plot of Velocity in the Exhaust Duct, Extension, and Detail Layer

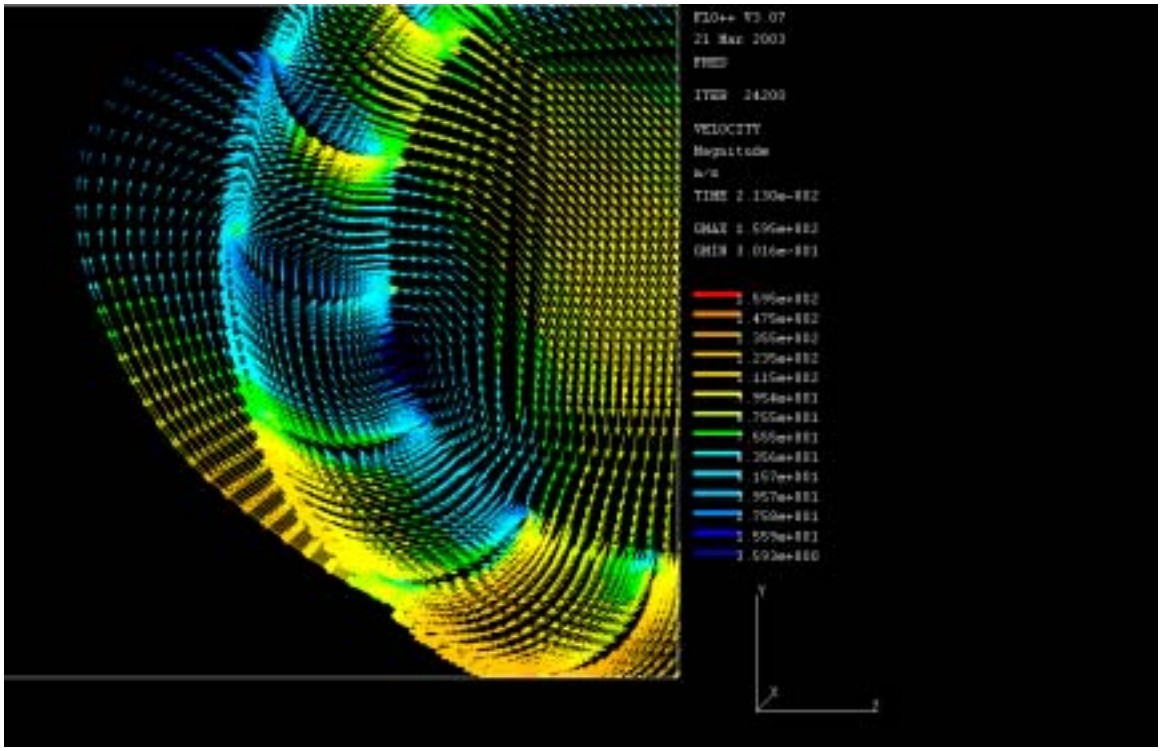

Figure 41. Vector Plot of Velocity in the Low-Pressure Cavity and Recirculation Area

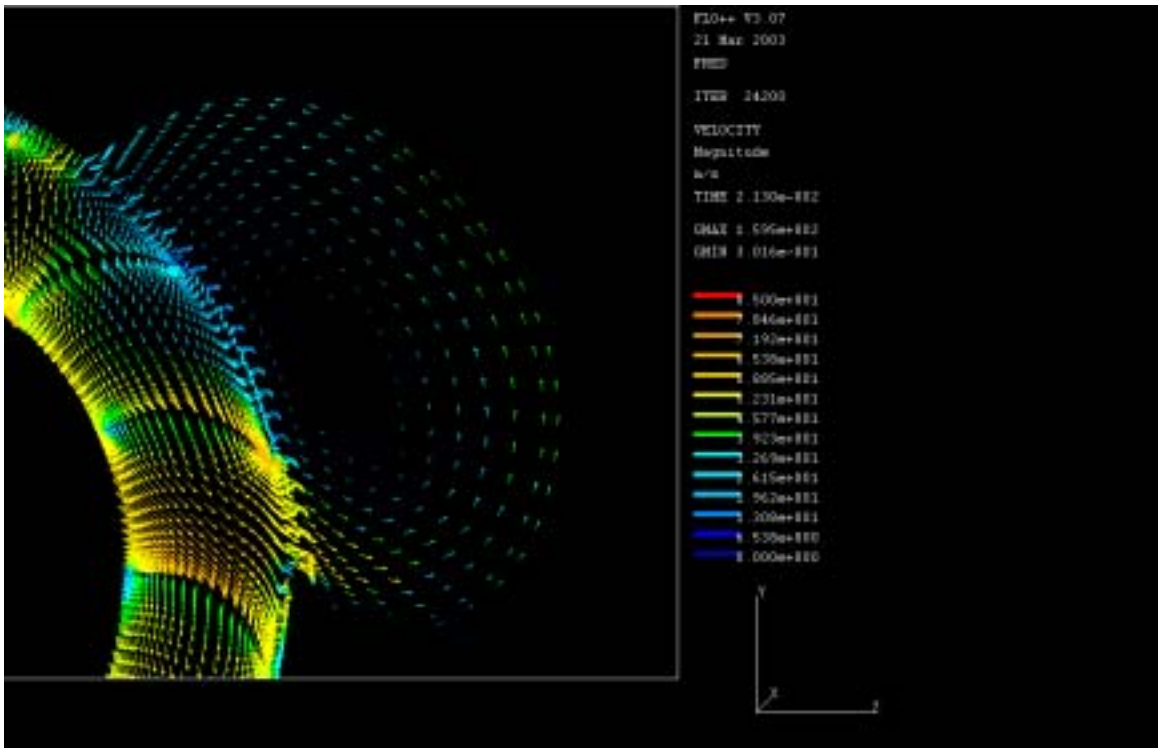

Figure 42. Vector Plot of Velocity in the High-Pressure Cavity and Recirculation Region

IV. FAN-IN-WING CONCEPT

A. DESCRIPTION

Analysis of the experimental and numerical simulation results led to the conceptualization of a crossflow fan-based lift / propulsion device. This concept consisted of a crossflow fan of the type and configuration studied in the experimental and numerical simulation phases of this research, installed within a wing section. The intake of the fan was located in such a manner as to coincide with the location of the low-pressure peak of the airfoil in forward flight, or with the location of the separation bubble at high angles of attack. This theoretically increased the lift produced by the wing by further reducing the pressure in the low-pressure region on the upper surface of the wing section. Additionally, it was theorized that the location of the intake would inhibit flow separation at high angles of attack. The crossflow fan exhaust exited the wing section from the trailing edge, providing both thrust and higher lift due to supercirculation effects. Figure 43 shows one possible installation of the "fan-in-wing" concept. It is important to emphasize that this particular installation may not represent an optimum configuration.

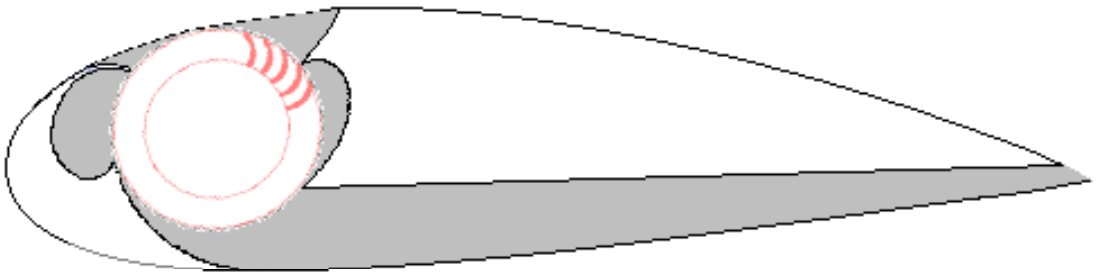

Figure 43. Conceptual Fan-In-Wing Installation

B. NUMERICAL SIMULATION

In order to investigate the usefulness of the fan-in-wing configuration as applied to a V/STOL aircraft, a relatively simple numerical simulation was performed using FLO++. A NACA 4244 airfoil was selected for use in this simulation, solely for its thickness. It was felt that a crossflow fan of the same dimensions as that used in the experimental phase could easily be incorporated into the 4244 airfoil of appropriate chord.

The airfoil coordinates were obtained from Ref. 13 and were used to create airfoil splines in the PFLO input command file. A very basic C-grid was created around the airfoil, utilizing 5094 vertices and 2400 cells. More information on this C-grid may be found in Appendix C.

The intake of the crossflow fan was modeled by defining four of the cells on the surface of the wing section as OUTLET boundaries. FREE mass flow was selected, but the mass flow fraction was here defined as the experimentally derived $\dot{m}_{CFF}$ divided by the mass flow through the C-grid's inlet boundary. This was calculated as $\rho A_{inlet} V_{\infty}$.

The exhaust of the crossflow fan was modeled by defining the terminal cell on the upper surface of the wing section as type INLET. Velocity here was specified using an experimentally derived exit velocity oriented in the chordwise direction. Figure 44 depicts the boundaries in this problem.

This solution was modeled as an incompressible flow, with steady boundary conditions. Convergence was reached extremely quickly, within approximately 30 seconds. Contour plots of pressure and velocity magnitude were created for a single regime of flight. Comparisons were made between the unaugmented wing section and the fan-in-wing augmented wing section.

Flight conditions of 10° angle of attack (AOA) and 100 knots airspeed were stipulated in order to simulate level flight. Mass flow and exit velocity quantities were derived from experimental data for a rotational speed of 5,000 RPM.

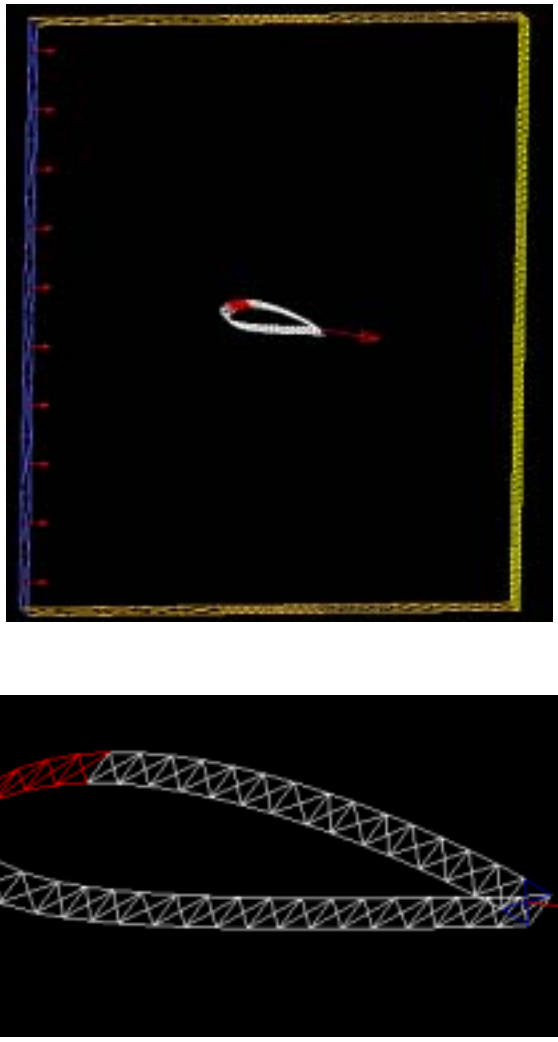

Figure 44 Fan-In-Wing Boundaries

Figure 45 is a comparison of static pressure between the unaugmented and fan-in-wing augmented case. It is obvious from inspection of the figure that there was a significant change in the pressure distribution over the upper surface of the wing. Both the low- and high-pressure regions on the upper and lower surface expanded. This resulted in a significant change in the lift developed by the wing.

Figure 46 is a comparison of velocity magnitude between the unaugmented and fan-in-wing augmented case. In the unaugmented case the wake profile exhibited a characteristic shape, and due to the high AOA, flow separation was present. In the augmented case, the wake profile velocities were much higher, indicating a reduction of

drag. Additionally, the air expelled from the trailing edge entrained the flow over the upper surface of the wing, which in turn reduced the effect of the separation bubble.

It is important to acknowledge that this was only a simple analysis of the possibilities of this type of crossflow fan configuration. A more detailed analysis is required. However, the results of this numerical simulation demonstrate that significant benefits may be obtained by drawing air through the leading edge and expelling it through the trailing edge, and that the crossflow fan may be an ideal device to accomplish this. Future efforts in this respect should center around incorporating the crossflow fan grid as previously reported into the NACA 4424 airfoil grid in this section.

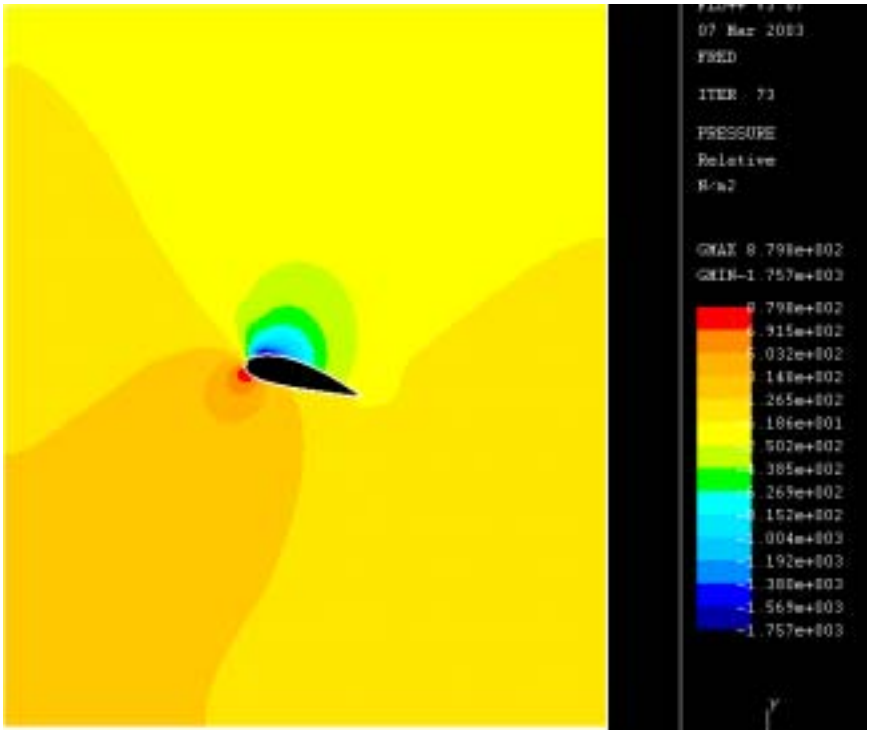

(a)

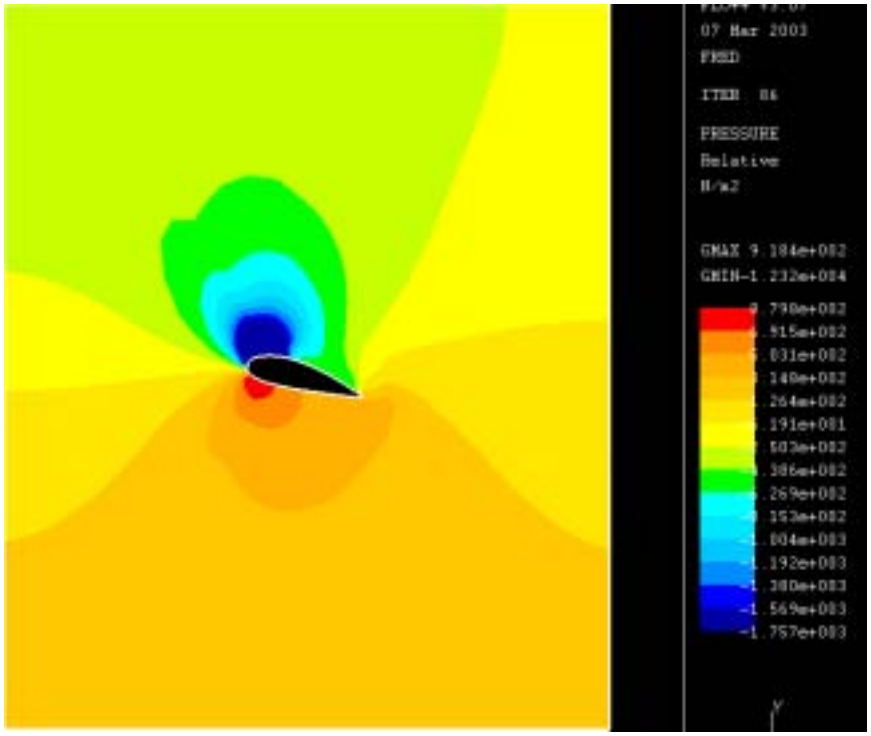

(b)

Figure 45 Pressure Contour Plot of the NACA 4424 Airfoil Without (a) and With (b) Fan-In-Wing Augmentation

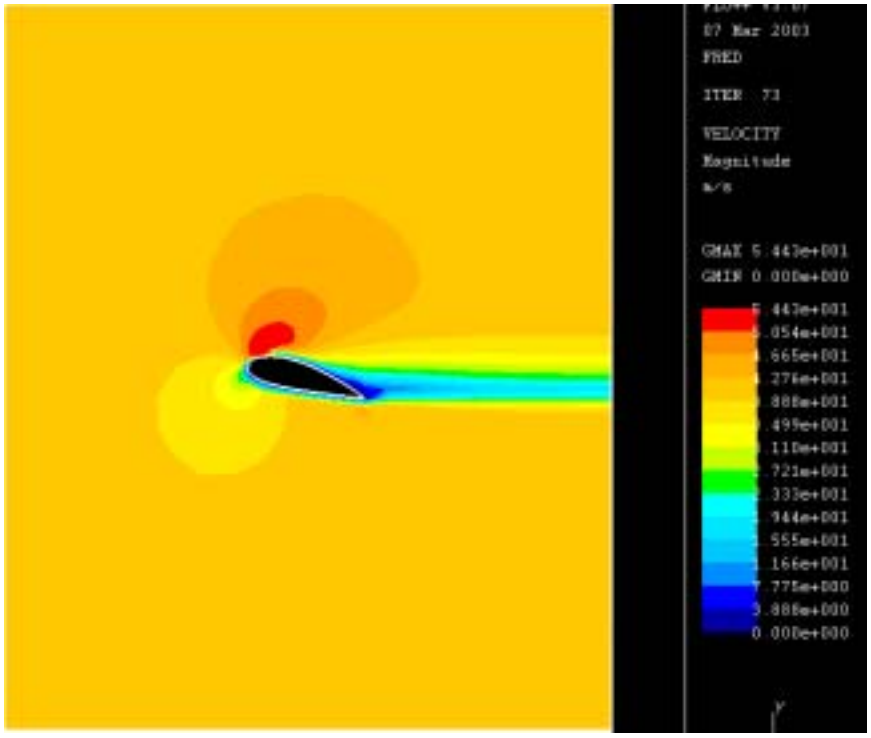

(a)

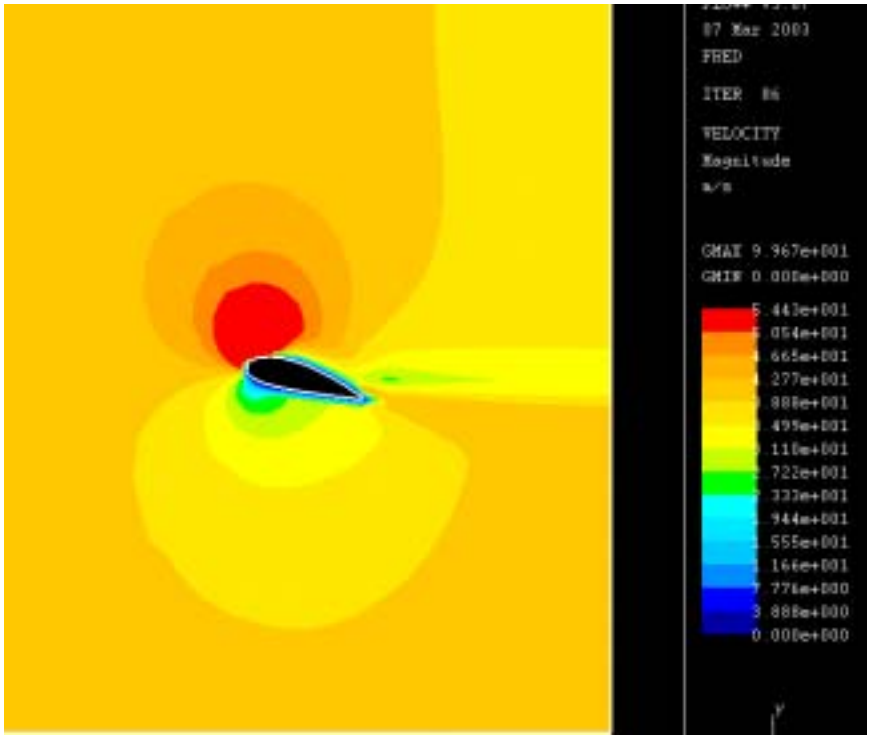

(b)

Figure 46 Velocity Magnitude Plot of the NACA 4424 Airfoil Without (a) and With (b) Fan-In-Wing Augmentation

C. SUGGESTED V/STOL CONFIGURATION

Gossett used a 20.6-inch span fan driven at 6,500 RPM by a 600-HP Wankel engine to produce 690 lbf thrust to augment the ducted propellers in his conceptual light VTOL aircraft. The design called for a crossflow fan assembly located along the centerline with the axis of the fan parallel to the longitudinal axis of the vehicle. A longer span fan was not considered in Gossett's design due to weight, engine size, and specifically, power limitations. Gossett extrapolated information for Fan #6 in the VSD study to arrive at his power requirements, leading him to conclude that the best thrust-to-power ratio of 1.15 would be achieved at 6,500 RPM. However, the VSD study did not test this fan below approximately 6,000 RPM. Inspection of Figures 22 and 23 reveals that a thrust to horsepower ratio (per foot of span) of 2 may be obtained by operating the fan at approximately 3,250 RPM.

In order to develop a useful amount of thrust in a light civil VTOL aircraft design, operation at this relatively low RPM called for a much longer span. For example, a 10-foot span fan will be required in order to produce 1,200 lbf thrust when powered by the 600-HP engine described in Ref. 8. A span this large was not useable in Gossett's design due to fuselage and wing section size limitations. However, the fan-in-wing concept takes advantage of the dimensions of the wing and may allow designers to take advantage of the higher thrust-to-power ratio of the lower-RPM fan.

A suggested aircraft configuration is given in Figure 47. This general configuration could be adapted and scaled to suit a number of applications. The basic design centers around the use of four fan-in-wing sections, which connect a separate fuselage to a twin boom-type tail assembly. The design is not unlike that of the Rockwell OV-10 Bronco observation aircraft. Two additional lifting surfaces strengthen the structure.

The fan-in-wing sections, shown in blue in Figure 47, rotate 90° around the crossflow fan axis to provide thrust for vertical takeoff. The lifting surfaces are staggered so that thrust from the forward fan-in-wing sections will not impinge on the center

structural member or the aft fan-in-wing section. A high-mounted horizontal stabilizer prevents impingement of the net thrust from both fan-in-wing sections.

Thrust in the VTOL mode would be provided by the crossflow fans in the fan-in-wing sections, rotated initially 90° downwards. Forward flight would be accomplished by slowly rotating the fan-in-wing sections upwards toward 0° relative to the longitudinal axis of the aircraft. As forward airspeed builds, lift would be generated by the airfoil starting at a high AOA. Stall characteristics of the wing would be reduced by the elimination of the separation bubble due to the crossflow fan intake.

Thrust vectoring in a hover could be accomplished by flaps on the upper and lower sides of the trailing edge. These flaps would move in concert with each other to provide longitudinal control. Thrust vectoring flaps could also move in opposition to each other, forming a linear “nozzle”. This would allow throttling of the crossflow fan for optimum performance. Lateral control in a hover could be accomplished by a system of vanes located in the exhaust duct. Yaw control could easily be accomplished by allowing left- and right-side fan-in-wing sections to rotate independently. Other controls would be as in current fixed-wing aircraft.

Use of two engines would allow the fore and aft fan-in-wing sections to be powered separately. This would provide emergency operation in forward-flight mode in case of a single engine failure. The aircraft could be landed at any suitable airport. In the case of dual engine failure, the aircraft would have the ability to glide as with other fixed-wing aircraft.

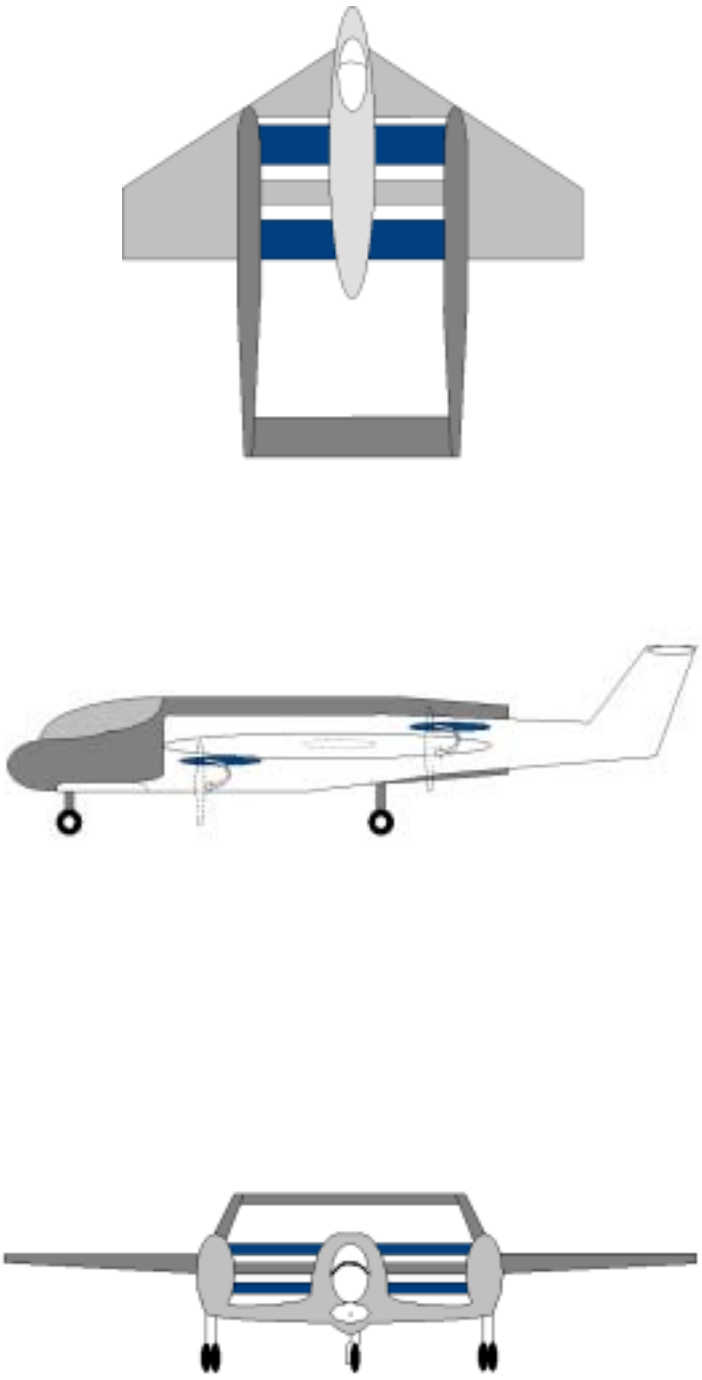

Figure 47 Three-View of Suggested V/STOL Aircraft Configuration Utilizing Fan-In-Wing Concept

THIS PAGE INTENTIONALLY LEFT BLANK

V. CONCLUSIONS AND RECOMMENDATIONS

A. EXPERIMENTAL APPARATUS

The Crossflow Fan Test Assembly (CFTA) was constructed and successfully operated. Comparison of results with the Vought Systems Division (VSD) experimental data confirmed the validity of the design of the fan used in the present research. Repeatability of the results was demonstrated in the course of seven different performance runs. The resulting data were extremely compact and exhibited little variance despite the different ambient conditions on the various dates on which data were taken. In addition to validation of the VSD study, data were provided for the 1,000-5,000 RPM range. This was critical in that it revealed a higher thrust-to-power ratio than that observed in the higher RPM range tested by VSD. A wide range of raw and reduced data were taken for this important speed range. Flow visualization results also supported the conclusions drawn from the experimental data. Similar streamlines and flow patterns to those predicted in the VSD study were noted in the present results.

The data acquisition system proved extremely effective and allowed the collection of both raw and reduced data in minimum time. However, further data reduction became necessary due to noticeable variations in TTR mass flow for a given speed. This was accomplished with Excel, but could easily be incorporated into the HPVEE program to eliminate post-processing altogether. Additionally, the HPVEE program should be rewritten to remove references to TTR measurements, as these became irrelevant through the use of dimensionless velocity and mass-averaging to calculate crossflow fan parameters independently.

A greater number of combination probes should be used in the crossflow fan inlet. This would allow a more accurate average of total temperature and pressure to be determined. Additionally, it would allow the inlet flow parameters to be mass-averaged.

The inner plate of the front blanking plate should be instrumented with a directional combination probe. This could be mounted through the instrumentation port already incorporated in the plate. The inner plate should be equipped with an actuator in

order to allow rotation of the plate for multiple measurements of pressure within the fan during a single run.

Seals should be considered for use between the Plexiglas-to-Plexiglas and Plexiglas-to-Aluminum interfaces on the viewing window to minimize air flow and dye loss through these areas. Labyrinth seals may perform this function, but may require permanent changes to the Plexiglas. Subsequent changes to the test assembly cavity shapes or arrangements would likely require fabrication of a new viewing window and blanking plate.

Experiments with the CFTA should continue in an effort to determine optimum configurations for various lift and propulsion applications. The most immediate need is to develop a throttling device for the crossflow fan exhaust duct. This will allow a true compressor map to be obtained for the crossflow fan, and will help suggest the optimum operating conditions for any particular regime of flight. Subsequently, efforts should center around determining optimum fan dimensions, number of blades, solidity, blade shape, and blade angle. Finally, different cavity, intake, and exhaust configurations should be tested.

B. NUMERICAL SOLUTION

A 15-bladed crossflow fan computational grid was created and mated with a grid modeled after the cavities, intake, and exhaust used in the CFTA. An incompressible solution was achieved at a fan speed of 3,000 RPM in a reasonable computational time. The results were similar to those obtained through experimental and flow visualization efforts.

An incompressible solution using a 30-bladed fan should be pursued immediately. A video card with more memory would be useful in this endeavor, as would the use of faster computers which will soon become available. Following this, a compressible solution should be attempted. This would facilitate an increase in fan speed up to 5,000 RPM or perhaps greater. A 3D solution will eventually be called for. A 3,000 RPM incompressible approach to this problem is recommended to spare computational time.

Testing of alternate intake, cavity, or exhaust duct shapes in an incompressible, 3,000-RPM solution will not require a great deal of effort. Since the computational grid was created in a modular fashion in the PFLO input file, it will not be difficult to make changes to the existing cavity shapes or locations without significantly affecting the remainder of the grid. Changes to the blade shape and number will require more effort, but could be accomplished in a similar manner.

C. FAN-IN-WING CONCEPT

Numerical simulation of a theoretical wing section augmented with a crossflow fan was performed. The results suggested a significant increase in lift may be obtained using a crossflow fan in a wing section as a lift / propulsion device. One possible configuration that implements this concept was introduced.

Refinement of the numerical solution should proceed by incorporation of a rotating crossflow fan grid inside the existing wing section; fabrication of a scale augmented wing section for testing in a low-speed wind tunnel; and construction of a flying model. The numerical simulation could be accomplished in a short period of time by modification of the numerical simulation used in Section III. A wing section for wind tunnel testing should be constructed, complete with a rotating crossflow fan. This would allow validation of the fan-in-wing concept as well as optimization of the intake, cavity, and exhaust duct configuration. A small-scale flying model would be more difficult and expensive to produce, but it is possible and would be the next logical step in attempting to prove the worth of the crossflow fan in a lift / propulsion application.

THIS PAGE INTENTIONALLY LEFT BLANK

LIST OF REFERENCES

1. Studevan, C. C., “Design of a Cold-Flow Test Facility for the High-Pressure Fuel Turbopump Turbine of the Space Shuttle Main Engine”, Master’s Thesis, Naval Postgraduate School, Monterey, California, December 1993.

2. Rutkowski, R. J., “Cold-Flow Simulation of the Alternate Turbopump Development Turbine of the Space Shuttle Main Engine High Pressure Fuel Turbopump”, Master’s Thesis, Naval Postgraduate School, Monterey, California, March 1994.

3. Greco, P. A., "Turbine Performance Mapping of the Space Shuttle Main Engine High-Pressure Fuel Turbopump", Master's Thesis, Naval Postgraduate School, Monterey, California, September 1995.

4. Southward, J. D., "Laser Doppler Velocimetry in the Space Shuttle Main Engine High-Pressure Fuel Turbopump", Master's Thesis, Naval Postgraduate School, Monterey, California, March 1998.

5. White, F. M., *Fluid Mechanics*, WCB/McGraw-Hill, San Francisco, 1999.

6. Naval Air Systems Command Contract N00019-74-C-0434, *Multi-Bypass Ratio Propulsion System Technology Development*, Vol. I-III, Vought Systems Division, LTV Aerospace Corporation, 24 July 1975.

7. Moller International, "The Skycar", [http://www.moller.com], 2003.

8. Gossett, D. H., "Investigation of Cross Flow Fan Propulsion for a Lightweight VTOL Aircraft", Master's Thesis, Naval Postgraduate School, Monterey, California, December 2000.

9. Peebles, Patrick, “Fanwing Pictures”, [www.fanwing.com], 2003

10. O’Brien, J. M., “Transonic Compressor Test Rig Rebuild and Initial Results with the Sanger Stage”, Master’s Thesis, Naval Postgraduate School, Monterey, California, June 2000.

11. Vavra, M. H., "Determination of Flow Rates of Allis-Chalmers Axial Flow Compressor VA-312 of Propulsion Laboratories by Means of Square-Edged Orifices", Naval Postgraduate School, Monterey, California, TN 63T-2 1963.

12 Shreeve, R. P., Class Notes, AA3451 Propulsion, Naval Postgraduate School, Monterey, California, 2001

13 University of Illinois at Urbana-Champaign, “Airfoil Coordinates Database”, [http://www.aae.uiuc.edu/m-selig/ads/coord_database.html], 2003

APPENDIX A DATA ACQUISITION PROGRAM

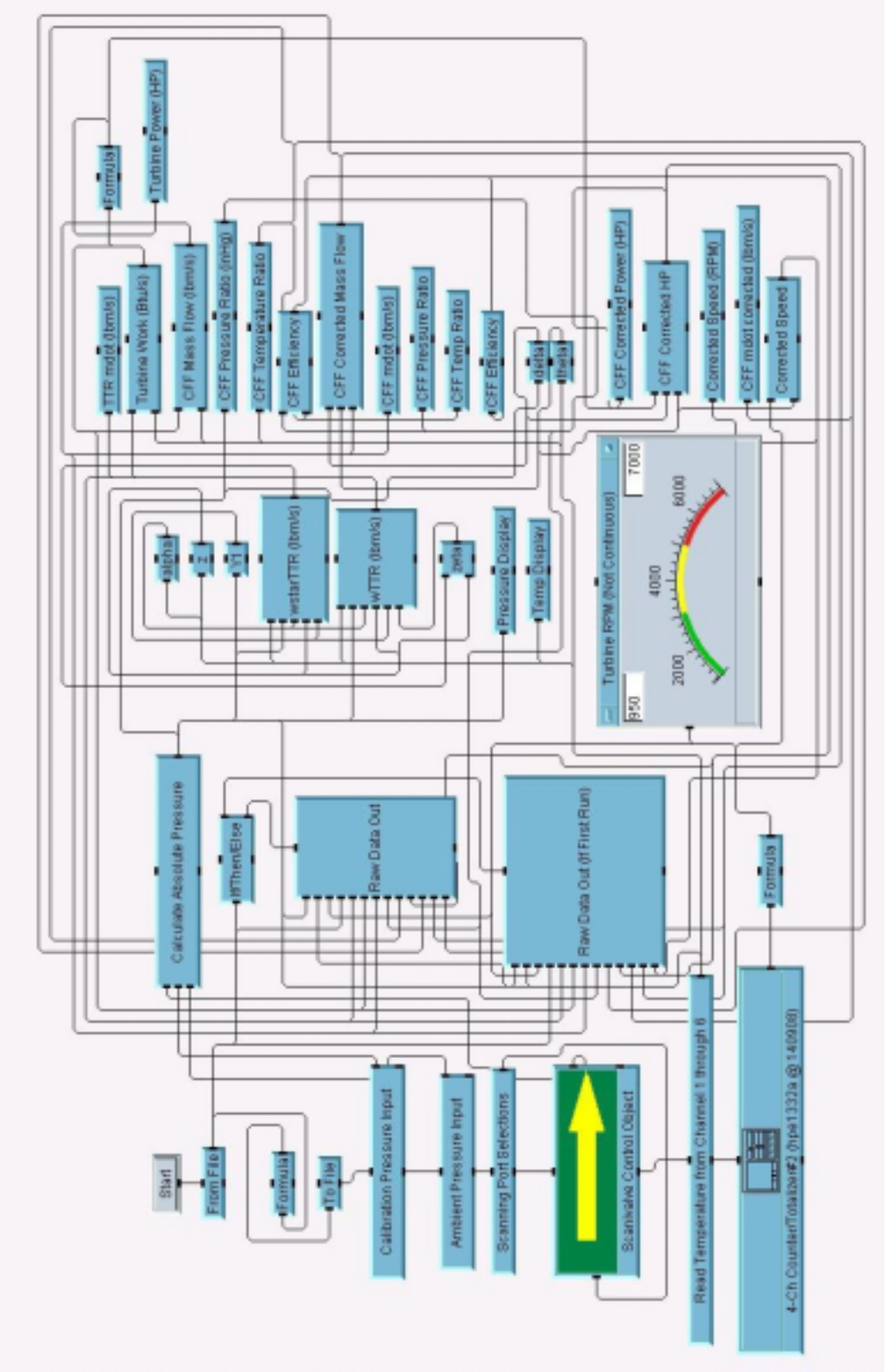

Figure A1. HPVEE Data Acquisition Program CFFdata.vee

THIS PAGE INTENTIONALLY LEFT BLANK

APPENDIX B CROSSFLOW FAN GRID GENERATION CODE

B1. MATLAB BLADE PASSAGE VERTEX GENERATION CODE

```
%   Program to draw the CFF airfoil profile and calculate the machine coordinates
%   of a 1/4" ball cutter tool
%
clear all
close all
%
%   Camber line first
%
%
thetac=linspace(80,165.22,100);
%   Center point of camber arc
xc0=4.4770;
yc0=1.4294;
rc0=1.4515;
%
xc=xc0-rc0*cos(thetac*pi/180);
yc=yc0-rc0*sin(thetac*pi/180);
figure(1)
plot(xc,yc,'b.')
%
%   Now the pressure side
%
thetap=linspace(85.65,159.58,100);
%   Center point of pressure arc
xp0=4.3454;
yp0=1.6305;
rp0=1.6102;
%
xp=xp0-rp0*cos(thetap*pi/180);
yp=yp0-rp0*sin(thetap*pi/180);
hold on
plot(xp,yp,'r.')
%
%   Then the suction side
%
thetas=linspace(74.54,170.48,100);
%   Center point of suction arc
xs0=4.5771;
ys0=1.2730;
rs0=1.3458;
%
xs=xs0-rs0*cos(thetas*pi/180);
ys=ys0-rs0*sin(thetas*pi/180);
plot(xs,ys,'g.')
%
%   So far so good! Now the leading edge
%
thetale=linspace(85.65,180+74.54,20);
%   Center point of leading edge arc
xle0=4.225;
```

```
yle0=0.000;
rle0=0.025;
%
xle=xle0+rle0*cos(thetale*pi/180);
yle=yle0+rle0*sin(thetale*pi/180);
plot(xle,yle,'m.')
%
%   Not quite there yet so lets try the trailing edge
%
thetate=linspace(159.58,-(180-170.68),20);
%   Center point of leading edge arc
xte0=5.88037;
yte0=1.05919;
rte0=0.025;
%
xte=xte0+rte0*cos(thetate*pi/180);
yte=yte0+rte0*sin(thetate*pi/180);
plot(xte,yte,'c.')
%
%   Concatenate the arrays into one for the complete airfoil
%
x=zeros(237,1);
y=zeros(237,1);
for i=1:3
   x(i)=xte(17+i);
   y(i)=yte(17+i);
end
for i=4:103
   x(i)=xs(104-i);
   y(i)=ys(104-i);
end
for i=104:120
   x(i)=xle(123-i);
   y(i)=yle(123-i);
end
for i=121:219
   x(i)=xp(i-120);
   y(i)=yp(i-120);
end
for i=220:237
   x(i)=xte(i-219);
   y(i)=yte(i-219);
end
%plot(x,y)
%
%         Plot the dowels on the camber line
%
thetai=linspace(0,2*pi);
plot(4.9161+0.030*cos(thetai),0.0459+0.030*sin(thetai))
%
thetai=linspace(0,2*pi);
plot(5.5490+0.030*cos(thetai),0.4508+0.030*sin(thetai))
%

figure(2)
```

```
plot(x,y)
%
%   Draw the passage between the blades
%
fid = fopen('vreadb1.txt','w t');
for i = 1:111
   xpass(i) = x(i);
   ypass(i) = y(i);
   Vreadb1(i,:)=[i xpass(i) ypass(i)];
   fprintf(fid,'    %5.4f    %5.4f    %5.4f\n',Vreadb1(i,1), Vreadb1(i,2), Vreadb1(i,3));
end
Vreada=[Vreadb1(:,2), Vreadb1(:,3)]
fclose(fid)
fid = fopen('vreadb2.txt','w t');
for i = 111:237
   xpass(i+1) =  x(i)*cos(pi*24/180)+y(i)*sin(pi*24/180);
   ypass(i+1) =- x(i)*sin(pi*24/180)+y(i)*cos(pi*24/180);
   Vreadb2(i+1,:)=[i+1 xpass(i+1) ypass(i+1)];
   fprintf(fid,'    %5.4f    %5.4f    %5.4f\n',Vreadb2(i+1,1), Vreadb2(i+1,2), Vreadb2(i+1,3));
end
for j=111:237
   Vreadb(j-110,:)=[Vreadb2(j+1,2), Vreadb2(j+1,3)];
end
fclose(fid)
figure(3)
plot(xpass,ypass,'r.')
axis([3 7 -2 2])
%
%         Plot the rotor endwall
%
thetai=linspace(pi*24/180,0);
hold on
plot(4.2*cos(thetai),-4.2*sin(thetai),'b.')

%
offset = atan(y(1)/x(1));
thetai=linspace(pi*24/180,0);
plot(6*cos(thetai-offset),-6*sin(thetai-offset),'g.')
%

Vread1=[xpass' ypass'];
Vreadc=[4.2*cos(thetai)',-4.2*sin(thetai)'];
Vreadc=flipud(Vreadc)
Vreadd=[6*cos(thetai-offset)',-6*sin(thetai-offset)'];

Vr=[Vreada;Vreadc;Vreadb;Vreadd];
for i=1:length(Vr)
   Vread(i,:)=[i Vr(i,:)];
end
```

B2. GRID GENERATION FLO++ INPUT CODE

```
reset
// *** crossflowfan : Flo++ input file
// *** Insert your Flo++ code here
reset
csys 0
#def span 1.5
#def spnblk 1
#def chordblk 30
#def cbr 1.2
#def cscblk 20
#def cscr 1.2
#def clnc 6.13
// *** Mesh generation ******************************
////Build fan passage splines//////////////////////
//vread c:\vread15mod.txt 0 ALL
vread c:\vread15mod.txt 0 ALL
vp
vset news vlist 338 339
vmerge vset 0.0001
vset news vlist 111 112
vmerge vset 0.0001
vset news vlist 211 212

vmax

spline 1 vran vmax - 436 vmax - 325 1
#def bp1 vmax - 378
splmodify 1 modify bp1 -bp1
spline 2 vran vmax - 325 vmax - 225 1
#def bp2 vmax - 277
splmodify 2 modify bp2 -bp2
spline 3 vran vmax - 225 vmax - 99 1
#def bp3 vmax - 162
splmodify 3 modify bp3 -bp3
spline 4 vlist vmax - 99 vmax - 89 vmax - 79 vmax - 69 vmax - 59 vmax - 49 vmax - 39 vmax - 29 vmax -
        19 vmax - 9 vmax - 436
#def bp4 vmax - 49
splmodify 4 modify bp4 -bp4
sp

vset all
vcopy 2 vmax vset span 0 0
vp

spline 5 vran vmax - 436 vmax - 325 1
#def bp5 vmax - 378
splmodify 5 modify bp5 -bp5
spline 6 vran vmax - 325 vmax - 225
#def bp6 vmax - 277
splmodify 6 modify bp6 -bp6
spline 7 vran vmax - 225 vmax - 99 1
#def bp7 vmax - 162
```

```
splmodify 7 modify bp7 -bp7
spline 8 vlist vmax - 99 vmax - 89 vmax - 79 vmax - 69 vmax - 59 vmax - 49 vmax - 39 vmax - 29 vmax -
        19 vmax - 9 vmax - 436
#def bp8 vmax - 49
splmodify 8 modify bp8 -bp8
sp

vmax

/////Build fan passage block//////////////////////
cgro 1
block 1 vmax - 873 vmax - 762 vmax - 662 vmax - 536 vmax - 436 vmax - 325 vmax - 225 vmax - 99
blplot
blfactors 1 chordblk cscblk spnblk 1
blcd 1 1 chordblk / 2 cbr chordblk / 2 1 / cbr
blcd 1 2 chordblk / 2 cbr chordblk / 2 1 / cbr
blcd 1 3 chordblk / 2 cbr chordblk / 2 1 / cbr
blcd 1 4 chordblk / 2 cbr chordblk / 2 1 / cbr
blcd 1 5 cscblk / 2 cscr cscblk / 2 1 / cscr
blcd 1 6 cscblk / 2 cscr cscblk / 2 1 / cscr
blcd 1 7 cscblk / 2 cscr cscblk / 2 1 / cscr
blcd 1 8 cscblk / 2 cscr cscblk / 2 1 / cscr

blex 1
view 1 0 0
cp

local 2 cyli 0 0 0 0 90 0 0
csys 2
mcrea 4.15 4.2 2 66 78.3752 10 0 span spnblk 1 cscr 1
mcrea 4.15 4.2 2 78.3752 90 10 0 span spnblk 1 1 / cscr 1

cp
mcrea 6 6.1 3 76.2039 88.0825 10 0 span spnblk 1.5 cscr 1
mcrea 6 6.1 3 88.0825 100.2038 10 0 span spnblk 1.5 1 / cscr 1
cp
save 12

resu 12
// Louis
// Here I have decided to vmerge and compress when finish
// with cell group 1
spldelete all
bldelete all
cset news cgro 1
vset news cset
vset unsel
vdel vset
vset all
cp
vcdist all
// VCDIST tell us that we should not merge closer than aprox 0.002181
vmerge all 0.002
vcomp all
vcdist all
```

```
cp

/////Copy fan passage and build complete fan///////
cset news cgro 1
local 2 cyli 0 0 0 0 90 0 0
csys 2
cgro 2
// Louis: Copy in 1 action
mcopy 15 vmax 0 24 0 active
vcdist all
vmerge all 0.0001
vcomp all
vcdist all

cset all
cgro 0
cgmodify all

save 13

resu 13

/////Build fan clearance layer//////////////////////
csys 2
cgro 2
mcrea 6.1 clnc 3 0 360 360 0 span spnblk 1 1 1

/////Build Intake/////////////////////////////////////////////////////////////
/////Intake First Block/////////////////


csys 3

spldelete all
v vmax + 1 0 4.8676 3.726
v vmax + 1 0 4.8852 3.7369
v vmax + 1 0 4.9001 3.7228
v vmax + 1 0 4.9211 3.7142
v vmax + 1 0 4.9415 3.7136
v vmax + 1 0 4.9571 3.7183

csys 2

v vmax + 1 6.1967 125 0
v vmax + 1 6.1967 120 0
v vmax + 1 6.1967 115 0
v vmax + 1 6.1967 110 0
v vmax + 1 6.1967 105 0
v vmax + 1 6.1967 100 0
v vmax + 1 6.1967 95 0
v vmax + 1 6.1967 90 0
v vmax + 1 6.1967 85 0
v vmax + 1 6.1967 80 0
v vmax + 1 6.1967 75 0
v vmax + 1 6.1967 70 0
```

```
v vmax + 1 6.1967 65 0
v vmax + 1 6.1967 60 0
v vmax + 1 6.1967 55 0
v vmax + 1 6.1967 50 0
v vmax + 1 6.1967 45 0
v vmax + 1 6.1967 40 0
v vmax + 1 6.1967 35 0
v vmax + 1 6.1967 30 0
v vmax + 1 6.1967 25 0

csys 3

v vmax + 1 0 2.4157 -5.6827
v vmax + 1 0 2.4057 -5.6731
v vmax + 1 0 2.3921 -5.6666
v vmax + 1 0 2.3789 -5.6648
v vmax + 1 0 2.3645 -5.6673
v vmax + 1 0 2.3603 -5.6574

csys 2

v vmax + 1 clnc 25 0
v vmax + 1 clnc 30 0
v vmax + 1 clnc 35 0
v vmax + 1 clnc 40 0
v vmax + 1 clnc 45 0
v vmax + 1 clnc 50 0
v vmax + 1 clnc 55 0
v vmax + 1 clnc 60 0
v vmax + 1 clnc 65 0
v vmax + 1 clnc 70 0
v vmax + 1 clnc 75 0
v vmax + 1 clnc 80 0
v vmax + 1 clnc 85 0
v vmax + 1 clnc 90 0
v vmax + 1 clnc 95 0
v vmax + 1 clnc 100 0
v vmax + 1 clnc 105 0
v vmax + 1 clnc 110 0
v vmax + 1 clnc 115 0
v vmax + 1 clnc 120 0
v vmax + 1 clnc 125 0

vmax
vp

spldelete all
#def bp1 vmax - 52
spline 1 vlist vmax - 53 -bp1 vmax - 51 vmax - 50 vmax - 49 vmax - 48
spline 2 vran vmax - 48 vmax - 26 1
#def bp3 vmax - 22
spline 3 vlist  vmax - 26 vmax - 25 vmax - 24 vmax - 23 -bp3 vmax - 21
spline 4 vlist vmax - 21 vmax - 20 vmax - 19 vmax - 18 vmax - 17 vmax - 16 vmax - 15 vmax - 14 vmax -
        13 vmax - 12 vmax - 11 vmax - 10 vmax - 9 vmax - 8 vmax - 7 vmax - 6 vmax - 5 vmax - 4 vmax
        - 3 vmax - 2 vmax - 1 vmax vmax - 53
```

```
sp

csys 3
vcopy 2 54 vran vmax - 53 vmax 1 span 0 0
vp

#def bp5 vmax - 52
spline 5 vlist vmax - 53 -bp5 vmax - 51 vmax - 50 vmax - 49 vmax - 48
spline 6 vran vmax - 48 vmax - 26 1
#def bp7 vmax - 22
spline 7 vlist  vmax - 26 vmax - 25 vmax - 24 vmax - 23 -bp7 vmax - 21
spline 8 vlist vmax - 21 vmax - 20 vmax - 19 vmax - 18 vmax - 17 vmax - 16 vmax - 15 vmax - 14 vmax -
          13 vmax - 12 vmax - 11 vmax - 10 vmax - 9 vmax - 8 vmax - 7 vmax - 6 vmax - 5 vmax - 4 vmax
          - 3 vmax - 2 vmax - 1 vmax vmax - 53
sp
vmax

bldelete all
block 9 vmax - 48 vmax - 26 vmax - 21 vmax - 53 vmax - 102 vmax - 80 vmax - 75 vmax - 107
blfactors 9 50 5 spnblk 3

blex 9


/////Intake Second Block//////////////////////////////
vset none

csys 3
v vmax + 1 0 4.9571 3.7183
v vmax + 1 0 5.0204 3.7809
v vmax + 1 0 5.0811 3.8448
v vmax + 1 0 5.1426 3.9136
v vmax + 1 0 5.2094 3.9943
v vmax + 1 0 5.4164 4.2939
v vmax + 1 0 5.6144 4.6854
v vmax + 1 0 5.7769 5.1999
v vmax + 1 0 5.8362 5.7068
v vmax + 1 0 5.7902 6.2869
v vmax + 1 0 5.6351 6.9151
v vmax + 1 0 5.2369 7.9234
v vmax + 1 0 3.35 11.56
v vmax + 1 0 -3.007 23.8109////
//v vmax + 1 0 9.16 6.56 //Adjusted point from z=11.56
//v vmax + 1 0 11.16 2 //Added to adjust grid
//v vmax + 1 0 11.16 -6.56 //Added for smoothness
csys 2
v vmax + 1 24 180 0
v vmax + 1 24 170 0
v vmax + 1 24 160 0
v vmax + 1 24 150 0
v vmax + 1 24 140 0
v vmax + 1 24 130 0
v vmax + 1 24 120 0
v vmax + 1 24 110 0
v vmax + 1 24 100 0
```

```
v vmax + 1 24 90 0
v vmax + 1 24 80 0
v vmax + 1 24 70 0
v vmax + 1 24 60 0
//v vmax + 1 24 160 0////
csys 3
v vmax + 1 0 19.3968 -14.1337////
v vmax + 1 0 9.16 -11.05
v vmax + 1 0 7.07 -10.42
v vmax + 1 0 4.26 -8.21
v vmax + 1 0 2.78 -6.41
v vmax + 1 0 2.53 -6.00 //added for continuity
v vmax + 1 0 2.4157 -5.6827

csys 2

v vmax + 1 6.1967 125 0
v vmax + 1 6.1967 120 0
v vmax + 1 6.1967 115 0
v vmax + 1 6.1967 110 0
v vmax + 1 6.1967 105 0
v vmax + 1 6.1967 100 0
v vmax + 1 6.1967 95 0
v vmax + 1 6.1967 90 0
v vmax + 1 6.1967 85 0
v vmax + 1 6.1967 80 0
v vmax + 1 6.1967 75 0
v vmax + 1 6.1967 70 0
v vmax + 1 6.1967 65 0
v vmax + 1 6.1967 60 0
v vmax + 1 6.1967 55 0
v vmax + 1 6.1967 50 0
v vmax + 1 6.1967 45 0
v vmax + 1 6.1967 40 0
v vmax + 1 6.1967 35 0
v vmax + 1 6.1967 30 0
v vmax + 1 6.1967 25 0
vp
vmax



spldelete all
spline 1 vran vmax - 54 vmax - 41 1
spline 2 vran vmax - 41 vmax - 27 1
spline 3 vran vmax - 27 vmax - 21 1
spline 4 vlist vmax - 21 vmax vmax - 1 vmax - 2 vmax - 3 vmax - 4 vmax - 5 vmax - 6 vmax - 7 vmax - 8
        vmax - 9 vmax - 10
spline 4 vlist vmax - 11 vmax - 12 vmax - 13 vmax - 14 vmax - 15 vmax - 16 vmax - 17 vmax - 18 vmax -
        19 vmax - 20 vmax - 54
sp
csys 3
vcopy 2 55 vran vmax - 54 vmax 1 span 0 0
vp
```

```
spline 5 vran vmax - 54 vmax - 41 1
spline 6 vran vmax - 41 vmax - 27 1
spline 7 vran vmax - 27 vmax - 21 1
spline 8 vlist vmax - 21 vmax vmax - 1 vmax - 2 vmax - 3 vmax - 4 vmax - 5 vmax - 6 vmax - 7 vmax - 8
        vmax - 9 vmax - 10
spline 8 vlist vmax - 11 vmax - 12 vmax - 13 vmax - 14 vmax - 15 vmax - 16 vmax - 17 vmax - 18 vmax -
        19 vmax - 20 vmax - 54
sp
vmax
bldelete all
block 10 vmax - 54 vmax - 41 vmax - 27 vmax - 21 vmax - 109 vmax - 96 vmax - 82 vmax - 76
blfactors 10 20 50 spnblk 4
blcd 10 1 20 1.1
blcd 10 4 20 1.1
blcd 10 2 20 1 / 1.1
blcd 10 3 20 1 / 1.1
blex 10

cset news cgro 4
cp
cset cgro 3

#def cm1 12310
/////Build inner fan mesh//////////////////////////
#def vm1 vmax
cgro 1
csys 2
v vmax + 1 3 135 0
v vmax + 1 4.15 135 0
v vmax + 1 4.15 125 0
v vmax + 1 4.15 115 0
v vmax + 1 4.15 105 0
v vmax + 1 4.15 95 0
v vmax + 1 4.15 85 0
v vmax + 1 4.15 75 0
v vmax + 1 4.15 65 0
v vmax + 1 4.15 55 0
v vmax + 1 4.15 45 0
v vmax + 1 3 45 0
vp
spline 9 vlist vmax - 11 vmax - 10
spline 10 vran vmax - 10 vmax - 1 1
spline 11 vlist vmax - 1 vmax
spline 12 vlist vmax vmax - 11
sp
vset none
vset news vran vmax - 11 vmax 1
vcopy 2 12 vset 0 0 span
vp

spline 13 vlist vmax - 11 vmax - 10
spline 14 vran vmax - 10 vmax - 1 1
spline 15 vlist vmax - 1 vmax
spline 16 vlist vmax vmax - 11
sp
```

```
block 2 vmax - 23 vmax - 22 vmax - 10 vmax - 11 vmax - 12 vmax - 13 vmax - 1 vmax
blplot
blfactors 2 10 spnblk 30 1
blcd 2 1 10 1 / 1.4
blcd 2 2 10 1 / 1.4
blcd 2 3 10 1.4
blcd 2 4 10 1.4

blex 2

cset cgro 1

view 1 0 0

vset news cset
vp
cset news cgro 1


#def vm2 vmax - vm1

mcopy 4 vm2 0 90 0 active
cset news cgro 1
cp

/////Build inner fan mesh center block//////////////
vmax
csys 0
cgro 1
mcrea 0 span spnblk -2.12132 2.12132 30 -2.12132 2.12132 30 1 1 1
cset cgro 1
cp


vset news cset
vp
vmerge vset
csys 0
/////Build LP cavity//////////////////////////
/////LP First Block////////////////
vset none
vset news
csys 3
v vmax + 1 0 2.3603 -5.6574
v vmax + 1 0 2.3645 -5.6673
v vmax + 1 0 2.3516 -5.6744
v vmax + 1 0 2.3407 -5.6866
v vmax + 1 0 2.3344 -5.7035
v vmax + 1 0 2.3351 -5.7205
vp
csys 2
v vmax + 1 6.1787 20 0
v vmax + 1 6.1787 15 0
v vmax + 1 6.1787 10 0
v vmax + 1 6.1787 5 0
```

```
v vmax + 1 6.1787 0 0
v vmax + 1 6.1787 -5 0
v vmax + 1 6.1787 -10 0
v vmax + 1 6.1787 -15 0
v vmax + 1 6.1787 -20 0
v vmax + 1 6.1787 -25 0
v vmax + 1 6.1787 -30 0
v vmax + 1 6.1787 -35 0
v vmax + 1 6.1787 -40 0
v vmax + 1 6.1787 -45 0
v vmax + 1 6.1787 -50 0
vp
csys 3
v vmax + 1 0 -4.8676 -3.8054
v vmax + 1 0 -4.8818 -3.7668
v vmax + 1 0 -4.8459 -3.7542
vp
csys 2
v vmax + 1 clnc -50 0
v vmax + 1 clnc -45 0
v vmax + 1 clnc -40 0
v vmax + 1 clnc -35 0
v vmax + 1 clnc -30 0
v vmax + 1 clnc -25 0
v vmax + 1 clnc -20 0
v vmax + 1 clnc -15 0
v vmax + 1 clnc -10 0
v vmax + 1 clnc -5 0
v vmax + 1 clnc 0 0
v vmax + 1 clnc 5 0
v vmax + 1 clnc 10 0
v vmax + 1 clnc 15 0
v vmax + 1 clnc 20 0
vp

vmax
spldelete all
#def bp1 vmax - 37
spline 1 vlist vmax - 38 -bp1 vmax - 36 vmax - 35 vmax - 34 vmax - 33
spline 2 vran vmax - 33 vmax - 17 1
#def bp3 vmax - 16
spline 3 vlist vmax - 17 -bp3 vmax - 15
spline 4 vlist vmax - 15 vmax - 14 vmax - 13 vmax - 12 vmax - 11 vmax - 10 vmax - 9 vmax - 8 vmax - 7
        vmax - 6 vmax - 5 vmax - 4 vmax - 3 vmax - 2 vmax - 1 vmax vmax - 38
sp

vcopy 2 39 vset 0 0 span
vp
#def bp5 vmax - 37
spline 5 vlist vmax - 38 -bp5 vmax - 36 vmax - 35 vmax - 34 vmax - 33
spline 6 vran vmax - 33 vmax - 17 1
#def bp7 vmax - 16
spline 7 vlist vmax - 17 -bp7 vmax - 15
spline 8 vlist vmax - 15 vmax - 14 vmax - 13 vmax - 12 vmax - 11 vmax - 10 vmax - 9 vmax - 8 vmax - 7
        vmax - 6 vmax - 5 vmax - 4 vmax - 3 vmax - 2 vmax - 1 vmax vmax - 38
```

sp

vmax
bldelete all
block 11 vmax - 38 vmax - 33 vmax - 17 vmax - 15 vmax - 77 vmax - 72 vmax - 56 vmax - 54
blplot
blfactors 11 5 30 spnblk 5
blex 11

/////LP Second Block//////////////////

vset news none

csys 3
v vmax + 1 0 2.3351 -5.7205
v vmax + 1 0 2.3576 -5.8582
v vmax + 1 0 2.3791 -6.0989
v vmax + 1 0 2.3753 -6.3741
v vmax + 1 0 2.3418 -6.649
v vmax + 1 0 2.2034 -7.0359
v vmax + 1 0 1.8774 -7.4162
v vmax + 1 0 1.4134 -7.7727
v vmax + 1 0 .4909 -7.9588
v vmax + 1 0 -.2726 -7.9034
v vmax + 1 0 -1.2811 -7.5651
v vmax + 1 0 -2.0786 -7.1576
v vmax + 1 0 -2.8812 -6.5783
v vmax + 1 0 -3.5716 -5.8094
v vmax + 1 0 -4.21 -4.9431
v vmax + 1 0 -4.6805 -4.188
v vmax + 1 0 -4.8676 -3.8054
v vmax + 1 0 -4.8676 -3.8054

csys 2

v vmax + 1 6.1787 20 0
v vmax + 1 6.1787 15 0
v vmax + 1 6.1787 10 0
v vmax + 1 6.1787 5 0
v vmax + 1 6.1787 0 0
v vmax + 1 6.1787 -5 0
v vmax + 1 6.1787 -10 0
v vmax + 1 6.1787 -15 0
v vmax + 1 6.1787 -20 0
v vmax + 1 6.1787 -25 0
v vmax + 1 6.1787 -30 0
v vmax + 1 6.1787 -35 0
v vmax + 1 6.1787 -40 0
v vmax + 1 6.1787 -45 0
v vmax + 1 6.1787 -50 0

csys 3
v vmax + 1 0 2.3351 -5.7205
vmax
vp

```
spldelete all
spline 1 vran vmax - 33 vmax - 17 1
spline 2 vlist vmax - 16 vmax - 1 vmax - 2 vmax - 3 vmax - 4 vmax - 5 vmax - 6 vmax - 7 vmax - 8 vmax -
        9 vmax - 10 vmax - 11 vmax - 12 vmax - 13 vmax - 14 vmax - 15 vmax
sp

csys 2

vcopy 2 34 vset 0 0 span
vp
vmax
spline 3 vran vmax - 33 vmax - 17 1
spline 4 vlist vmax - 16 vmax - 1 vmax - 2 vmax - 3 vmax - 4 vmax - 5 vmax - 6 vmax - 7 vmax - 8 vmax -
        9 vmax - 10 vmax - 11 vmax - 12 vmax - 13 vmax - 14 vmax - 15 vmax
sp

bldelete all
block 12 vmax - 33 vmax - 17 vmax - 16 vmax vmax - 67 vmax - 51 vmax - 50 vmax - 34
blfactors 12 30 10 spnblk 6
blcd 12 1 30 1 / 1.01
blcd 12 4 30 1 / 1.01
blex 12
cset news cgro 6
cp
/////Build Exhaust Wall////////////////////////////////////////////////////////
/////First Block//////////////////
save 22

resu 22
vset none

cset news
cgro 4
vset none
#def vmo vmax

csys 3
v vmax + 1 0 -4.8459 -3.7542
v vmax + 1 0 -4.8818 -3.7668
v vmax + 1 0 -4.8863 -3.7626
v vmax + 1 0 -4.9088 -3.7547
v vmax + 1 0 -4.9347 -3.7653
v vmax + 1 0 -4.9454 -3.7909
vp
csys 2
v vmax + 1 6.2312 305 0
v vmax + 1 6.2312 300 0
v vmax + 1 6.2312 295 0
v vmax + 1 6.2312 290 0
v vmax + 1 6.2312 285 0
v vmax + 1 6.2312 280 0
v vmax + 1 6.2312 275 0
v vmax + 1 6.2312 270 0
v vmax + 1 6.2312 265 0
v vmax + 1 6.2312 260 0
```

```
v vmax + 1 6.2312 255 0
v vmax + 1 6.2312 250 0
v vmax + 1 6.2312 245 0
v vmax + 1 6.2312 240 0
v vmax + 1 6.2312 235 0
v vmax + 1 6.2312 230 0
v vmax + 1 6.2312 225 0
v vmax + 1 6.2312 220 0
v vmax + 1 6.2312 215 0
v vmax + 1 6.2312 210 0
v vmax + 1 6.2312 205 0
v vmax + 1 6.2312 200 0
v vmax + 1 6.2312 195 0
v vmax + 1 6.2312 190 0

csys 3
v vmax + 1 0 -1.0097 6.1489
v vmax + 1 0 0.0089 6.1376
v vmax + 1 0 0.0089 6.13

csys 2
v vmax + 1 6.13 305 0
v vmax + 1 6.13 300 0
v vmax + 1 6.13 295 0
v vmax + 1 6.13 290 0
v vmax + 1 6.13 285 0
v vmax + 1 6.13 280 0
v vmax + 1 6.13 275 0
v vmax + 1 6.13 270 0
v vmax + 1 6.13 265 0
v vmax + 1 6.13 260 0
v vmax + 1 6.13 255 0
v vmax + 1 6.13 250 0
v vmax + 1 6.13 245 0
v vmax + 1 6.13 240 0
v vmax + 1 6.13 235 0
v vmax + 1 6.13 230 0
v vmax + 1 6.13 225 0
v vmax + 1 6.13 220 0
v vmax + 1 6.13 215 0
v vmax + 1 6.13 210 0
v vmax + 1 6.13 205 0
v vmax + 1 6.13 200 0
v vmax + 1 6.13 195 0
v vmax + 1 6.13 190 0
// Louis added these in order to
// get a better interface between groups 2 and 7
v vmax + 1 6.13 187 0
v vmax + 1 6.13 185 0
v vmax + 1 6.13 183 0
v vmax + 1 6.13 181.5 0
#def dvm vmax - vmo
save 18

resu 18
```

```
vp

spldelete all
#def bp1 vmax - 59
spline 1 vlist vmax - 60 -bp1 vmax - 58 vmax - 57 vmax - 56 vmax - 55
#def bp2 vmax - 30
spline 2 vran vmax - 55 vmax - 29
splm 2 modi vmax - 30 vmax - 30 * -1
spline 3 vlist vmax - 29 vmax - 28
save 19

resu 19
sp
// Louis: I ran out of line lenght
// Only 256 characters allowed in one line
// so I added the vertices like below
spline 4 vlist vmax - 28 vmax * -1 vmax - 1 vmax - 2 vmax - 3 vmax - 4 vmax - 5 vmax - 6 vmax - 7 vmax
        - 8
spline 4 vlist vmax - 9 vmax - 10 vmax - 11 vmax - 12 vmax - 13 vmax - 14 vmax - 15 vmax - 16 vmax -
        17
spline 4 vlist vmax - 18 vmax - 19 vmax - 20 vmax - 21 vmax - 22 vmax - 23 vmax - 24 vmax - 25 vmax -
        26 vmax - 27 vmax - 60
sp

vcopy 2 dvm vset 0 0 span

#def bp5 vmax - 59
spline 5 vlist vmax - 60 -bp5 vmax - 58 vmax - 57 vmax - 56 vmax - 55
#def bp6 vmax - 30
spline 6 vlist vmax - 55 vmax - 54 vmax - 53 vmax - 52 vmax - 51 vmax - 50 vmax - 49 vmax - 48 vmax -
        47
spline 6 vlist vmax - 46 vmax - 45 vmax - 44 vmax - 43 vmax - 42 vmax - 41 vmax - 40 vmax - 39 vmax -
        38 vmax - 37 vmax - 36 vmax - 35 vmax - 34 vmax - 33 vmax - 32 vmax - 31 -bp6 vmax - 29
spline 7 vlist vmax - 29 vmax - 28
spline 8 vlist vmax - 28 vmax * -1 vmax - 1 vmax - 2 vmax - 3 vmax - 4 vmax - 5 vmax - 6 vmax - 7 vmax
        - 8
spline 8 vlist vmax - 9 vmax - 10 vmax - 11 vmax - 12 vmax - 13 vmax - 14 vmax - 15 vmax - 16 vmax -
        17 vmax - 18 vmax - 19 vmax - 20 vmax - 21 vmax - 22 vmax - 23 vmax - 24 vmax - 25 vmax - 26
        vmax - 27 vmax - 60
sp

bldelete all
block 13 vmax - 29 vmax - 28 vmax - 60 vmax - 55 vmax - 90 vmax - 89 vmax - 121 vmax - 116

blfactors 13 5 70 spnblk 7
blex 13
cset news cglist 7 2
VIEW      1.0000e+000     0.0000e+000     0.0000e+000
VUP       0.0000e+000     1.0000e+000     0.0000e+000
FOCAL  COORD     2.5000e-001    -6.5494e-001     6.0758e+000
SCALE  VALUE     4.0470e-001
cp
save 23

resu 23
```

```
autosc on
focal center
/////Exhaust Duct Second Block///////////////
vset none
csys 3
v vmax + 1 0 -4.9454 -3.7909
v vmax + 1 0 -7.2027 -3.7909//bp?
v vmax + 1 0 -9.46 -3.7909
vp
csys 0
local 4 cyli 0 -0.57 -2.72 0 90 0 0 0
csys 4
v vmax + 1 8.89 -90 0
v vmax + 1 8.89 -95 0
v vmax + 1 8.89 -100 0
v vmax + 1 8.89 -105 0
v vmax + 1 8.89 -110 0
v vmax + 1 8.89 -115 0
v vmax + 1 8.89 -120 0
v vmax + 1 8.89 -125 0
v vmax + 1 8.89 -130 0
v vmax + 1 8.89 -135 0
v vmax + 1 8.89 -140 0
v vmax + 1 8.89 -145 0
v vmax + 1 8.89 -150 0
v vmax + 1 8.89 -155 0
v vmax + 1 8.89 -160 0
v vmax + 1 8.89 -165 0
v vmax + 1 8.89 -170 0

csys 3
v vmax + 1 0 -1.0097 6.1489
v vmax + 1 0 -1.0097 6.1489

vp

csys 2
v vmax + 1 6.2312 305 0
v vmax + 1 6.2312 300 0
v vmax + 1 6.2312 295 0
v vmax + 1 6.2312 290 0
v vmax + 1 6.2312 285 0
v vmax + 1 6.2312 280 0
v vmax + 1 6.2312 275 0
v vmax + 1 6.2312 270 0
v vmax + 1 6.2312 265 0
v vmax + 1 6.2312 260 0
v vmax + 1 6.2312 255 0
v vmax + 1 6.2312 250 0
v vmax + 1 6.2312 245 0
v vmax + 1 6.2312 240 0
v vmax + 1 6.2312 235 0
v vmax + 1 6.2312 230 0
v vmax + 1 6.2312 225 0
v vmax + 1 6.2312 220 0
```

```
v vmax + 1 6.2312 215 0
v vmax + 1 6.2312 210 0
v vmax + 1 6.2312 205 0
v vmax + 1 6.2312 200 0
v vmax + 1 6.2312 195 0
v vmax + 1 6.2312 190 0

vp
vmax

spldelete all
spline 1 vran vmax - 45 vmax - 43 1
spline 2 vran vmax - 43 vmax - 25 1
spline 3 vlist vmax - 24 vmax vmax - 1 vmax - 2 vmax - 3 vmax - 4 vmax - 5 vmax - 6 vmax - 7 vmax - 8
spline 3 vlist vmax - 9 vmax - 10 vmax - 11 vmax - 12 vmax - 13 vmax - 14 vmax - 15 vmax - 16 vmax -
        17 vmax - 18 vmax - 19 vmax - 20 vmax - 21 vmax - 22 vmax - 23 vmax - 45
sp
vmax

save 44

resu 44
vcopy 2 46 vset 0 0 span
vp
vmax

spline 4 vran vmax - 45 vmax - 43 1
spline 5 vran vmax - 43 vmax - 25 1
spline 6 vlist vmax - 24 vmax vmax - 1 vmax - 2 vmax - 3 vmax - 4 vmax - 5 vmax - 6 vmax - 7 vmax - 8
spline 6 vlist vmax - 9 vmax - 10 vmax - 11 vmax - 12 vmax - 13 vmax - 14 vmax - 15 vmax - 16 vmax -
        17 vmax - 18 vmax - 19 vmax - 20 vmax - 21 vmax - 22 vmax - 23 vmax - 45
sp

bldelete all
block 14 vmax - 25 vmax - 24 vmax - 45 vmax - 43 vmax - 71 vmax - 70 vmax - 91 vmax - 89

blfactors 14 10 30 spnblk 8
blcd 14 5 30 1 / 1.01025
blcd 14 6 30 1 / 1.01025
blcd 14 7 30 1
blcd 14 8 30 1
blex 14

cset news cgro 8
cp

vmax


/////Build Exhaust Wall Extension//////////////////////////////////////////////////

csys 3
vset none
v vmax + 1 0 -4.9454 -3.7909
v vmax + 1 0 -7.2027 -3.7909//bp?
```

```
v vmax + 1 0 -9.46 -3.7909
v vmax + 1 0 -4.9454 -8.825
v vmax + 1 0 -7.2027 -8.825
v vmax + 1 0 -9.46 -8.825
vp

spldelete all
#def bp1 vmax - 4
spline 1 vlist vmax - 3 -bp1 vmax - 5
spline 2 vlist vmax - 5 vmax - 2
#def bp3 vmax - 1
spline 3 vlist vmax - 2 -bp3 vmax
spline 4 vlist vmax vmax - 3
sp

vcopy 2 6 vset span 0 0
vp
#def bp5 vmax - 4
spline 5 vlist vmax - 3 -bp5 vmax - 5
spline 6 vlist vmax - 5 vmax - 2
#def bp7 vmax - 1
spline 7 vlist vmax - 2 -bp7 vmax
spline 8 vlist vmax vmax - 3
sp

vmax

bldelete all
block 6 vmax - 3 vmax - 5 vmax - 2 vmax vmax - 9 vmax - 11 vmax - 8 vmax - 6
blfactors 6 10 10 spnblk 9
blex 6


/////Build HP Cavity////////////////////////////////////////////////////
/////HPC First Block///////////////
csys 0
csys 3
vset none
vset news

v vmax + 1 0 4.8676 3.726
v vmax + 1 0 4.8852 3.7369
v vmax + 1 0 4.8757 3.7578
v vmax + 1 0 4.8741 3.7775
v vmax + 1 0 4.8790 3.7954
v vmax + 1 0 4.8871 3.8086
v vmax + 1 0 4.9406 3.8754

csys 2

v vmax + 1 6.2792 175 0
v vmax + 1 6.2792 170 0
v vmax + 1 6.2792 165 0
v vmax + 1 6.2792 160 0
v vmax + 1 6.2792 155 0
```

```
v vmax + 1 6.2792 150 0//breakpoint
v vmax + 1 6.2792 145 0
v vmax + 1 6.2792 140 0
v vmax + 1 6.2792 135 0
v vmax + 1 6.2792 130 0

csys 3

v vmax + 1 0 -.0605 6.2789
v vmax + 1 0 .0075 6.2675
v vmax + 1 0 .0329 6.262
v vmax + 1 0 .053 6.249
v vmax + 1 0 .0655 6.2324
v vmax + 1 0 .0729 6.2016
v vmax + 1 0 .0676 6.1767
v vmax + 1 0 .0516 6.1543
v vmax + 1 0 .0324 6.1423
v vmax + 1 0 .0089 6.1376
v vmax + 1 0 .0089 6.13

csys 2

v vmax + 1 clnc 175 0
v vmax + 1 clnc 170 0
v vmax + 1 clnc 165 0
v vmax + 1 clnc 160 0
v vmax + 1 clnc 155 0
v vmax + 1 clnc 150 0//breakpoint
v vmax + 1 clnc 145 0
v vmax + 1 clnc 140 0
v vmax + 1 clnc 135 0
v vmax + 1 clnc 130 0
v vmax + 1 clnc 127.5 0
vp

vmax
spldelete all
#def bp1 vmax - 37
spline 1 vlist vmax - 38 -bp1 vmax - 36 vmax - 35 vmax - 34 vmax - 33 vmax - 32
spline 2 vlist vmax - 32 vmax - 22 vmax - 23 vmax - 24 vmax - 25 vmax - 26 vmax - 27 vmax - 28 vmax -
        29 vmax - 30 vmax - 31 vmax - 21
#def bp3 vmax - 12
spline 3 vlist vmax - 21 vmax - 20 vmax - 19 vmax - 18 vmax - 17 vmax - 16 vmax - 15 vmax - 14 vmax -
        13 -bp3 vmax - 11
spline 4 vlist vmax - 11 vmax - 10 vmax - 9 vmax - 8 vmax - 7 vmax - 6 vmax - 5 vmax - 4 vmax - 3 vmax
        - 2 vmax - 1 vmax vmax - 38
sp

csys 3
vcopy 2 39 vset span 0 0
vp

#def bp5 vmax - 37
spline 5 vlist vmax - 38 -bp5 vmax - 36 vmax - 35 vmax - 34 vmax - 33 vmax - 32
```

```
spline 6 vlist vmax - 32 vmax - 22 vmax - 23 vmax - 24 vmax - 25 vmax - 26 vmax - 27 vmax - 28 vmax -
        29 vmax - 30 vmax - 31 vmax - 21
#def bp7 vmax - 12
spline 7 vlist vmax - 21 vmax - 20 vmax - 19 vmax - 18 vmax - 17 vmax - 16 vmax - 15 vmax - 14 vmax -
        13 -bp7 vmax - 11
spline 8 vlist vmax - 11 vmax - 10 vmax - 9 vmax - 8 vmax - 7 vmax - 6 vmax - 5 vmax - 4 vmax - 3 vmax
        - 2 vmax - 1 vmax vmax - 38
sp

vmax

bldelete all
block 7 vmax - 21 vmax - 32 vmax - 38 vmax - 11 vmax - 60 vmax - 71 vmax - 77 vmax - 50
blfactors 7 20 10 spnblk 10
blex 7
cset news cgro 10
cp

/////HPC Second Block////////////////////////////////
vset none
csys 3

v vmax + 1 0 4.9406 3.8754
v vmax + 1 0 5.29 4.5
v vmax + 1 0 5.59 5.68
v vmax + 1 0 5.29 6.99
v vmax + 1 0 5.05 7.4156
v vmax + 1 0 4.2003 8.3185
v vmax + 1 0 3.3509 8.9136//breakpoint ?????
v vmax + 1 0 2.9006 9.1322
v vmax + 1 0 2.502 9.2577
v vmax + 1 0 1.77 9.35
v vmax + 1 0 .8759 9.221
v vmax + 1 0 0 8.84
v vmax + 1 0 -.58 8.16
v vmax + 1 0 -.79 7.39
v vmax + 1 0 -.6908 7.0132
v vmax + 1 0 -.5907 6.7994
v vmax + 1 0 -.3601 6.4987
v vmax + 1 0 -.2105 6.3704
v vmax + 1 0 -.0605 6.2789
v vmax + 1 0 -.0605 6.2789
vp

csys 2

v vmax + 1 6.2792 175 0
v vmax + 1 6.2792 170 0
v vmax + 1 6.2792 165 0
v vmax + 1 6.2792 160 0
v vmax + 1 6.2792 155 0
v vmax + 1 6.2792 150 0//breakpoint
v vmax + 1 6.2792 145 0
v vmax + 1 6.2792 140 0
v vmax + 1 6.2792 135 0
```

```
v vmax + 1 6.2792 130 0

csys 3

v vmax + 1 0 4.9406 3.8754
vp
vmax

spldelete all
spline 1 vran vmax - 30 vmax - 12 1
spline 2 vran vmax - 11 vmax 1
sp

vcopy 2 31 vset span 0 0
vp

spline 3 vran vmax - 30 vmax - 12 1
spline 4 vran vmax - 11 vmax 1
sp

bldelete all
block 8 vmax - 12 vmax - 30 vmax vmax - 11 vmax - 43 vmax - 61 vmax - 31 vmax - 42
blfactors 8 30 10 spnblk 11
blex 8
cset news cgro 11
cset all
cp

view -1 0 0
cp
////////////////////////////////////////////////////////////////////////////////////////////
////////////////////////////COMPLETE WITH STRUCTURE/////////////////////////////////////////
////////////////////////////////////////////////////////////////////////////////////////////
save 33

resu 33
/////Merge vertices in non-sliding cell groups//////////
cset none
cset news cgro 2
cset cgro 3
cset cgro 4
cset cgro 5
cset cgro 6
cset cgro 7
cset cgro 8
cset cgro 9
cset cgro 10
cset cgro 11
cp

vset news cset
vmerge vset 0.0005

cset news cgro 3
cset cgro 10
```

```
cp
vset news cset
vmerge vset 0.0001

cset news cgro 8
cset cgro 9
cp
vset news cset
vmerge vset 0.0001

save 66

resu 66
/////Find embedded cell sets//////////////////////////
cset news cgro 3
vcdis cset
cset cgro 2
cp
esfind 2 3 0.01 10 11 12

cset news cgro 2
csys 2
cset gxyzrange 5 6.13 6.135 0 22 0 span
cset gxyzrange 5 6.13 6.135 300 360 0 span
cp

cp
esfind 2 5 0.02 30 11 12

cset news cgro 5
cset cgro 6
cp
esfind 5 6 0.01 30 11 12

cset news cgro 3
cset cgro 4
cp
esfind 3 4 0.005 30 11 12

cset news cglist 2 7
csys 2
cp
esfind 2 7 0.02 30 11 12

cset news cgro 2
cset cgro 10
cp
esfind 2 10 0.05 30 11 12

cset news cgro 7
cset cgro 8
cp
esfind 8 7 0.02 10 11 12

cset news cgro 7
```

```
cset cgro 10
cp
esfind 10 7 0.0001 10 11 12

cset news cgro 7
cset cgro 5
cp
esfind 5 7 0.0001 10 11 12

cset news cgro 10
cset cgro 11
cp
esfind 10 11 0.005 30 11 12

/////Compress all vertex and cell numbers//////////////////

save 1
resu 1

// Boundaries
// Inlet
cset none
cset cgro 4
view 1 0 0
cp
bface 1 east
bset news bgro 1
bp


// Outlet
cset none
cset cgro 9
view 0 0 -1
cp
bface 2 north
bset bgro 2
bp


// Symmetry
// Merge vertices first otherwise
// boundaries will be created on axis
csys 3
cset all
view 1 0 0
pltype hsurf
cp
bview 3 10
view -1 0 0
pltype hsurf
cp
 bview 3 10

// Attached boundary 1
```

```
csys 2
cset news cgro 0
cset news gxyzrange 0 6 6.2 0 360 0 span
view 1 1 1
cp
bface 4 east
bset news bgro 4
bp

// Attached boundary 2
cset news cgro 2
view 1 1 1
cp
bface 5 west
bset bgro 5
bp

//Attached Boundary 3
csys 2
cset news cgro 0
cset news gxyzrange 0 4.15 4.2 0 360 0 span
view 1 1 1
cp
bface 6 west
bset news bgro 6
bp

//Attached Boundary 4

cset news cgro 1
cset news gxyzrange 1 4.0 4.15 0 360 0 span
view 1 1 1
cp
bface 7 east
bset news bgro 7
bp
bset bgro 6
bp

save 2

resu 2
movi on stand //yes
#def step 1.5e-6 0
// Note 1
// NB Watch out for this:
// #def speed 5000 //in RPM
// rather use this:
#def speed 3000   0            //in RPM

// Must fill in at least up to 'ratio'
// otherwise the dt will stay the same...
// in cases where it can automatically and with safety use a bigger time step
// Note 2
unst on step fixed 10 1 //1 1.05
```

```
unst on step adjust 10 1.2 10

#def dpt speed * 360 / 60 * step 0
slide on
//ssdef 1 2 0 0 dpt 0 arbitr 4 5 0.000001 20 const 1 1 2
//ssdef 2 2 0 0 dpt 0 arbitr 6 7 0.000001 20 const 1 1 1

ssdef 1 2 0 0 speed / 2 0 arbitr 4 5 0.000001 20 const 0 0 2
ssdef 2 2 0 0 speed / 2 0 arbitr 6 7 0.000001 20 const 0 0 1

ssdef 1 2 0 0 speed / 2 0 arbitr 4 5 0.0001 10 const 0 0 2
ssdef 2 2 0 0 speed / 2 0 arbitr 6 7 0.0003 10 const 0 0 1

bgdef 4 attach
2 0
bgdef 5 attach
2 0
bgdef 6 attach
2 0
bgdef 7 attach
2 0

bgdef 3 symm

bgdef 1 pres
0 300 0.05 0.001
//bgdef 1 inlet const
//2 -12.62 0 0 1.2 0.05 0.001 0.001
bgdef 2 pres
0 300 0.05 0.001


mdef 0 fluid

cgdef 0 0
cgdef 1 0
cgdef 2 0
cgdef 3 0
cgdef 4 0
cgdef 5 0
cgdef 6 0
cgdef 7 0
cgdef 8 0
cgdef 9 0
cgdef 10 0
cgdef 11 0

save 5

resu 5
/*
cset news cglist  3 4 5
cp
vset news cset
csys 0
```

```
vmerge vset
cp

cset news cglist  1
cp
vset news cset
csys 0
vmerge vset
cp
*/

// Note 3
// No unused vertices are allowed for... do away with them
cset all
vset news cset
vset unsel
vdel vset

vcomp all
ccomp all
wmesh .0254

mate 0
turb on
dens const 1.204
visc const 0.000018
pgrad zero
pref 100000 cm1

rest init
iter 20000 100 10
restart previous 1640
unst on 5.5e-7 adjust 1 1.5 50
conv 0.01
switch 21 on
wdef

save

plty wire
view 1 2 3
bset news bgro 1

bset bgro 0
bset bgro 1
bset bgro 2
bset bgro 4
bset bgro 5
bset bgro 6
bset bgro 7
bp
```

THIS PAGE INTENTIONALLY LEFT BLANK

APPENDIX C FAN-IN-WING GRID GENERATION CODE

SYMMETRY boundaries were applied to the front and back faces, as well as to the north and south faces of the grid. Additionally, the north and south faces of the grid were placed relatively far from the surfaces of the wing section to minimize effects from these surfaces. The west face was defined as an INLET type, with velocity specified as the desired freestream velocity. The east face was defined as an OUTLET type, with FREE mass flow. The mass flow fraction set at this boundary equated to the total mass flow entering the inlet boundary less the mass flow that entered the intake. Figure C1 depicts the C-grid used for numerical simulation of the fan-in-wing section.

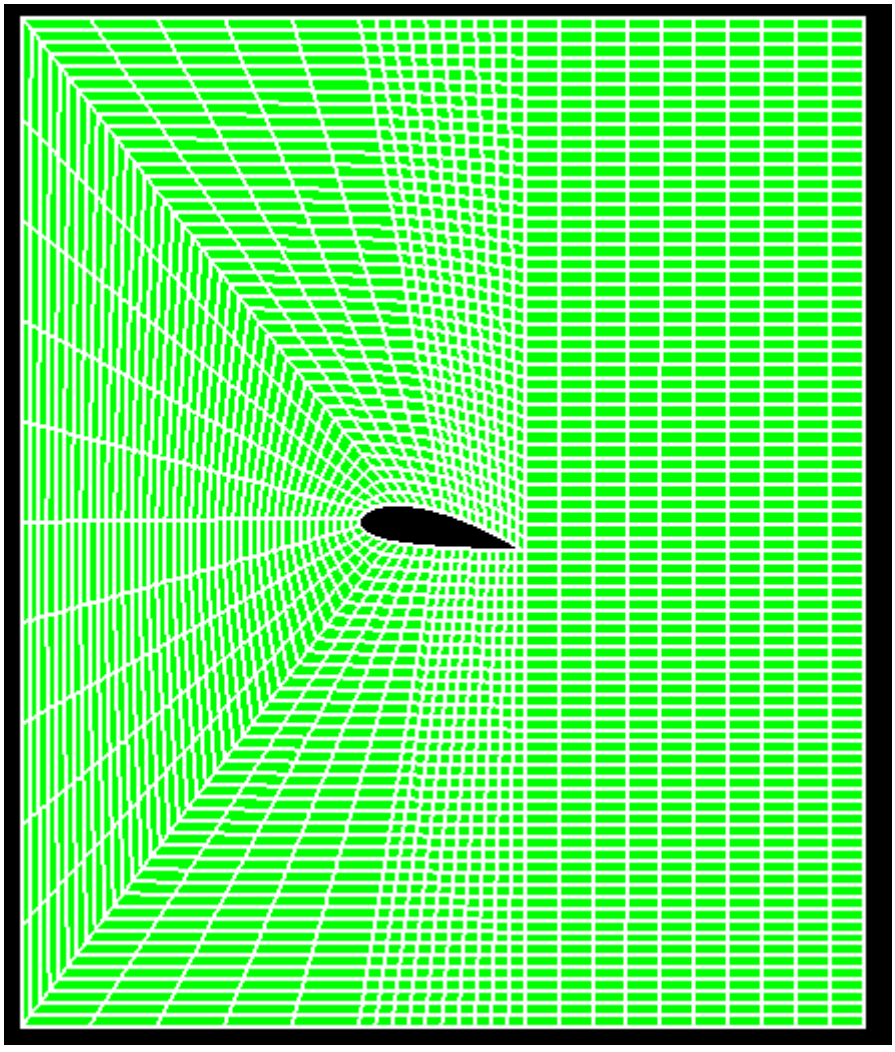

Figure C1. Fan-In-Wing C-Grid (10° AOA)

C1. FAN-IN-WING C-GRID FLO++ INPUT CODE

```
reset

// *** Mesh generation ****************************
// Define some user variables to
// First define some spline points and their locations
// Points for Spline 1 (5)
#def AOA -30 0
#def SPD 60 0 //in KNOTS
#def EXH 0    //in M/S
#def Wgrid 1.2 * 3 * .51444 * SPD
#def W 0 * 10.7153 / Wgrid//.058        //in percent of total mass flow through grid
#def SPAN .5

#def sinAOA AOA sine 0
#def cosAOA AOA cosi 0
vread c:\naca4424.txt
vp
vset all
csys 1
vmove 0 AOA 0
vp
csys 0
v vmax + 1 -2 0 0
v vmax + 1 -2 3 0
v vmax + 1 3 3 0
v vmax + 1 3 sinAOA  0
v vmax + 1 3 sinAOA  0
v vmax + 1 3 -3 0
v vmax + 1 -2 -3 0

v vmax + 1 cosAOA 3 0
v vmax + 1 cosAOA -3 0

v vmax + 1 0 3 0
v vmax + 1 0 -3 0

vp
vmax
#def bp1 vmax - 3
#def bp2 vmax - 1
#def bp3 vmax - 2
#def bp4 vmax
#def sp1a vmax - 9
#def sp1b vmax - 4


spline 1 vlist vmax - 8 -bp1  -bp2 -sp1a vmax - 10 -sp1b -bp4 -bp3 vmax - 5
sp

#def sp2a vmax - 45
#def sp2b vmax - 11
```

```
spline 2 vlist vmax - 7 -sp2a vmax - 44 vmax - 43 vmax - 42 vmax - 41 vmax - 40 vmax - 39 vmax - 38
vmax - 37 vmax - 36 vmax - 35
spline 2 vlist vmax - 34 vmax - 33 vmax - 32 vmax - 31 vmax - 30 vmax - 29 vmax - 28 vmax - 27
spline 2 vlist vmax - 26 vmax - 25 vmax - 24 vmax - 23 vmax - 22 vmax - 21 vmax - 20 vmax - 19
spline 2 vlist vmax - 18 vmax - 17 vmax - 16 vmax - 15 vmax - 14 vmax - 13 vmax - 12
spline 2 vlist -sp2b vmax - 6
sp

vset all
vcopy 2 46 vset 0 0 SPAN
vp
vmax

#def bp5 vmax - 3
#def bp6 vmax - 1
#def bp7 vmax - 2
#def bp8 vmax
#def sp3a vmax - 9
#def sp3b vmax - 4

spline 3 vlist vmax - 8 -bp5 -bp6 -sp3a vmax - 10 -sp3b -bp8 -bp7 vmax - 5
sp

#def sp4a vmax - 45
#def sp4b vmax - 11
spline 4 vlist vmax - 7 -sp4a vmax - 44 vmax - 43 vmax - 42 vmax - 41 vmax - 40 vmax - 39 vmax - 38
vmax - 37 vmax - 36 vmax - 35
spline 4 vlist vmax - 34 vmax - 33 vmax - 32 vmax - 31 vmax - 30 vmax - 29 vmax - 28 vmax - 27
spline 4 vlist vmax - 26 vmax - 25 vmax - 24 vmax - 23 vmax - 22 vmax - 21 vmax - 20 vmax - 19
spline 4 vlist vmax - 18 vmax - 17 vmax - 16 vmax - 15 vmax - 14 vmax - 13 vmax - 12
spline 4 vlist -sp4b vmax - 6
sp


block 1 vmax - 53 vmax - 54 vmax - 51 vmax - 52 vmax - 7 vmax - 8 vmax - 5 vmax - 6
blpl
blfactors 1 40 60 1 1

blcd 1 5 10 1 40 1 10 1
blcd 1 7 10 1 10 1 5 1 10 1 5 1 10 1 10 1
blcd 1 8 10 1 10 1 5 1 10 1 5 1 10 1 10 1
blcd 1 6 10 1 40 1 10 1

blex 1
cp

cset all
vcdist cset
//vmerge all 0.018

cset news gxyzrange 1 2.0 3.1 -3 3 0 SPAN
view 1 0 0
cp
bview 2
bp
```

```
cset news cgro 1
view 0 0 -1
cp
bview 3
bp


cset news cgro 1
view 0 0 1
cp
bview 3


cset news gxyzrange 1 -2 3 2.9 3.1 0 SPAN
cp
view 0 1 0
bface 4 east
bp

cset news gxyzrange 1 -2 3 -3.1 -2.9 0 SPAN
cp
view 0 -1 0
bface 4 east
bp
cset news gxyzrange 1 -2.1 -1.9 -3 3 0 SPAN
cp
view -1 0 0
cp
bview 1
bp
//cset news gxyzrange 1 -1.1 -0.9 -2 2 0 SPAN
//view -1 0 0
//cp
//bview 1
//bp
bset news bgro 4
bp
cp
cset news cran 1121 1121 1
cset cran 1081 1081 1
cset cran 1041 1041 1
cset cran 1001 1001 1
cp
bface 5 west
bp
cset all
cp
cset news cran 401 401 1
cp
bface 6 west
bp
cset all
cp
// *** Fluid type definition **************************
```

```
energy on
// turb on
tref 273
pref 100000 1
// *** Material properties and initial conditions ***
dens ideal
visc const 1.8e-5
// *** Cell and boundary group definitions ********
bgdef 1 inlet const
0 SPD * .514444 0 0 1 0.05 0.001 0.001
bgdef 2 outlet const
free 1 - W
bgdef 3 symmetry
bgdef 4 symm
bgdef 5 outlet const
free W
bgdef 6 inlet const
0 cosAOA * EXH sinAOA * EXH 0 1 0.05 0.001 0.001
//save 99
//resu 99
cset all
vcdist cset
vmerge all 0.01
wmesh
// *** Solution control ********************************
iter 1000 1
conv 0.001
monit 4
// *** Writing data for the solution stage **********
wdef
// *** Save the modelling status ********************
save
view 1 2 3
plty norm
bset none
bset bglist 1 2 4 5 6 0
bp
```

THIS PAGE INTENTIONALLY LEFT BLANK

APPENDIX D COMPLETE DATA LISTING

Date	Run #	RPM	Patm	Pcal	Pin TTR (5 o/c)	Pout TTR	Pin TTR (8 o/c)	Pin CFF (2 o/c)	Pin CFF (10 o/c)	Pout CFF (Top)	Pout CFF (Mid)	Pout CFF (Bot)	PA	PB	PC	PD	PE	PF	PG	PH	PI	PJ
12-Mar-03	1	4007.91	29.915	39.915	30.01177	30.82329	35.39967	29.90694	29.88255	33.03513	32.93059	32.75082	30.04177	26.92398	27.86993	29.54284	30.34437	29.7156	28.83954	28.73711	28.90555	30.28405
	2	4984.176	29.91	39.91	30.08067	31.31579	38.3769	29.89977	29.86183	34.8148	34.64465	34.43378	30.14158	25.22351	26.44574	29.02262	30.35273	29.60159	28.18129	28.04129	28.27832	30.45179
	3	5020.334	29.91	39.91	30.17326	31.31836	38.39609	29.89889	29.85529	34.83842	34.70758	34.43426	30.15047	25.33848	26.43721	28.95622	30.28715	29.60028	28.2085	28.05964	28.32001	30.45464
	4	2993.46	29.91	39.91	30.1775	30.42135	32.91546	29.90388	29.88979	31.54044	31.55588	31.46411	29.97223	28.33048	28.8438	29.74718	30.16362	29.79163	29.32601	29.27024	29.38331	30.12038
	5	3016.227	29.889	39.889	30.12854	30.4219	33.00929	29.88871	29.87569	31.55864	31.57554	31.48812	29.95877	28.43151	28.88968	29.76895	30.18032	29.77964	29.31772	29.25602	29.37715	30.10799
	6	4013.942	29.889	39.889	30.15687	30.79619	35.28187	29.88437	29.8577	32.98845	32.89756	32.73125	30.01978	27.25088	27.99028	29.52885	30.30656	29.69394	28.84692	28.7422	28.92947	30.25163
	7	5013.579	29.889	39.889	30.18482	31.22523	38.30866	29.88033	29.84195	34.7689	34.64464	34.43115	30.12725	25.7764	26.74534	29.08275	30.33688	29.58743	28.25165	28.10579	28.35445	30.42701
	8	5496.772	29.889	39.889	30.22351	31.48411	40.00836	29.87642	29.82524	35.79985	35.80268	35.37594	30.19476	25.00366	26.03919	28.76458	30.30182	29.52815	27.90805	27.74767	28.09647	30.50174
	9	5993.468	29.889	39.889	30.25464	31.82932	42.0174	29.87131	29.8123	37.17311	37.17908	36.54715	30.2773	24.08855	25.1674	28.26901	30.14695	29.47378	27.47536	27.27188	27.58007	30.55831
	10	6498.149	29.889	39.889	30.30477	32.23154	44.18715	29.86852	29.79153	38.24192	38.48933	37.84382	30.3586	23.22706	24.28056	27.65514	29.81851	29.41189	27.08331	26.85379	27.21198	30.58063
	11	7022.144	29.889	39.889	30.32025	32.67074	46.63439	29.86693	29.78284	39.87407	39.98784	39.22866	30.50484	22.24592	23.18941	26.8273	29.35083	29.34713	26.49577	26.26049	26.64927	30.55778
	12	7008.61	29.889	39.889	30.33454	32.6868	46.59722	29.86521	29.78581	39.8001	39.94766	39.19628	30.49863	22.25719	23.21587	26.8691	29.36114	29.34636	26.50496	26.25999	26.66749	30.57086
	13	5999.041	29.889	39.889	30.34803	31.87912	41.87659	29.87041	29.80856	37.12073	37.14766	36.50587	30.26618	24.04813	25.17619	28.31937	30.20619	29.476	27.46285	27.2654	27.56771	30.56019
	14	5007.93	29.889	39.889	30.32657	31.29217	38.15807	29.87489	29.82604	34.74819	34.63784	34.42517	30.11575	25.72317	26.78777	29.15749	30.40153	29.57888	28.23539	28.08281	28.31521	30.41778
	15	4004.298	29.889	39.889	30.30335	30.8058	35.15823	29.87911	29.84862	32.97117	32.9073	32.73314	30.01411	27.22264	28.01953	29.56235	30.33559	29.68367	28.83348	28.7341	28.91205	30.239
	16	2991.415	29.889	39.889	30.28142	30.41402	32.83494	29.88099	29.86746	31.52502	31.5298	31.45936	29.94644	28.42961	28.91183	29.77784	30.17632	29.76452	29.30408	29.24532	29.36107	30.09044
19-Feb-03	1	1012.356	30.1	40.1	29.70405	30.17218	30.65707	30.09982	30.09651	30.25735	30.26511	30.2755	30.10565	29.9593	30.0109	30.08458	30.11704	30.08916	30.05184	30.04634	30.07274	30.13297
	2	2002.583	30.1	40.1	29.76827	30.29854	31.62076	30.09972	30.0917	30.81089	30.80483	30.81581	30.12612	29.42599	29.64387	30.03839	30.22226	30.05137	29.85586	29.831	29.90439	30.20824
	3	3005.606	30.1	40.1	29.86097	30.54717	33.26515	30.09688	30.07963	31.8005	31.79553	31.69846	30.16677	28.4797	29.00381	29.93586	30.36726	29.98707	29.50767	29.45264	29.56973	30.32256
	4	4004.432	30.095	40.095	29.93266	30.92902	35.61672	30.08793	30.06103	33.2622	33.15762	32.95134	30.22495	27.11026	28.0152	29.70547	30.52403	29.89431	29.00628	28.9149	29.07989	30.46593
	5	4519.468	30.095	40.095	29.96872	31.23489	37.08035	30.0852	30.04917	34.16144	34.01651	33.76764	30.26935	26.25888	27.32577	29.49495	30.58308	29.84395	28.66505	28.53978	28.884	30.55084
	6	5014.752	30.095	40.095	30.01799	31.49818	38.68181	30.08414	30.04733	35.11112	34.95254	34.69494	30.32678	25.36913	26.53322	29.13726	30.49957	29.78771	28.34855	28.21123	28.47474	30.63653
	7	5021.51	30.095	40.095	30.08229	31.51452	38.70246	30.08294	30.04822	35.10823	34.94917	34.69503	30.32863	25.27978	26.52293	29.14147	30.49515	29.78474	28.3318	28.18235	28.42934	30.64417
	8	4008.017	30.095	40.095	30.08608	31.01855	35.53113	30.08557	30.05934	33.20282	33.14166	32.94582	30.22105	27.05963	28.00375	29.70055	30.50961	29.89139	29.00475	28.90104	29.06882	30.46322
	9	2991.922	30.095	40.095	30.05839	30.62015	33.16106	30.0878	30.07204	31.75778	31.75374	31.68036	30.15591	28.46389	29.01868	29.94814	30.3705	29.97309	29.49566	29.4413	29.55023	30.30863
	10	3020.418	30.08	40.08	29.96136	30.5982	33.21059	30.07676	30.06304	31.77389	31.797	31.68909	30.15362	28.45038	29.00222	29.93243	30.35551	29.96338	29.48627	29.43064	29.54767	30.3024
	11	4005.047	30.08	40.08	30.07855	31.0004	35.52925	30.07051	30.04715	33.16914	33.10573	32.91951	30.20941	27.08057	28.02516	29.70576	30.50216	29.87383	28.99452	28.89177	29.05764	30.44539
	12	4501.666	30.08	40.08	30.12702	31.23481	36.98861	30.06974	30.04438	34.06396	33.94362	33.7421	30.25692	26.25186	27.3629	29.5126	30.56782	29.83255	28.67084	28.55041	28.85822	30.53893
	13	5010.146	30.07	40.07	30.11963	31.50573	38.67817	30.05705	30.01575	35.01613	34.90215	34.63734	30.30402	25.30694	26.53814	29.14174	30.48404	29.75779	28.31963	28.17388	28.41536	30.61738
	14	5036.135	30.07	40.07	30.16072	31.51396	38.70137	30.05673	30.01722	35.07799	34.96421	34.69873	30.30182	25.27979	26.52205	29.12104	30.49331	29.75446	28.30821	28.15692	28.40214	30.61626
	15	3998.561	30.07	40.07	30.16504	31.00101	35.52101	30.06026	30.03197	33.19759	33.14601	32.93408	30.19664	27.03697	27.99563	29.67883	30.49209	29.86177	28.97523	28.87727	29.03898	30.43409
	16	2989.82	30.07	40.07	30.1752	30.59533	33.09997	30.0625	30.05	31.71637	31.7312	31.653	30.13083	28.45577	29.01135	29.92905	30.34418	29.94816	29.47675	29.42002	29.53331	30.2795
	17	3003.65	30.08	40.08	30.03505	30.61041	33.16804	30.07666	30.05993	31.73999	31.73692	31.66548	30.1478	28.46903	29.00818	29.93108	30.35441	29.96556	29.49028	29.43332	29.54476	30.30063
	18	4010.883	30.08	40.08	30.12608	31.01	35.53754	30.07192	30.04903	33.18494	33.09414	32.9224	30.20822	27.07736	28.02079	29.69296	30.5115	29.8781	28.99652	28.89429	29.06058	30.4485
	19	4996.836	30.08	40.08	30.1785	31.51285	38.69239	30.06947	30.02737	35.0308	34.84229	34.66662	30.31356	25.35021	26.57325	29.1516	30.51419	29.77405	28.34231	28.19631	28.42643	30.63136
	20	5006.091	30.075	40.075	30.2063	31.51226	38.66379	30.06348	30.01752	35.0553	34.87352	34.662	30.30821	25.32054	26.53571	29.12453	30.47939	29.76318	28.32601	28.17768	28.41484	30.62205
	21	4000.721	30.075	40.075	30.21785	31.00892	35.54733	30.0654	30.03953	33.1922	33.12721	32.95352	30.20033	27.04546	27.98219	29.67275	30.48713	29.87029	28.98172	28.8807	29.03351	30.44453
	22	3012.774	30.075	40.075	30.21673	30.60875	33.15449	30.06749	30.04787	31.75097	31.74345	31.66916	30.1361	28.42725	28.99052	29.92792	30.35685	29.95213	29.47043	29.41471	29.52909	30.29052
7-Feb-03	1	2002.436	29.925	39.925	29.85831	30.11081	31.42075	29.9201	29.91346	30.61852	30.62196	30.61176	29.94424	29.29371	29.51116	29.88835	30.06291	29.86492	29.66955	29.64393	29.72813	30.0186
	2	3007.383	29.925	39.925	29.94619	30.34332	33.02303	29.91983	29.90431	31.60491	31.62294	31.51341	29.99146	28.44968	28.93258	29.82081	30.23155	29.80712	29.34262	29.29583	29.40262	30.1437
	3	4027.306	29.925	39.925	29.99325	30.76922	35.38493	29.91473	29.88608	33.08373	32.98331	32.79999	30.05751	27.22987	28.00138	29.58639	30.37568	29.71707	28.85678	28.76021	28.94155	30.30269
	4	4504.302	29.925	39.925	30.02457	30.98939	36.74827	29.91322	29.87878	33.87749	33.74819	33.56891	30.09967	26.5154	27.42651	29.41817	30.42237	29.6668	28.56598	28.44921	28.76727	30.38184
	5	5012.114	29.925	39.925	30.05364	31.25843	38.3669	29.91152	29.86717	34.8402	34.70473	34.49757	30.15446	25.72728	26.75784	29.14152	30.40703	29.60419	28.25543	28.11848	28.35439	30.47561
	6	5505.649	29.925	39.925	30.09794	31.55087	40.11754	29.90959	29.84971	35.89141	35.90778	35.47718	30.22765	24.84944	26.0098	28.82811	30.39395	29.55472	27.88604	27.71833	28.01715	30.54956
	7	6023.673	29.925	39.925	30.13311	31.90931	42.29569	29.90377	29.84452	37.39958	37.39111	36.70564	30.31784	23.93554	25.08535	28.25182	30.18024	29.49165	27.43887	27.23421	27.60692	30.6113
	8	6502.55	29.925	39.925	30.16844	32.27588	44.46424	29.90229	29.81628	38.44922	38.73611	38.06402	30.40469	23.07853	24.19294	27.61484	29.79652	29.42618	27.04323	26.80927	27.16547	30.61284
	9	6516.498	29.925	39.925	30.17724	32.29144	44.4719	29.90226	29.82969	38.44305	38.75193	38.10366	30.3961	23.06445	24.16897	27.58897	29.78056	29.42215	27.03401	26.81106	27.13942	30.60377
	10	5995.325	29.925	39.925	30.19575	31.90538	42.06491	29.90589	29.84928	37.25882	37.25357	36.58427	30.30144	23.97498	25.16051	28.3232	30.22093	29.49463	27.4653	27.27456	27.54737	30.59151
	11	5511.87	29.925	39.925	30.21007	31.59086	40.11606	29.90553	29.84639	35.89411	35.94042	35.46402	30.21669	24.78586	25.97138	28.82565	30.41661	29.55079	27.8645	27.69815	27.97946	30.52835
	12	4996.961	29.925	39.925	30.21753	31.28859	38.29881	29.90866	29.86368	34.83558	34.75139	34.49792	30.13818	25.66009	26.76132	29.17993	30.44859	29.60736	28.23606	28.08052	28.29804	30.44963
	13	4502.781	29.925	39.925	30.21589	31.03058	36.62947	29.91144	29.87229	33.87565	33.75037	33.56936	30.088	26.48305	27.47011	29.45195	30.46733	29.6627	28.55205	28.42224	28.71582	30.35091
	14	3995.233	29.925	39.925	30.21567	30.80908	35.24014	29.9131	29.8852	33.01982	32.97665	32.75759	30.04861	27.20958	28.04957	29.62316	30.40048	29.71655	28.86104	28.7662	28.91254	30.27911
	15	3740.299	29.925	39.925	30.22337	30.70443	34.58546	29.91336	29.88965	32.59891	32.55986	32.43319	30.03023	27.54137	28.29245	29.69001	30.37288	29.73839	28.98971	28.90248	29.05088	30.23304
	16	3494.386	29.925	39.925	30.22614	30.60231	33.96707	29.91404	29.89317	32.23406	32.22322	32.07611	30.01503	27.86122	28.5456	29.74954	30.32611	29.7568	29.10674	29.03475	29.21891	30.1877
	17	3002.507	29.925	39.925	30.21868	30.42977	32.93048	29.91423	29.89916	31.57839	31.59282	31.49008	29.98147	28.42715	28.93567	29.82304	30.23005	29.79687	29.32673	29.27056	29.38047	30.12377
	18	1992.078	29.925	39.925	30.21114	30.16097	31.34228	29.91868	29.90979	30.61086	30.61648	30.60733	29.94082	29.28786	29.5165	29.89172	30.06025	29.86052	29.66942	29.64197	29.7156	30.00785
29-Jan-03	1	2056.013	30.18	40.18	30.16796	30.3971	31.71224	30.17762	30.16709	30.92533	30.91478	30.91529	30.20588	29.50551	29.7344	30.13187	30.31694	30.12181	29.90768	29.88086	29.96032	30.28153
	2	2054.858	30.18	40.18	30.17614	30.39676	31.72128	30.17586	30.16898	30.91686	30.90675	30.90737	30.20525	29.50687	29.73406	30.13105	30.31651	30.12076	29.90756	29.87967	29.96617	30.28095
	3	3002.958	30.195	40.195	30.21657	30.68723	33.29744	30.18693	30.16942	31.8625	31.88858	31.80282	30.25886	28.68766	29.16755	30.04953	30.46931	30.06999	29.58699	29.53181	29.64759	30.39888
	4	3503.507	30.195	40.195	30.23553	30.86916	34.36949	30.18793	30.16198	32.54991	32.54554	32.37273	30.29738	28.11865	28.73351	29.93639	30.53429	30.03316	29.36649	29.29338	29.50112	30.46293
	5	4004.031	30.195	40.195	30.25109	31.07483	35.63196	30.18612	30.15527	33.34348	33.26484	33.07106	30.33353	27.46744	28.24384	29.79117	30.57857	29.98505	29.10657	29.01272	29.18332	30.54629
	6	4484.607	30.195	40.195	30.27496	31.30228	37.01203	30.18489	30.1519	34.13886	33.99636	33.85923	30.37765	26.75435	27.66613	29.61382	30.61207	29.93634	28.802	28.69144	28.99781	30.62244
	7	5003.795	30.195	40.195	30.27897	31.55826	38.69161	30.18336	30.13693	35.0871	35.00603	34.79126	30.42935	25.96179	26.98814	29.33082	30.55519	29.87966	28.47846	28.33745	28.55476	30.70229
	8	5502.922	30.195	40.195	30.30987	31.86276	40.50519	30.18058	30.11982	36.16861	36.22814	35.79718	30.50972	25.14096	26.25458	29.99365	30.51983	29.81827	28.10533	27.94894	28.23978	30.77043
	9	4984.549	30.195	40.195	30.31702	31.57539	38.64951	30.18418	30.13333	35.0754	34.97282	34.8129	30.42934	25.97054	26.98994	29.34688	30.58491	29.88149	28.48159	28.34096	28.56932	30.70456

Table D1. Complete Data Listing

Date	Run #	PK	PL	Pin	Pin (Flange)	Pout (Flange)	Pout (Vena)	Tin CFF (2 o/c)	Tin CFF (11 o/c)	Tin TTR (8 o/c)	Tout TTR	Tin Orifice	Tout CFF (Bot)	Tout CFF (Mid)	Tout CFF (Top)	TTR Mass Flow (lbm/s)	Turbine Power (HP)	CFF Mass Flow (lbm/s)	Pi CFF	Tau CFF	CFF Efficiency	CFF Corrected Mass Flow (lbm/s)
12-Mar-03	1	30.52937	29.909	39.5379	30.36939	39.40675	39.42151	525.2055	525.747	533.4655	519.97	538.36	546.47	548.77	550.25	2.3274	-7.4933	1.3564	1.1007	1.0438	0.6345	1.3651
	2	30.83467	29.89719	42.06413	30.63058	41.88869	41.87134	525.2055	525.2143	535.8227	515.96	540.35	557.73	561.22	564.04	3.0754	-14.603	1.7003	1.159	1.0681	0.6319	1.7116
	3	30.85734	29.89719	42.03722	30.63407	41.83996	41.83566	526.9159	526.2374	537.1464	517.26	540.52	559.29	563.06	565.41	3.1424	-14.912	1.7255	1.1601	1.0684	0.6338	1.7394
	4	30.25444	29.89514	35.22137	30.14788	35.12471	35.12003	528.0936	529.4577	536.8282	528.98	540.44	540.58	542.45	543.11	2.0487	-3.7955	1.1914	1.0543	1.0251	0.6063	1.2027
	5	30.25075	29.88634	36.3711	30.14463	36.32236	36.32238	528.3116	529.0604	535.6364	527.61	539.98	540.28	542.03	542.33	1.451	-2.7552	0.8927	1.0555	1.0243	0.6394	0.9015
	6	30.51107	29.88093	38.79422	30.34044	38.67224	38.67774	528.8548	528.222	536.1638	522.94	539.49	549.43	551.5	552.26	2.3042	-7.275	1.3457	1.1005	1.0426	0.6507	1.3593
	7	30.84838	29.87813	42.47195	30.60945	42.30033	42.27528	527.7684	526.4536	536.5733	516.9	539.39	559.66	563.04	564.42	3.1236	-14.669	1.7335	1.1592	1.0669	0.6445	1.7493
	8	30.99457	29.87407	43.93429	30.74488	43.71392	43.71644	527.1356	525.2003	536.9565	514.35	539.59	564.84	569.7	571.23	3.3411	-18.09	1.7768	1.1946	1.0806	0.6463	1.792
	9	31.16535	29.87164	45.55206	30.91093	45.31479	45.30009	527.3993	524.8628	538.1096	513.43	541.96	572.6	579.09	581.33	3.6482	-21.549	1.7419	1.2387	1.098	0.6439	1.7573
	10	31.25056	29.86738	47.91632	31.03719	47.82826	47.82609	527.322	524.005	538.8093	513.84	541.79	580.95	587.69	589.7	4.0134	-23.982	1.653	1.2803	1.115	0.6361	1.6675
	11	31.31035	29.86752	50.77958	31.22962	50.50756	50.45302	526.095	522.829	539.1046	511.88	541.81	589.35	597.46	599.25	4.3799	-28.525	1.6766	1.331	1.1352	0.6297	1.6896
	12	31.32116	29.86617	50.8315	31.21841	50.50891	50.47976	526.872	523.1876	539.21	512.37	541.76	590.05	597.69	599.13	4.5466	-29.195	1.7232	1.3293	1.1345	0.6302	1.7375
	13	31.17298	29.86523	45.37818	30.90541	45.12757	45.10178	527.1532	525.8542	539.1538	513.6	541.33	572.98	579.78	582.39	3.8141	-23.313	1.8723	1.2374	1.0986	0.6369	1.8896
	14	30.83554	29.86342	44.2213	30.59089	44.02934	44.01851	528.8723	528.0251	538.8339	519.41	540.78	561.35	564.86	566.71	3.2317	-15.047	1.7485	1.1592	1.0679	0.6355	1.7672
	15	30.49833	29.86427	43.06224	30.32559	42.9587	42.93924	529.1354	529.2309	538.4612	525.52	540.17	550.42	552.97	554.18	2.4915	-7.7056	1.3761	1.1007	1.0441	0.6302	1.3912
	16	30.23345	29.86415	39.27833	30.12526	39.21123	39.25622	528.0514	529.9622	538.4067	530.71	541.31	540.97	543.14	543.72	1.0214	-1.8701	0.5727	1.0546	1.0257	0.5948	0.5787
19-Feb-03	1	30.14521	30.10336	33.62557	30.13256	33.59354	33.60307	515.912	521.9589	527.4696	526	536.29	521.19	522.52	522.54	0.9589	-0.3016	0.399	1.0056	1.0061	0.262	0.3964
	2	30.26227	30.10425	33.3764	30.21536	33.31636	33.34681	519.1499	522.6585	529.9077	525.62	539.6	525.56	527.02	527.52	1.0892	-1.098	0.7894	1.0238	1.0111	0.6048	0.7857
	3	30.45951	30.10215	36.51247	30.36032	36.44848	36.42233	521.8305	524.5886	531.7376	523.5	539.38	534.56	536.69	537.09	1.9702	-3.8409	1.2402	1.0557	1.0247	0.633	1.2375
	4	30.71198	30.09093	39.06743	30.55277	38.91182	38.9296	524.0032	524.8294	533.6026	520	538.32	545.46	547.91	548.93	2.5154	-8.1522	1.4757	1.1014	1.0439	0.6373	1.4747
	5	30.87278	30.08932	41.20012	30.67856	41.01614	40.99767	524.0296	524.5956	534.9843	518.17	540.57	550.91	553.89	555.99	3.1177	-12.508	1.7796	1.1302	1.0659	0.6371	1.7787
	6	31.03399	30.08726	42.17799	30.82096	41.95266	41.93143	523.3845	523.6657	535.7085	515.68	539.72	554.97	559.29	562.48	3.4802	-16.64	1.9592	1.1614	1.0676	0.6463	1.9569
	7	31.04327	30.08338	42.17071	30.82425	41.96052	41.94711	525.0966	524.7766	536.6559	516.64	539.63	558	561.75	564.51	3.3159	-15.851	1.8103	1.1614	1.0695	0.6283	1.8106
	8	30.70921	30.08288	39.65885	30.54534	39.53086	39.5506	524.3003	526.5204	536.9214	523.42	541.15	546.34	549.13	551.05	2.2403	-7.1961	1.2797	1.1006	1.0446	0.6224	1.2802
	9	30.4436	30.08082	36.20557	30.34025	36.18045	36.14643	522.5864	526.8069	536.22	528.26	538.96	536.14	538.61	539.61	1.5942	-3.0033	0.9323	1.0549	1.0256	0.6013	0.9318
	10	30.43988	30.07527	36.88141	30.33877	36.82776	36.83219	527.5557	528.0356	535.3552	527.34	539.81	539.54	541.37	541.84	1.4687	-2.7823	0.8835	1.056	1.0249	0.6309	0.886
	11	30.69139	30.06924	39.77405	30.53089	39.66383	39.65212	527.8159	527.1761	536.5259	523.07	541.27	548.25	550.58	552.37	2.3825	-7.6279	1.3877	1.1	1.0434	0.6358	1.3916
	12	30.86066	30.07604	40.4829	30.66623	40.2976	40.27842	527.1163	525.6802	535.995	519.59	538.52	552.82	555.38	558.19	3.1116	-12.187	1.7472	1.1284	1.0552	0.636	1.7504
	13	31.01864	30.0586	42.15737	30.80232	41.95731	41.9605	527.3518	525.4305	536.9952	516.99	540.98	559.84	562.9	565.81	3.1091	-14.807	1.6923	1.1603	1.0693	0.6266	1.6966
	14	31.01485	30.05709	42.1565	30.8022	41.97014	41.98237	527.6524	525.7153	537.2835	517.28	540.34	559.96	563.19	566.12	2.9275	-13.984	1.6004	1.1624	1.0691	0.6354	1.6049
	15	30.68506	30.05448	40.21264	30.51742	40.0595	40.04241	529.0288	528.1534	537.0145	523.69	540.38	549.74	552.08	553.86	2.8276	-8.9705	1.6041	1.1014	1.0441	0.6346	1.611
	16	30.41576	30.05406	39.17285	30.3103	39.10952	39.09459	529.8286	529.8409	537.12	529.29	541.77	541.39	543.15	544.08	1.8985	-3.5102	1.1218	1.0547	1.0246	0.623	1.1275
	17	30.43569	30.07298	36.66271	30.33341	36.5935	36.56335	528.8319	528.9725	535.6434	527.83	539.67	540.7	542.44	542.89	2.0709	-3.8416	1.2209	1.0547	1.0248	0.6189	1.2256
	18	30.69608	30.07216	39.37631	30.5338	39.25099	39.23641	528.403	527.4731	536.6577	523.28	541.37	549.02	551.43	553.09	2.5372	-8.0674	1.447	1.1	1.044	0.6275	1.4516
	19	31.02626	30.07198	41.70804	30.80705	41.44991	41.46084	527.3958	525.2759	536.6507	516.88	539.39	558.95	562.33	565.03	3.4663	-16.347	1.9045	1.1597	1.068	0.6362	1.9084
	20	31.01497	30.06273	41.70022	30.80276	41.49573	41.46027	528.0831	526.0054	537.2835	517.47	541.43	560.11	563.35	566.23	3.409	-16.118	1.856	1.1606	1.0687	0.633	1.8616
	21	30.68613	30.06114	38.73657	30.52367	38.62475	38.62798	529.2221	528.338	537.403	524.02	541.07	549.94	552.29	554.17	2.221	-7.0746	1.2622	1.1011	1.0442	0.6317	1.2676
	22	30.4269	30.0601	37.0248	30.32108	36.97009	36.97554	529.1975	529.6845	536.7069	528.74	539.16	541.09	543.15	544.21	1.473	-2.7732	0.864	1.0553	1.0253	0.614	0.8681
7-Feb-03	1	30.07611	29.91149	33.09907	30.02353	33.05272	33.05163	522.5038	525.0561	530.8552	526.46	538.01	528.71	529.65	529.71	1.3696	-1.4087	1.0525	1.0234	1.0106	0.6232	1.0567
	2	30.28521	29.91523	36.03746	30.17542	35.97606	35.97188	524.3811	526.2005	533.1614	524.99	538	536.89	538.73	538.8	1.6751	-3.2348	1.0489	1.0558	1.0245	0.6388	1.0548
	3	30.55756	29.91112	39.62787	30.38509	39.52287	39.53625	524.5288	525.2829	535.0757	521.36	540.57	546.06	548.57	549.42	2.0661	-6.7251	1.2124	1.1022	1.044	0.6401	1.2192
	4	30.70847	29.90993	41.88408	30.49962	41.67043	41.6692	525.6573	524.9823	535.6013	519.08	539.1	551.84	554.29	555.46	3.2418	-12.73	1.8584	1.1283	1.0543	0.6458	1.8699
	5	30.87547	29.90568	41.84632	30.63799	41.66904	41.67793	525.311	524.629	536.7122	516.71	540.81	557.85	561.41	562.62	2.8676	-13.659	1.5961	1.1603	1.0679	0.6389	1.6058
	6	31.03074	29.90491	43.866	30.78804	43.64357	43.64367	524.7391	523.7114	537.0901	513.86	539.69	563	567.89	569.47	3.3719	-18.702	1.8314	1.1968	1.0812	0.6487	1.8418
	7	31.19632	29.90425	45.96643	30.96918	45.7496	45.70346	525.1194	523.4354	537.7001	510.42	541.14	571.13	577.89	580.11	3.7458	-24.401	1.9515	1.244	1.0994	0.6478	1.9631
	8	31.25252	29.90259	46.58622	31.09024	46.2699	46.2743	524.4989	521.9764	537.8495	506.86	539.71	578.32	585.09	587.61	4.1087	-30.349	2.0924	1.2866	1.1155	0.6463	2.1038
	9	31.24667	29.90196	46.66363	31.09211	46.40939	46.39661	524.2071	521.8429	538.2679	507.09	541.09	578.62	585.62	588.27	3.803	-28.34	1.9312	1.2868	1.1169	0.6391	1.9409
	10	31.17646	29.89963	44.20894	30.9353	43.92257	43.93443	526.4694	524.172	538.4858	511.69	540.73	572	578.1	580.47	3.7539	-23.983	1.939	1.2395	1.0981	0.6448	1.9522
	11	31.01821	29.89853	42.26522	30.78151	42.01173	42.02035	527.2798	525.4059	538.4366	515.09	540.88	566.37	570.83	572.73	3.4683	-19.301	1.843	1.1972	1.0829	0.6364	1.8575
	12	30.85533	29.89854	40.2647	30.6245	40.05904	40.03562	528.1411	527.0214	538.6651	519.07	541.35	561.01	564.05	566.06	3.2742	-15.268	1.761	1.1609	1.0685	0.636	1.7763
	13	30.68511	29.89798	38.33824	30.47894	38.13132	38.13401	528.2044	527.8106	537.9304	521.84	539.37	554.93	557.51	559.78	3.0241	-11.575	1.6405	1.1285	1.0557	0.631	1.6551
	14	30.53025	29.90083	36.62991	30.36556	36.48418	36.49179	529.2749	529.1993	538.31	525.21	541.2	550.48	552.88	553.97	2.4326	-7.5998	1.3645	1.101	1.0438	0.6354	1.378
	15	30.45617	29.90006	35.95125	30.30022	35.83953	35.82491	529.7882	529.7302	538.1096	526.52	540.3	548.45	550.46	551.16	2.308	-6.3547	1.3066	1.0879	1.0383	0.6371	1.32
	16	30.38058	29.89897	35.19306	30.2409	35.08605	35.1492	529.0288	529.8971	537.5981	527.49	538.87	545.68	547.85	548.48	1.3571	-3.2528	0.7584	1.0761	1.0338	0.627	0.7659
	17	30.26264	29.8994	34.09151	30.15729	34.02663	34.03908	528.846	530.3331	537.9638	530.12	541.24	541.49	543.47	543.77	1.4556	-2.6983	0.8441	1.0551	1.0252	0.6137	0.8525
	18	30.06371	29.90285	33.07519	30.01209	33.03524	33.0486	529.3346	531.5952	537.5032	533.58	540.25	536.19	537.45	537.22	1.0285	-0.9367	0.6015	1.0233	1.0122	0.54	0.6078
29-Jan-03	1	30.34443	30.17342	33.38856	30.29736	33.34264	33.33953	526.9721	529.129	535.095	530.96	538.95	534.21	535.19	534.91	1.3967	-1.3399	0.8311	1.0247	1.0127	0.5505	0.8311
	2	30.34223	30.17151	33.39957	30.29525	33.33909	33.35902	524.8891	528.4786	535.1917	531.07	539.35	532.3	533.78	534.26	1.2721	-1.2142	0.7481	1.0245	1.0128	0.5395	0.7471
	3	30.54374	30.18231	35.72753	30.44994	35.67087	35.65158	526.5819	528.5173	536.3009	528.4	541.22	539.43	541.49	541.77	1.7882	-3.3194	1.0361	1.0554	1.0253	0.614	1.0354
	4	30.66072	30.18372	37.57776	30.54075	37.49177	37.48847	527.2182	528.1903	536.1936	525.91	539.05	543.77	546.03	546.45	1.9897	-4.8542	1.142	1.0767	1.0336	0.6358	1.1414
	5	30.80353	30.18215	39.6606	30.66489	39.55363	39.51284	527.5118	527.8721	537.1024	523.9	540.93	548.92	551.34	551.92	2.617	-8.197	1.4826	1.1013	1.0437	0.6401	1.482
	6	30.95124	30.18157	41.93271	30.78514	41.75382	41.76234	525.8296	526.153	536.9425	520.9	539.4	551.99	555.2	556.91	2.8908	-11.034	1.6013	1.1269	1.0546	0.6364	1.5983
	7	31.11285	30.18054	41.61274	30.93448	41.40218	41.39661	526.327	525.7891	537.8179	518.3	541.06	558.97	562.52	563.64	3.2348	-15.031	1.7568	1.1592	1.0678	0.6361	1.7541
	8	31.26457	30.17853	43.69213	31.08462	43.44746	43.43734	525.4833	523.6886	537.8688	514.7	540.73	563.55	568.52	570.77	3.5968	-19.925	1.9296	1.1962	1.082	0.6402	1.9245
	9	31.11543	30.18121	41.27962	30.93089	41.0497	41.05391	527.0778	525.9807	537.8513	518.46	539.98	559.54	563.12	564.39	3.295	-15.278	1.7773	1.159	1.068	0.6329	1.7754

Table D1. Complete Data Listing (Continued)

Date	Run #	Corrected Power (HP)	Corrected Speed (RPM)	X1	mdot1	X2	mdot2	X3	mdot3	Computed MA Mdot	Computed MA HP	Corrected Computed MA Mdot	Corrected Computed MA HP	Ttbar Out	Ptbar Out	MA Exit Mach	Static Temp CFF Out	Exit Vel (fps)	Exit Vel (m/s)	Corrected Thrust	C. Thrust Normalized to 12"	C. Power Norm. to 12"
12-Mar-03	1	10.543	3985.8	0.1636	0.5725	0.1609	0.3219	0.1561	0.5467	1.4411	11.256	1.4517	11.193	548.48	32.904	0.3629	534.41	411.08	125.3	18.564	148.51	89.544
	2	20.561	4958	0.2009	0.7063	0.1975	0.3973	0.1932	0.6811	1.7847	21.685	1.7982	21.579	561	34.632	0.4498	539.18	511.81	156	28.642	229.14	172.63
	3	20.972	4987.4	0.2011	0.7067	0.1985	0.399	0.193	0.6795	1.7853	21.805	1.8014	21.673	562.55	34.655	0.4505	540.61	513.22	156.43	28.776	230.2	173.38
	4	5.3232	2967.7	0.1203	0.4173	0.1208	0.2398	0.1174	0.408	1.0652	4.7802	1.0763	4.7381	541.99	31.515	0.2687	534.28	304.33	92.761	10.189	81.508	37.905
	5	3.8664	2990.5	0.1215	0.4217	0.1221	0.2423	0.1188	0.4131	1.0772	4.6772	1.0889	4.6387	541.48	31.535	0.2717	533.6	307.5	93.725	10.42	83.359	37.109
	6	10.214	3980.2	0.163	0.5689	0.1607	0.3203	0.1562	0.5453	1.4346	10.947	1.4505	10.862	551.02	32.87	0.3623	536.92	411.38	125.39	18.577	148.61	86.896
	7	20.631	4978.2	0.2003	0.7036	0.1978	0.3972	0.1935	0.6806	1.7814	21.275	1.7993	21.146	562.29	34.612	0.4497	540.43	512.24	156.13	28.703	229.62	169.17
	8	25.473	5462.9	0.2179	0.7685	0.218	0.4399	0.2103	0.7434	1.9518	28.017	1.9703	27.882	568.45	35.639	0.4925	542.15	561.84	171.25	34.487	275.9	223.06
	9	30.354	5956.7	0.2386	0.8449	0.2387	0.4839	0.2288	0.8123	2.1411	37.349	2.1621	37.182	577.51	36.937	0.5406	545.62	618.73	188.59	41.687	333.49	297.45
	10	33.809	6461.2	0.2526	0.8971	0.256	0.5214	0.247	0.8811	2.2996	47.018	2.3219	46.847	585.89	38.145	0.5806	548.89	666.46	203.14	48.242	385.94	374.77
	11	40.267	6990.2	0.2714	0.9709	0.2728	0.5589	0.2633	0.9454	2.4752	59.328	2.4968	59.189	595.06	39.653	0.6238	552.1	718.15	218.89	55.909	447.27	473.51
	12	41.19	6972.9	0.2706	0.9674	0.2724	0.5578	0.263	0.9433	2.4685	58.918	2.4914	58.747	595.33	39.603	0.6224	552.52	716.9	218.51	55.69	445.52	469.98
	13	32.83	5960.2	0.238	0.8415	0.2384	0.4828	0.2283	0.81	2.1343	37.48	2.1561	37.301	578.23	36.893	0.5395	546.43	617.88	188.33	41.518	332.14	298.41
	14	21.143	4966.3	0.2001	0.7013	0.1979	0.3967	0.1936	0.6799	1.7779	21.607	1.7987	21.457	564.25	34.6	0.4498	542.31	513.19	156.42	28.757	230.05	171.65
	15	10.815	3968.2	0.1628	0.5668	0.1611	0.3207	0.1564	0.5455	1.433	11.329	1.4502	11.237	552.48	32.966	0.3625	538.33	412.07	125.6	18.608	148.86	89.894
	16	2.6242	2965	0.1207	0.4183	0.1209	0.2395	0.1182	0.4106	1.0684	4.9067	1.0806	4.8661	542.53	31.501	0.2698	534.75	305.75	93.194	10.285	82.278	38.929
19-Feb-03	1	0.4241	1013.1	0.0379	0.1328	0.0388	0.0778	0.0401	0.1407	0.3514	0.3651	0.3494	0.3629	522	30.266	0.0872	521.2	97.585	29.744	1.0536	8.4285	2.9029
	2	1.5413	2000.3	0.08	0.2808	0.0797	0.1598	0.0803	0.2824	0.723	1.409	0.7204	1.3978	526.64	30.811	0.1796	523.27	201.25	61.341	4.4795	35.836	11.182
	3	5.381	2995.5	0.1223	0.4297	0.1221	0.2453	0.1185	0.4171	1.0921	4.7546	1.0907	4.7076	536.03	31.76	0.2722	528.21	306.51	93.426	10.333	82.66	37.661
	4	11.413	3986.4	0.1643	0.5791	0.1616	0.3255	0.1561	0.5507	1.4553	11.351	1.4558	11.231	547.39	33.121	0.3639	533.27	411.79	125.51	18.537	148.29	89.848
	5	17.517	4499.5	0.1843	0.6512	0.1811	0.3659	0.1754	0.6206	1.6377	16.281	1.6385	16.114	553.6	33.98	0.4098	535.61	464.72	141.65	23.55	188.4	128.91
	6	23.322	4996.4	0.2025	0.7178	0.1994	0.4045	0.1942	0.6908	1.8132	21.779	1.8128	21.573	558.91	34.917	0.4533	536.85	514.6	156.85	28.853	230.83	172.58
	7	22.187	4996.4	0.2024	0.7162	0.1993	0.4034	0.1942	0.6888	1.8085	22.396	1.8105	22.155	561.41	34.915	0.4531	539.27	515.55	157.14	28.871	230.97	177.24
	8	10.066	3986.2	0.1629	0.5727	0.1613	0.3245	0.1561	0.55	1.4472	11.506	1.4492	11.375	548.83	33.091	0.3624	534.78	410.61	125.15	18.401	147.21	90.999
	9	4.2027	2977.6	0.1212	0.4244	0.121	0.2425	0.1183	0.4154	1.0823	4.9075	1.0828	4.8534	538.05	31.727	0.2704	530.3	305.05	92.979	10.212	81.692	38.827
	10	3.8834	2997.2	0.1218	0.426	0.1227	0.2452	0.1187	0.4156	1.0868	4.818	1.0908	4.7525	540.85	31.747	0.2722	532.96	307.9	93.848	10.387	83.096	38.02
	11	10.653	3975.3	0.1623	0.5698	0.1607	0.3227	0.1557	0.5475	1.44	11.197	1.4454	11.052	550.4	33.06	0.3612	536.4	409.93	124.95	18.331	146.65	88.419
	12	17.04	4472.9	0.1825	0.6428	0.1798	0.3624	0.1751	0.6182	1.6234	16.047	1.6279	15.857	555.52	33.915	0.4071	537.7	462.52	140.98	23.295	186.36	126.85
	13	20.718	4978.2	0.2011	0.7101	0.1989	0.4019	0.1936	0.6848	1.7968	22.259	1.8031	22.011	562.88	34.846	0.4512	540.86	514.12	156.7	28.7	229.6	176.08
	14	19.56	5002.6	0.2024	0.7146	0.2002	0.4045	0.1949	0.6897	1.8088	22.373	1.8156	22.116	563.12	34.908	0.4542	540.8	517.54	157.75	29.091	232.73	176.93
	15	12.521	3964.8	0.1634	0.5729	0.1621	0.3251	0.1565	0.5493	1.4473	11.45	1.4549	11.295	551.9	33.086	0.3637	537.67	413.19	125.94	18.606	148.85	90.36
	16	4.892	2961.1	0.1206	0.4204	0.1211	0.2415	0.1182	0.4129	1.0748	4.7446	1.0814	4.6732	542.84	31.695	0.2699	535.04	305.89	93.235	10.234	81.876	37.385
	17	5.3564	2977.4	0.1208	0.4218	0.1207	0.2409	0.118	0.4127	1.0754	4.7641	1.0806	4.6947	541.95	31.711	0.2697	534.18	305.4	93.087	10.207	81.654	37.558
	18	11.262	3979.5	0.1628	0.5711	0.1604	0.3218	0.1558	0.5475	1.4404	11.354	1.4464	11.202	551.16	33.065	0.3616	537.11	410.63	125.16	18.374	146.99	89.616
	19	22.864	4965.2	0.2012	0.711	0.1975	0.3992	0.1939	0.687	1.7972	21.824	1.8027	21.572	562.1	34.85	0.4508	540.15	513.38	156.48	28.641	229.13	172.58
	20	22.535	4971.1	0.2018	0.7124	0.1982	0.4003	0.194	0.6863	1.7991	22.116	1.8062	21.852	563.25	34.865	0.4518	541.16	515	156.97	28.796	230.37	174.82
	21	9.8706	3966.2	0.1632	0.5719	0.1615	0.3238	0.1569	0.5508	1.4465	11.471	1.4541	11.311	552.14	33.087	0.3635	537.92	413.07	125.9	18.586	148.69	90.486
	22	3.8661	2984.9	0.1217	0.4242	0.1214	0.2421	0.1186	0.4146	1.0808	4.8921	1.087	4.82	542.77	31.718	0.2713	534.9	307.48	93.719	10.34	82.722	38.56
7-Feb-03	1	1.9837	1994.6	0.0796	0.2773	0.0798	0.1588	0.0792	0.2761	0.7122	1.337	0.7158	1.3306	529.31	30.617	0.1784	525.96	200.47	61.103	4.4604	35.683	10.645
	2	4.5495	2991.3	0.1219	0.4251	0.1226	0.2443	0.1185	0.4137	1.0831	4.6937	1.0902	4.6654	538.06	31.574	0.272	530.21	306.92	93.55	10.403	83.223	37.324
	3	9.4655	4007.3	0.1644	0.5762	0.1618	0.3241	0.157	0.5504	1.4507	11.353	1.4603	11.293	547.96	32.954	0.3649	533.74	413.07	125.9	18.761	150.09	90.342
	4	17.914	4480.1	0.1823	0.6402	0.1793	0.3599	0.1752	0.6157	1.6159	15.633	1.6274	15.547	553.82	33.731	0.4067	536.08	461.39	140.63	23.357	186.85	124.38
	5	19.231	4986.9	0.2011	0.7083	0.1984	0.3994	0.1942	0.6851	1.7928	21.641	1.8054	21.534	560.53	34.679	0.4514	538.58	513.29	156.45	28.833	230.66	172.27
	6	26.358	5481.8	0.2188	0.7741	0.2191	0.4436	0.2115	0.7499	1.9676	28.33	1.9807	28.218	566.65	35.737	0.495	540.18	563.69	171.81	34.749	277.99	225.74
	7	34.395	5997.3	0.2412	0.8572	0.2411	0.4906	0.2306	0.8214	2.1693	38.244	2.1843	38.099	576.21	37.133	0.5461	543.77	623.98	190.19	42.427	339.42	304.79
	8	42.842	6480.5	0.2547	0.9084	0.2586	0.5292	0.2493	0.8938	2.3314	47.678	2.3464	47.567	583.48	38.367	0.5861	545.96	671.06	204.54	49.038	392.31	380.54
	9	40.006	6495.8	0.2548	0.9079	0.2589	0.5296	0.2501	0.8962	2.3338	48.28	2.3477	48.167	583.96	38.383	0.5871	546.31	672.33	204.93	49.148	393.18	385.33
	10	33.769	5963.2	0.2395	0.8495	0.2394	0.4863	0.2289	0.8139	2.1497	37.518	2.1665	37.334	576.73	37.002	0.5419	544.73	619.77	188.91	41.792	334.34	298.67
	11	27.151	5477	0.2191	0.7727	0.2199	0.444	0.2115	0.7474	1.9641	29.031	1.9814	28.862	569.88	35.741	0.4957	543.19	566.06	172.54	34.911	279.29	230.89
	12	21.445	4969.5	0.2013	0.7068	0.1997	0.401	0.1946	0.6843	1.7921	21.965	1.8095	21.804	563.68	34.688	0.4527	541.49	516.16	157.33	29.062	232.5	174.43
	13	16.248	4467.2	0.1825	0.6384	0.1797	0.3595	0.1755	0.6149	1.6129	16.108	1.6288	15.98	557.42	33.731	0.4074	539.52	463.65	141.32	23.494	187.95	127.84
	14	10.653	3959.1	0.163	0.5686	0.1619	0.3229	0.1561	0.5448	1.4362	11.294	1.4517	11.189	552.4	32.911	0.3629	538.23	412.49	125.73	18.625	149	89.512
	15	8.9028	3704.6	0.1522	0.5301	0.1511	0.3008	0.1475	0.5141	1.345	9.2279	1.3601	9.1367	549.97	32.527	0.3397	537.56	385.92	117.63	16.324	130.59	73.094
	16	4.5581	3462	0.142	0.494	0.1417	0.2817	0.1371	0.4774	1.2531	7.5748	1.2667	7.5015	547.27	32.171	0.3164	536.53	359.09	109.45	14.146	113.16	60.012
	17	3.7802	2974.3	0.1213	0.4209	0.1218	0.2417	0.118	0.41	1.0727	4.8218	1.0843	4.7741	542.83	31.548	0.2707	534.99	306.8	93.514	10.345	82.756	38.192
	18	1.3109	1971.8	0.0794	0.2744	0.0797	0.1574	0.0792	0.274	0.7059	1.5352	0.714	1.5184	536.87	30.611	0.1781	533.49	201.54	61.429	4.473	35.784	12.147
29-Jan-03	1		2039.7	0.0819	0.2862	0.0813	0.1623	0.0813	0.2844	0.733	1.6541	0.7334	1.6257	534.7	30.919	0.1829	531.14	206.53	62.951	4.6682	37.346	13.006
	2		2041.2	0.0814	0.2848	0.0809	0.1617	0.0809	0.2835	0.73	1.6625	0.7294	1.636	533.39	30.911	0.1819	529.88	205.21	62.547	4.6134	36.907	13.088
	3		2980.5	0.121	0.4246	0.122	0.2446	0.1188	0.4175	1.0867	4.8918	1.0865	4.8091	540.81	31.845	0.2712	532.97	306.76	93.502	10.271	82.168	38.473
	4		3476.8	0.1424	0.5009	0.1423	0.2861	0.1369	0.4821	1.2692	7.5969	1.2693	7.4682	545.34	32.482	0.3169	534.6	359.05	109.44	14.045	112.36	59.746
	5		3973.6	0.1633	0.576	0.1613	0.325	0.1562	0.551	1.4521	11.32	1.4524	11.129	550.65	33.223	0.3629	536.53	411.82	125.52	18.437	147.49	89.036
	6		4457.7	0.1811	0.6409	0.1779	0.3598	0.1747	0.6196	1.6204	15.764	1.6183	15.526	554.65	34	0.4044	537.08	459.24	139.98	22.909	183.27	124.21
	7		4973.5	0.1997	0.7088	0.1981	0.4019	0.1938	0.689	1.7998	21.717	1.7981	21.393	561.6	34.956	0.4495	539.78	511.75	155.98	28.372	226.98	171.14
	8		5477.2	0.2178	0.7765	0.2189	0.4469	0.2113	0.7557	1.9792	28.835	1.9752	28.454	567.5	36.04	0.4937	541.12	562.72	171.52	34.282	274.26	227.63
	9		4952.1	0.1995	0.7075	0.1974	0.4003	0.1942	0.6904	1.7981	21.801	1.7973	21.467	562.24	34.952	0.4494	540.42	511.84	156.01	28.366	226.93	171.73

Table D1. Complete Data Listing (Continued)

THIS PAGE INTENTIONALLY LEFT BLANK

INITIAL DISTRIBUTION LIST

1. Defense Technical Information Center
   Ft. Belvoir, VA

2. Dudley Knox Library
   Naval Postgraduate School
   Monterey, CA

3. Dr. Max F. Platzer
   Department of Aeronautics and Astronautics
   Naval Postgraduate School
   Monterey, CA

4. Dr. Garth V. Hobson
   Department of Aeronautics and Astronautics
   Naval Postgraduate School
   Monterey, CA

5. Dr. Raymond P. Shreeve
   Department of Aeronautics and Astronautics
   Naval Postgraduate School
   Monterey, CA

6. Dr. Kevin D. Jones
   Department of Aeronautics and Astronautics
   Naval Postgraduate School
   Monterey, CA

7. Dr. M. S. Chandrasekhara
   Department of Aeronautics and Astronautics
   Naval Postgraduate School
   Monterey, CA

8. Gary J. Skoch
   NASA Glenn Research Center
   Cleveland, OH

9. Louis LeGrange
   Softflo, Inc.
   Noordbrug, South Africa

10. Scot Seaton
    Santee, CA